PB85-173821

# Microwave System for Locating Faults in Hazardous Material Dikes

Drexel Univ., Philadelphia, PA

Prepared for

Environmental Protection Agency, Cincinnati, OH

Mar 85

U.S. Department of Commerce
National Technical Information Service
NTIS

PB85-173821

EPA/600/2-85/014
March 1985

# MICROWAVE SYSTEM FOR LOCATING FAULTS IN HAZARDOUS MATERIAL DIKES

by

Robert M. Koerner and Arthur E. Lord, Jr.
Drexel University
Philadelphia, Pennsylvania 19104

Cooperative Agreement No. R80476301

Project Officer

John E. Brugger
Land Pollution Control Division
Hazardous Waste Engineering Research Laboratory
Edison, New Jersey 08837

HAZARDOUS WASTE ENGINEERING RESEARCH LABORATORY
OFFICE OF RESEARCH AND DEVELOPMENT
U.S. ENVIRONMENTAL PROTECTION AGENCY
CINCINNATI, OH 45268

REPRODUCED BY
NATIONAL TECHNICAL
INFORMATION SERVICE
U.S. DEPARTMENT OF COMMERCE
SPRINGFIELD, VA. 22161

| TECHNICAL REPORT DATA (Please read Instructions on the reverse before completing) | | |
|---|---|---|
| 1. REPORT NO. EPA/600/2-85/014 | 2. | 3. RECIPIENT'S ACCESSION NO. PB85 173821/AS |
| 4. TITLE AND SUBTITLE MICROWAVE SYSTEM FOR LOCATING FAULTS IN HAZARDOUS MATERIAL DIKES | | 5. REPORT DATE March 1985 |
| | | 6. PERFORMING ORGANIZATION CODE |
| 7. AUTHOR(S) Robert Koerner and Arthur Lord | | 8. PERFORMING ORGANIZATION REPORT NO. |
| 9. PERFORMING ORGANIZATION NAME AND ADDRESS Drexel University Philadelphia, PA 19104 | | 10. PROGRAM ELEMENT NO. CBR1DA |
| | | 11. CONTRACT/GRANT NO. R-80476301 |
| 12. SPONSORING AGENCY NAME AND ADDRESS Hazardous Waste Engineering Research Laboratory Office of Research and Development U.S. Environmental Protection Agency Cincinnati, OH 45268 | | 13. TYPE OF REPORT AND PERIOD COVERED Final 9/76-9/82 |
| | | 14. SPONSORING AGENCY CODE EPA/600/14 |
| 15. SUPPLEMENTARY NOTES Project Officer: John Brugger (201) 321-6634 | | |


16. ABSTRACT

Continuous-wave microwave (CW-μW) and pulsed radio-frequency (ground-penetrating radar, GPR) methods were developed and assessed for nondestructive monitoring of sub-surface environmental problems concerning hazardous material impoundments. The primary objective of the project was to conduct a technological assessment of these systems for identifying dike failure characteristics (seepage, soil stratigraphic discontinuity, voids, grouting breakthrough). These technologies were also evaluated for the detection of related subsurface objects such as waste drums.

The CW-μW method that was designed and constructed during the course of this project successfully located subsurface seepage layers and rock profiles. More subtle details such as soil stratigraphy or void detection were not successfully defined.

The GPR method was investigated by modifying a commercially available system for use on a number of problems. Buried metal drums were successfully located and soil stratigraphy was defined; however, equivocal results were obtained in locating polluted water or detecting of small voids. The technique was also used to evaluate the completeness of chemical grout curtains and warrants further investigation.

The CW-μW system should be commercialized, and the GPR system should include some type of signal enhancement capability. Signal enhancement is needed because the GPR system receives a large amount of subsurface information that is difficult to interpret visually.


| 17. KEY WORDS AND DOCUMENT ANALYSIS | | |
|---|---|---|
| a. DESCRIPTORS | b. IDENTIFIERS/OPEN ENDED TERMS | c. COSATI Field/Group |
| | | |
| 18. DISTRIBUTION STATEMENT RELEASE TO PUBLIC | 19. SECURITY CLASS (This Report) UNCLASSIFIED | 21. NO. OF PAGES 141 |
| | 20. SECURITY CLASS (This page) UNCLASSIFIED | 22. PRICE |

EPA Form 2220-1 (9-73)

NOTICE

This document has been reviewed in accordance with U.S. Environmental Protection Agency policy and approved for publication. Mention of trade names or commercial products does not constitute endorsement or recommendation for use.

## FOREWORD

The U.S. Environmental Protection Agency was created because of increasing public and government concern about the dangers of pollution to the health and welfare of the American people. Noxious air, foul water, and spoiled land are tragic testimonies to the deterioration of our natural environment. The complexity of that environment and the interplay of its components require a concentrated and integrated attack on the problem.

Research and development is that necessary first step in problem solution; it involves defining the problem, measuring its impact, and searching for solutions. The Hazardous Waste Engineering Research Laboratory develops new and improved technology and systems to prevent, treat, and manage wastewater and solid and hazardous waste pollutant discharges from municipal and community sources, to preserve and treat public drinking water supplies, and to minimize the adverse economic, social, health, and aesthetic effects of pollution. This publication is one of the products of that research and provides a most vital communications link between the researcher and the user community.

This report describes the development and application of a significant new technological approach for monitoring subsurface environmental problems involving hazardous materials. The technology developed in this report (i.e. continuous wave microwave and pulsed radio frequency methods) will be of use to those involved in the prevention and amelioration of hazardous waste spills and in hazardous waste site investigations. This report will be particularly useful to agencies, companies, and individuals involved in detecting seepage (groundwater, salt intrusion, hazardous waste) and for locating buried objects (containers, drums, and tanks).

David G. Stephan
Director
Hazardous Waste Engineering Research Laboratory

## ABSTRACT

Continuous-wave microwave (CW-μW) and pulsed radio-frequency (ground-penetrating radar, GPR) methods were developed and assessed for nondestructive monitoring of sub-surface environmental problems concerning hazardous material impoundments. The primary objective of the project was to conduct a technological assessment of these systems for identifying dike failure characteristics (seepage, soil stratigraphic discontinuity, voids, grouting breakthrough). These technologies were also evaluated for the detection of related subsurface objects such as waste drums.

The CW-μW method that was designed and constructed during the course of this project successfully located subsurface seepage layers and rock profiles. More subtle details such as soil stratigraphy or void detection were not successfully defined.

The GPR method was investigated by modifying a commercially available system for use on a number of problems. Buried metal drums were successfully located and soil stratigraphy was defined; however, equivocal results were obtained in locating polluted water or detecting of small voids. The technique was also used to evaluate the completeness of chemical grout curtains and warrants further investigation.

The CW-μW system should be commercialized, and the GPR system should include some type of signal enhancement capability. Signal enhancement is needed because the GPR system receives a large amount of subsurface information that is difficult to interpret visually.



This report was submitted in fulfillment of Grant No. R80476301 by Drexel University under the sponsorship of the U.S. Environmental Protection Agency. This report covers the period September 1976 to September 1982 and work was completed as of January 1984.

CONTENTS


Foreword . . . . . iii
Abstract . . . . . iv
Figures . . . . . vii
Tables . . . . . xi
Acknowledgments. . . . . xiii

1. Introduction. . . . . 1
2. Conclusions . . . . . 3
3. Recommendations . . . . . 4
4. Summary . . . . . 5
5. Overview . . . . . 8
   (a) Electromagnetic Methods. . . . . 8
   (b) Continuous-Wave Microwave Method . . . . . 8
   (c) Pulsed Radio-Frequency Method . . . . . 9
   (d) Report Format. . . . . 11
6. Electrical Properties in Soils. . . . . 12
   (a) Dielectric Constant ($\varepsilon_r$) . . . . . 12
   (b) Attenuation Coefficient ($\alpha$). . . . . 29
   (c) Penetration Depth (d). . . . . 40
7. Continuous-Wave Microwave Method. . . . . 43
   (a) Laboratory Tests . . . . . 43
      1. Water Location . . . . . 43
      2. Interface Detection. . . . . 51
      3. Void Detection . . . . . 60
   (b) Field Tests . . . . . 68
      1. Steel-Plate Detection. . . . . 68
      2. Water-Table Detection. . . . . 69
      3. Top of Rock Detection. . . . . 72
      4. Void Detection . . . . . 75
8. Pulsed Radio-Frequency Method . . . . . 78
   (a) Laboratory Tests . . . . . 78
      1. Sensitivity Study. . . . . 78
      2. Polluted-Water Detection . . . . . 84
      3. Small Void Detection . . . . . 87
   (b) Field Tests . . . . . 92
      1. Defining Water Table and Stratigraphy. . . . . 92
      2. Buried-Container Location. . . . . 100
      3. Void Detection . . . . . 113
      4. Chemical Grout Monitoring. . . . . 115

References . . . . . 121

CONTENTS (Continued)

Appendices

A. List of Technical Papers Generated During the Course of This Project . . . . . 124

B. List of (Masters) Theses Generated During the Course of This Project . . . . . 126

FIGURES


| Number | | Page |
|---|---|---|
| 1 | Photograph and Schematic Diagram of OWL-I . . . . . | 14 |
| 2 | Dielectric Constant Behavior of Atlantic City Beach Sand from OWL-I Probe . . . . . | 17 |
| 3 | Dielectric Constant Behavior of Delaware River Silt from OWL-I Probe . . . . . | 18 |
| 4 | Dielectric Constant Behavior of Kaolinite Clay from OWL-I Probe . . . . . | 19 |
| 5 | Effect of Moisture Content on Relative Dielectric Constant for Soils at Constant Density . . . . . | 21 |
| 6 | Relative Dielectric Constant for Atlantic City Beach Sand At Various Moisture Contents and for Water versus Temperature (Values in Parentheses Are for the Volumetric Water Content of the Soil Sample.). . . . . | 23 |
| 7 | Relative Dielectric Constant of Atlantic City Beach Sand At Various Volumetric Seawater Content (Data Taken At 22 C) . . . . . | 26 |
| 8 | Relative Dielectric Constant as a Function of Temperature for Atlantic City Beach Sand and for Seawater . . . . . | 27 |
| 9 | Photographs of OWL-II Setup with Associated Equipment for Monitoring Attenuation Coefficients ($\alpha$). . . . . | 30 |
| 10 | Smith Chart for OWL-II Results with Container Empty, i.e., Air. . . . . | 32 |
| 11 | Smith Chart for OWL-II Results with Container Filled with Dry Ottawa Sand. . . . . | 33 |
| 12 | Smith Chart for OWL-II Results with Container Filled with Ottawa Sand at 3% Water Content. . . . . | 34 |
| 13 | Attenuation Results for Atlantic City Beach Sand with Different Water Contents . . . . . | 37 |

FIGURES (Continued)


| Number | | Page |
|---|---|---|
| 14 | Attenuation Results for Delaware River Silt with Different Water Contents . . . . . | 38 |
| 15 | Attenuation Coefficients of Kaolinite Clay with Different Water Contents . . . . . | 39 |
| 16 | Ray Diagram for Penetration Depth Calculation . . . . . | 41 |
| 17 | Schematic Diagram of Variable Frequency Microwave System Used to Determine Depth to Water Surface. . . . . | 45 |
| 18 | Variation of Microwave Power Received as a Function of Various Depths to Water Surface Over a Frequency Sweep from 2.1 to 4.2 GHz. . . . . | 46 |
| 19 | Comparison of Calculated and Actual Depths to Water Surface for Frequency Sweep Tests Shown in Fig. 18 . . . . . | 48 |
| 20 | Signal Response for Buried Objects at Various Indicated Depths . . . . . | 50 |
| 21 | Seepage Box and Flow Channel. . . . . | 52 |
| 22 | Location of the Nine Microwave Stations . . . . . | 54 |
| 23 | Peak Amplitude Increase versus Interface Depth . . . . . | 55 |
| 24 | Soil Water Content Interface Test Results for Quartz Sand (Total Sand Depth 79 cm for All Tests). . . . . | 61 |
| 25 | Photographs of Continuous-Wave Microwave Experimental Test Setup Used to Detect Voids Under Paved Areas. . . . . | 63 |
| 26 | Schematic Diagrams of Single-Layer and Double-Layer Test Setups. . . . . | 64 |
| 27 | Seepage Study #1 at Bellmawr, New Jersey, . . . . . | 70 |
| 28 | Seepage Study #2 at Bellmawr, New Jersey, . . . . . | 71 |
| 29 | Seepage Study #3 at Bellmawr, New Jersey, . . . . . | 73 |
| 30 | Results of Microwave Survey at King of Prussia, Pennsylvania, Site . . . . . | 74 |

FIGURES (Continued)


| Number | | Page |
|---|---|---|
| 31 | Three Dimensional Plot of Area Surveyed Showing Ground Surface, Microwave Predicted Depth to Rock and Actual Probed Depth to Rock | 76 |
| 32 | Photograph and Schematic Diagrams of Ground-Probing Radar (GPR) Equipment and Test Setup | 82 |
| 33 | GPR Traces of Two Different Test Setups Showing the Differences that Density Variation Causes | 83 |
| 34 | GPR Traces of Well Graded Sand Varying Water Contents Using Fresh Water with Steel Plate Beneath Box | 85 |
| 35 | GPR Traces of Well Graded Sand at Varying Water Contents Using Salt Saturated Water with Steel Plate Beneath Box. | 86 |
| 36 | Pulse/Reflection Bands Showing Differences Between Fresh Water and Salt Water Tests at All Saturation States from Dry to Saturated. | 88 |
| 37 | GPR Traces of Uniform Well Graded Sand in Other Possible Situations | 89 |
| 38 | Two Types of Test Configurations Used in This Study to Detect the Presence and Location of Small Voids. | 91 |
| 39 | Photographs of Pulsed-RF Monitoring to Detect Water Table and/or Subsurface Stratigraphy | 93 |
| 40 | Pulsed-RF Survey of Wharton Site Made on April 3, 1981, with Actual Water Table Elevations Indicated by Horizontal Line in Circle | 97 |
| 41 | Pulsed-RF Survey of Springfield Site Made on April 3, 1981, with Actual Water Table Elevations Indicated by Horizontal Line in Circle. | 98 |
| 42 | Pulsed-RF Survey of Penrose Site Made on April 3, 1981, with Actual Water Table Elevations Indicated by Horizontal Line in Circle. | 99 |
| 43 | Plan of Buried Container Patterns at the Gibbsboro Site (Overall Site Dimensions Are Approximately 30 cm x 60 cm). | 102 |
| 44 | GPR Printout Showing Various Size Steel Drums with 1.1 m (3.5 ft) of Soil Cover | 104 |

FIGURES (Continued)


| Number | | Page |
|---|---|---|
| 45 | GPR Printout Showing Survey of 30-Gallon Steel Drums (Empty) at Various Depths . . . . . | 105 |
| 46 | GPR Printout Showing Survey of 40-Gallon Plastic Drums (Empty) at Various Depths All Drums Surveyed with 120 MHz Antenna; Burial Locations and Depths are the Same As in Figure 45 . . . . . | 106 |
| 47 | GPR Printout Showing Survey of 40-Gallon Plastic Drums Buried 0.6 m (2 ft) Beneath the Surface (120 MHz), where (a) Indicates the Saltwater Filled Drum and (b) Indicates the Fresh Water Filled Drum . . . . . | 107 |
| 48 | GPR Printout Showing Survey of 30-Gallon Steel Drums At Various Orientations Buried 1.0 m (3 ft) Beneath the Surface . . . . . | 109 |
| 49 | GPR Printout Showing Survey of Resolution Study of 55-Gallon Steel Drums, Buried 1.4 m (4.5 ft) Beneath the Surface . . . . . | 110 |
| 50 | GPR Printout Showing Two Surveys Over the Trash Dump. . . . . | 111 |
| 51 | GPR Printout Showing Spatial Sensitivity of the System (120 MHz Antenna). . . . . | 114 |
| 52 | GPR Printout Showing Survey of 40-Gallon Plastic Drums (Empty) at Various Depths, All Drums Surveyed with 120 MHz Antenna; Burial Locations and Depths are the Same As in Figure 45. . . . . | 116 |
| 53 | Insertion of Downhole Pulsed-RF Antennas to Monitor the Effectiveness of Chemical Grouting. . . . . | 117 |
| 54 | GPR Traces Between Boreholes 20 and 22 on Sixth Avenue in Front of the Oliver Building. . . . . | 119 |

TABLES


| Number | | Page |
|---|---|---|
| 1 | Summary of Continuous Wave Microwave Tests Conducted During This Project and an Assessment of Their Success via Their Stated Objective. . . . . | 6 |
| 2 | Summary of Pulsed Radio Frequency (Also Called Ground Penetrating Radar or GPR) Tests Conducted During This Project and an Assessment of Their Success via the Stated Objective. . . . . | 7 |
| 3 | Details of Continuous Wave Microwave Methods . . . . . | 9 |
| 4 | Details of Pulsed Radio Frequency Methods (Also Called Ground Probing Radar). . . . . | 10 |
| 5 | Some Pure "Dry" Salts Typically Found in Groundwater and Their Respective $\varepsilon_r$ . . . . . | 24 |
| 6 | Cations and Anions Present in Large Quantity in Sea Water Excluding Dissolved Gases . . . . . | 25 |
| 7 | Attenuation Coefficients Resulting for OWL-II Testing . . . . . | 35 |
| 8 | Calculated Penetration Depth for Various Soils at a Microwave Frequency ≈ 1 GHz . . . . . | 42 |
| 9 | Predicted versus Actual Depth to Water Surface . . . . . | 47 |
| 10 | Seepage Test Results . . . . . | 51 |
| 11 | Summary of Measurement Reproducibility Tests (A and C) and Density and Soil Interface Tests (B and D). Measurements for A, B, and C compared to the case with uniform quartz sand ($D_R$ = 70%) filling the soil box, Eccosorb betweem antennae, antennae on the soil surface. $D_R$ refers to relative density. Measurements for D are compared to case C.). . . . . | 59 |
| 12 | Results of Single Layer Tests on Calculated "n" Values Using Known Thickness of Upper Material . . . . . | 65 |

TABLES (Continued)


| Number | | Page |
|---|---|---|
| 13 | Results of Single Layer Tests on Calculated Thickness of Upper Material Based on n Value of Sand, Air, and Water, Respectively | 66 |
| 14 | Results of Double Layer Tests on Effect of Void Thickness On Signal Strength at Minimum Frequency | 68 |
| 15(a) | Electrical Parameters of Gray San Antonio Clay Loam, After Hipp (20) | 80 |
| 15(b) | Electrical Parameters of Goodrich Clay and Suffield Silty Clay, after Hoekstra and Delancy (21) | 80 |
| 15(c) | Electrical Parameters of Kaolin Clay, after Rosenfarb, et al. (22) | 81 |
| 16 | Calculated Powers of Reflection. | 81 |
| 17 | Summary of GPR Test Results Used to Detect Voids in Clayey Silt Soil. | 90 |
| 18 | Physical Properties of Soils Encountered at Various Test Sites | 94 |
| 19 | Summary of Results from All Drum Burial Patterns | 112 |

## ACKNOWLEDGMENTS

We would like to acknowledge the help and assistance of a number of individuals, companies, and municipalities that contributed in the performance of this project.

The bulk of the work was carrried out by a consecutive series of superb research assistants. These graduate students, all of whom performed at the masters degree level and wrote theses related to this project, were Thomas A. Okrasinski, Jonathan S. Reif, Michael J. Burlingame, William M. Dougherty and John J. Bowders, Jr. Laboratory assistance by Albert Bangs and Joseph Hughes was indispensible. Monthly progress reports (there were 69 in all) and this final report were expertly typed and often nicely edited by Elizabeth T. Fox.

The field work was usually accomplished by friends of the authors in the contracting business who cooperated with equipment, material, and labor in a most exemplary manner. They are the following:

- Contec Construction Company (formerly Rockland Construction Company) of North Wales, Pennsylvania, and, in particular, Francis A. Canuso III, Wallace A. Rutecki, and Anthony Guarino.
- Terrecon, Inc., of Gibbsboro, New Jersey, and, in particular, Steven R. Sahns and Bernard C. Sharp.
- Hayward Baker Company of Odenton, Maryland, and, in particular, Joseph P. Welsh and H. Wallace Baker.
- City of Reading, Pennsylvania, and, in particular, Joseph C. Mitchell.

Our sincere thanks to all.

Section 1

# INTRODUCTION

The investigation of subsurface phenomena (either buried beneath the ground surface or under water) can be approached in two very different ways. The first approach is the use of a suitable destructive test method. In this category are the following:

Test pits
Excavation trenches
Auger holes
Core borings
Observation wells

Though these methods do indeed permit the investigator to see the subsurface materials as they are excavated, such methods have drawbacks in identifying and monitoring many environmental problems. Some disadvantages of destructive test methods are the following:

- The information obtained is discontinuous over the area investigated.
- Permission to enter the properties in question (and excavate therein) may be hard to obtain or unobtainable.
- Access for excavation equipment may not be available at the site.
- Costs are generally high (e.g., small amounts of excavation can easily be $500/cu yd and boring costs of $20/ft are not uncommon).
- Danger is posed to personnel from containers of hazardous, toxic or radioactive materials that have been inadvertently ruptured or pierced by the excavations or borings.
- Danger is posed to the environment if such materials empty out of ruptured or pierced containers.

The second type of approach to identify and locate subsurface phenomena and buried containers is use of a suitable nondestructive testing (NDT) method. Within this category are the following techniques, which are grouped according to their basic operating principles. Most of these techniques eliminate the aforementioned disadvantages, but because of their recent development or uniqueness, they have not been widely used in shallow subsurface investigations.

- Thermally induced methods
  - Infrared
  - Heat pulse

- Elastic wave methods
  - Seismic refraction
  - Seismic reflection
  - Ultrasonics
  - Acoustic Emission
  - Sonar (active and passive)
- Nuclear methods
  - Neutron
- Electromagnetic methods
  - Resistivity
  - Very low frequency
  - Eddy current (metal detector)
  - Radio frequency (pulsed and continuous)
  - Microwave (pulsed and continuous)
  - Magnetometer
  - Penetrating radiation
- Optical

Some of the methods have background information available (e.g., the general area of geophysics, which includes seismic refraction and reflection, resistivity, and magnetometry), but others are quite recent in their development, (e.g., heat pulse, acoustic emission, and very low frequency). An individual report has recently been prepared on each of the above listed methods under separate U.S. Environmental Protection agency grants to the authors.[1])

This project dealt entirely with the development and deployment of electromagnetic methods, in particular the continuous-wave microwave (CW-μW) and pulsed radio-frequency (GPR) methods, which will be described in detail in this report. Emphasis was placed on both laboratory and field investigations using both techniques and including the following:

- CW-μW method
  - Laboratory tests
    - Water location
    - Interface detection
    - Void detection
  - Field tests
    - Steel-plate detection
    - Water-table detection
    - Top-of-rock detection
    - Void detection
- Pulsed radio-frequency (GPR) method
  - Laboratory tests
    - Sensitivity study
    - Polluted-water detection
    - Small-void detection
  - Field Tests
    - Defining water table and stratigraphy
    - Buried-container location
    - Void detection
    - Chemical grout monitoring

## Section 2

## CONCLUSIONS

Investigation of subsurface phenomena (e.g., location of buried drums, monitoring of seepage streams, etc.) can be achieved with techniques that require disturbances of the ground (borings, auger holes, test pits) or by nondestructive test (NDT) methods. This latter category is simpler, since no holes are created, no heavy equipment is involved, no cleanup is necessary, permission to do the survey may be easier to obtain, continuous profiles are obtained, and the cost is usually much lower than with destructive test methods. Of the variety of NDT methods that are available, electromagnetic wave concepts, (particularly those methods using the microwave frequency range) are very attractive. One reason these methods are attractive is that off-the-shelf equipment to generate the waves is readily available and inexpensive. In the course of this project, two methods were used-- CW-μW and GPR.

Continuous-wave microwaves were used in a system built by the authors during this contract. The system successfully located subsurface water zones and top-of-rock surfaces. Containers, voids, and soil stratigraphy were not easily located. To accomplish this, an electronics manufacturing firm will need to upgrade the present system. Indeed, such commercialization is the next step if this area is to be further developed.

The GPR method is a useful tool for environmental monitoring purposes, but [redacted]ve limitations, as noted here. The highlight of the laboratory and testing work performed using the GPR system was its use in chemical grout monitoring. Here, two adjacent boreholes are entered with transmitting and receiving antennas to obtain travel time printouts. Comparing traces before and after grouting allows instantaneous assessment of the completeness and uniformity of the grouting operation. As the contractor returns to an unsatisfactory area, the GPR system can again be used for actual control of the field operation. Obviously, a very significant feature of the equipment is the real-time printout of the subsurface detail to the limit of the penetrability of the signals. The system was successful in detecting a cylindrical drum buried at a shallow depth in dry sand. However, the system often records too much information, making interpretation difficult. At times, the background is overwhelming and completely obscures the desired trace. For a solution to this problem, signal enhancement techniques are definitely needed. Two approaches are possible: computer-aided systems and empirical comparisons. Both approaches should be pursued to develop GPR systems further.

## Section 3

## RECOMMENDATIONS

Additional investigation is warranted and recommended in numerous areas. Rather than contrasting CW-μW to GPR, each technique will be discussed separately. The reason for this lack of head-to-head comparison is that one system is in the development stage (CW-μW), whereas the other (GPR) is a commercially available item.

Development of a CW-μW system definitely lies with an electronics equipment manufacturer. The current system (individual components patched together and placed in a garden cart) requires a microcomputer to count wave cycles displayed on an oscilloscope and calculate depths to the reflecting anomalies. A real-time printout could easily be developed. This would provide continuous operation and greatly upgrade the system. In addition, the current power pack is a not-so-mobile electric generator. A built-in, 110-Volt electrical system would aid in moving rapidly over the ground surface. In general, the entire system needs streamlining.

The point just described was precisely where the GPR method was at the beginning of this project. Thus, a system was purchased, modified as required, and deployed in a number of rather challenging laboratory and field tests. Upon viewing the results, we feel that signal enhancement methods are required to aid in the interpretation of the return signals for heterogeneous soil conditions. Since this is usually the situation, such methods should be part of GPR systems. (Note that one manufacturer has recently included an option of a signal-enhanced real-time printout, but at a cost increase from $45,000 to $80,000.) Whether these signal-enhanced methods are computer-based or empirical is not so much the consideration. It is more important that a major, directed effort be made.

One particularly fruitful area for GPR monitorig, which was initiated during this project, is monitoring chemical grout curtain walls. In comparisons before grouting and after grouting, GPR traces provided a real-time printout of the completeness and possibly the integrity and stability of the grout between the monitoring locations. Better constructed, waterproof borehole antennas are needed for further investigation in this important area.

## Section 4

## SUMMARY

Of the wide variety of possible nondestructive testing (NDT) techniques and, in particular, those based on electromagnetic concepts, systems employing microwaves seem very promising. Toward assessing their applicability in problems of environmental concern, two specific techniques were investigated in this project: continuous-wave microwave (CW-μW) and pulsed radio-frequency, also called ground-penetrating radar, or simply, GPR.

The first system, CW-μW, was designed and manufactured by the authors under the auspices of this project. The system sweeps through a range of frequencies, displays alternating constructive and destructive interference peaks, and by counting these peaks and knowing their frequencies, obtains a depth to the interface. As described in the report, the "interface" seen is actually a material with different dielectric properties from the one above it. Such properties as dielectric constant ($\varepsilon_r$), attenuation coefficient ($\alpha$), and penetration depth (d) are of critical concern and are treated in Section 6. To evaluate the adequacy of the continuous-wave microwave system, a series of laboratory and field experiments was conducted. Table 1 lists these tests and a qualitative assessment of the results. The technique does show promise in a number of areas. Basically, the technique works best when the differences between the dielectric properties of the soil and the anomaly are the greatest. In this regard, dry soil to saturated soil or soil to rock boundaries can be distinguished, but the boundary between two different soil types cannot be easily identified.

Several GPR commercial systems are available. Thus, a system was purchased and modified for our specific site situations. These included rough terrain (where new and modified transceiver carriages were constructed) and downhole boring monitoring (where two narrow torpedo antennas, a transmitter, and a receiver were constructed). GPR systems are basically electromagnetic reflection systems in which a short pulse is transmitted into the ground, reflects off an anomaly, and returns to the ground surface. Travel time is measured, and if the propagation speed of the electromagnetic waves in the soil is known, a depth can be obtained. The system produces a continuous printout as the transceiver antenna is moved across the ground surface. The stronger the dielectric difference between the soil and the anomaly, the stronger will be the return signal and the sharper will be the recorder trace. These systems are extremely sensitive to all subsurface anomalies, and a tremendous amount of information is always received. Thus the systems must be properly tuned and visually interpreted.

TABLE 1. Continuous-Wave Microwave Tests Conducted During This Project and an Assessment of Their Success

| Test No. | Objective | Result | Comments |
|---|---|---|---|
| Lab. 1 | water location | excellent | -depth ranged from 0 to 50 cm<br>-spatial location very good<br>-requires sharp boundary |
| Lab. 2 | interface detection | poor | -frequency peaks not distinguishable<br>-requires soil layers to have different moisture contents<br>-amplitude distinction possible but difficult |
| Lab. 3 | void detection | doubtful | -frequency peaks not sharp enough<br>-amplitude distinction possible<br>-needs good area to contrast against void area for relative assessment |
| Field 1 | steel plate detection | possible | -depends on nature of backfill soil; dry granular good, wet cohesive poor |
| Field 2 | water table detection | good | -limited to 60 cm depth<br>-must be sharp and distinct |
| Field 3 | top-of-rock detection | good | -rock probed to 4 m with good correlation to predicted values |
| Field 4 | void detection | possible | -thorough tunnel survey conducted but no "ground truth" determined |

To evaluate the adequacy of the GPR system, a series of laboratory and field experiments was conducted. Table 2 lists these tests and a qualitative assessment of the results. A casual review of the table makes it appear as though the technique is not effective. Note, however, that the tests conducted were quite challenging, and most have never been attempted previously. Those tests in which a sharp dielectric difference occurred between upper and lower materials gave better results than tests in which small differences occurred. Therefore, buried containers were easily detected, but polluted water and small voids in dry soils were not as easily defined.

TABLE 2. Summary of Pulsed Radio-Frequency (Also Called Ground Penetrating Radar or GPR) Tests Conducted During This Project and an Assessment of Their Success

| Test No. | Objective | Result | Comments |
|---|---|---|---|
| Lab. 1 | sensitivity study | -- | -dielectric constant difference less than one results in a detectable signal |
| Lab. 2 | polluted water detection | poor | -salt saturation was difficult to quantify<br>-salt boundary not observable<br>-acetone was not responsive |
| Lab. 3 | small void detection | possible | -steel pipe easily detected<br>-smooth hole reasonable<br>-roughened hole marginal |
| Field 1(a) | defining water table | possible | -good in granular soil<br>-no good in fine-grained soil |
| Field 1(b) | defining soil stratigraphy | good | -soils in different categories (sands, silts, clays) are distinguishable<br>-vertical boundaries are detectable |
| Field 2 | buried container location | excellent<br>poor | -metal drums in granular soil<br>-metal drums in fine-grained soil |
| Field 3 | void detection | poor | -insufficient dielectric contrast unless void is water filled |
| Field 4 | chemical grout monitoring | possible | -qualitative tool at present<br>-perhaps quantifiable<br>-tremendous potential if additional work is successful |

## Section 5

## OVERVIEW

This section is presented to preview electromagnetic wave concepts in a unified manner and then to treat specifically the two techniques developed or used in this project. These techniques are the CW-μW and GPR methods.

### (a) Electromagnetic Methods

Electromagnetic (EM) wave methods to determine the location and extent of subsurface anomalies, such as water or seepage plumes, buried pipes or containers, and subsurface voids, are currently undergoing active development and hold much promise as valuable nondestructive testing methods. In each of the various EM methods, an electromagnetic wave is intentionally beamed by a transmitting antenna into the ground or water surface. The wave travels essentially unaltered through the material until it encounters an object or area with different electrical properties. Examples of such discontinuities are changes in soil strata or water content, metal or plastic objects of numerous types, or voids within the mass or in partially filled containers. The incident wave is then partly reflected and the reflected wave travels upward to the receiving antenna located at the ground surface. The amplitude of the reflected wave or the strength of the interference pattern between ground reflection and object reflection is the information used for the subsurface profiling. (The VLF and optical methods to be described use different principles.) The methods can be categorized on the basis of the frequency of the waves, namely:

- resistivity - essentially dc
- very low frequency - 10 Hz to 20 Hz
- eddy current (metal detector) - about 1 kHz
- radio frequency - 1 MHz to 600 MHz
- microwave - 0.2 GHz to 8 GHz
- magnetometer - about 10 GHz
- optical - about $10^{15}$ Hz
- penetrating radiation - about $10^{18}$ Hz

### (b) Continuous-Wave Microwave Method

The difficulty of obtaining very near surface information from some of the above EM methods suggests the use of generating and directing continuous waves into the material being investigated. Since frequencies of about 1 GHz are used, the method can appropriately be called a continuous wave microwave method, or "CW microwaves." As with other EM methods, the waves are reflected by a material with different electrical properties, e.g., a drum filled with

air or liquid, and, when received back at the surface, form an interference pattern consisting of alternating constructive and destructive peaks. From theoretical analyses the following equation for depth to the reflecting interface (2) comes about:

$$d = \frac{c}{2n}\left[1 - \frac{1}{n^2}\cos^2\Theta\right]^{-1/2}\left[\frac{x}{f_2 - f_1}\right] \qquad (1)$$

in which d = distance to reflecting surface; c = speed of light; n = index of refraction of the material ($=\sqrt{\varepsilon_r}$); $\varepsilon_r$ = relative dielectric constant; $\Theta$ = angle of incidence; x = number of peaks separating $f_1$ and $f_2$ (plus 1); $f_1$ = arbitrarily chosen initial frequency peak; and $f_2$ = arbitrarily chosen final frequency peak.

The strength of the interference is presented as a function of lateral position of the antennas to map out subsurface details. Some systems of this type are in an advanced research stage and should be available shortly; see Table 3. This is the case with the system developed under this particular contract (3).

TABLE 3. Details of Continuous-Wave Microwave Methods

| Investigators | Approximate frequency range in gigahertz | Maximum depth in meters | Major application area |
|---|---|---|---|
| Okrasinski, et al. (3) | 0.5-4 | 4 | Determining water table, buried metal objects, cavities |
| Unterberger (4) | 4.3 | 150 | Salt thickness measurement |
| Holser, et al. (5) | 4.3 | 150 | Salt thickness measurement |
| Lundien (6) | 0.5-8.0 | 3 | Defining subsurface layers |
| Ellerbruch and Adams (7) | 0.5-4 | 3 | Determining coal layer thickness |

(c) Pulsed Radio-Frequency Method

The bulk of subsurface probing at shallow depths has been based on transmitting pulsed radio-frequency waves in the frequency range from about 1 MHz to 200 MHz. The method is also called ground-probing radar, ground-piercing radar, or simply GPR. The transmitted pulse travels through the surface material until it encounters an object or material with dissimilar electrical characteristics. Part of it is then reflected back to the surface where it is received, and the time of travel is measured. The depth "d" to the interface is calculated from $d = (vt)/2$, in which v = the wave speed (which is equal to $c/\sqrt{\varepsilon_r}$, in which c = the speed of light and $\varepsilon_r$ = the relative dielectric constant of the material in which the wave is propagating), and t = the pulse travel time. As shown in Table 4,

this technique has been evaluated by many workers, and some commercially available systems are available.

For the purposes addressed in this project, however, the pulsed radio-frequency method has a basic drawback in that it cannot be used at very shallow depths. The high amplitude transmitted pulses swamp the receiver via direct transmission across the surface. This is sometimes called the "main bang effect" and is a function of the pulse frequency. The receiver cannot record reflected information until the transmitted pulse amplitude falls significantly. An approximate calculation of the depth associated with this amplitude decrease is

$$d = \frac{(y)(c)}{(n)(f)} \qquad (2)$$

in which d = depth from surface where no information is received; y = number of high amplitude cycles transmitted; c = speed of electromagnetic waves in air ($\approx 3 \times 10^8$ m/s); n = index of refraction of the material ($\approx \sqrt{\epsilon_r}$, the relative dielectric constant); and f = frequency of transmitted pulses, e.g., if y = 1.5, n = 4, f = 200 MHz ($0.2 \times 10^9$ Hz), and then d = 0.55 m. Thus it is seen that this limitation is so severe that it completely negates the use of the method in certain situations.

TABLE 4. Details of Pulsed Radio-Frequency Methods (Also Called Ground-Probing Radar)

| Investigators | Approximate frequency range in megahertz | Maximum depth in meters | Major application area |
|---|---|---|---|
| Cook (8,9) | 1-100 | 225 | Locating faults, walls, holes |
| Rosetta (10) | 100-200 | 15 | Locating faults, caverns, water utilities |
| Morey (11) | 100-200 | 15 | Locating faults, caverns, utilities |
| Dolphin, et al. (12) | 15-50 | 40 | Locating rock cavities |
| Unterberger (13) | 230 | 500 | Salt thickness measurement |
| Harrison (14) | 35 | 2,000 | Determining ice thickness |
| Rubin, et al. (15) | 100-200 | 10 | Detecting tunnels |
| Rubin and Fowler (16) | 100-200 | 15 | Drilling guidance, tunnel monitoring, coal thickness |
| Benson and Glaccum (17, 18) | 100-200 | 10 | General subsurface probing, locate and follow pollutants in ground, detection of buried containers of industrial wastes |
| Sandness, et al. (19) | 100-200 | 10 | General subsurface probing as described in Refs. (17, 18) |

(d) Report Format

With this background information in mind, the importance of defining and determining the basic electrical properties of soil is obvious. The most relevant properties are the dielectric constant ($\varepsilon_r$), the attenuation coefficient ($\alpha$) and the penetration depth (d) at the frequency involved. These three parameters are discussed in Section 6 of this report.

Following Section 6 are chapters on the two methods used in this project, namely continuous-wave microwave (Section 7) and pulsed radio-frequency (Section 8). Each contains laboratory and field sections. These two chapters represent the major effort in this project. They form the basis of the summary (Section 2), conclusions (Section 3) and recommendations (Section 4) portions that have been presented in the beginning of this report.

## Section 6

## ELECTRICAL PROPERTIES IN SOILS

The propagation of electromagnetic waves in a medium such as soil depends on two constants: the dielectric constant and the complex permeability. Since most soils are only weakly magnetic, only the complex dielectric constant need be evaluated for a given soil. It must, however, be evaluated for a wide range of conditions, such as the density, water content, soil type, etc.

### (a) Dielectric Constant ($\varepsilon_r$)

The literature reviewed suggested many methods for determining dielectric constant. These include active radar, interferometry, and capacitance analysis. In choosing a particular method for determining the complex dielectric constant of a material, the following criteria can govern the final choice of a method:

- type and nature of materials to be tested
- particular environmental conditions to which the test materials will be subjected
- interest in a specific frequency range
- degree of accuracy for dielectric properties required
- ease of mathematical computation
- convenience of method
- equipment needs of method
- portability of method

The method we selected uses a five wire, fixed-center-tap transmission line device. The device, shown in Figure 1, was initially used by Lundien (6) of the U.S. Army Engineer Waterways Experiment Station to study curing of concrete samples. Lundien named the device an "open wire line" probe or OWL-I probe.

Briefly, the OWL-I probe: (1) is capable of accurately determining a material's complex dielectric constant, (2) is adaptable to a host of environmental conditions, (3) can be easily modified for a particular frequency range under consideration, (4) uses minimal equipment, (5) and is portable and relatively easy to operate.

In operation, the soil is placed around the OWL-I probe with only the connectors exposed. The volume of the soil must be large enough that, when more soil is added, no effect is noted in the measurements. The soil in which the probe is placed must be homogeneous relative to the wavelength

of the electromagnetic waves used. For measurements in a liquid, there is no problem, but for emplacement in soil samples, a reasonable amount of care must be taken to compact the sample uniformly around the wires of the probe.

The OWL-I probe was constructed as shown in the schematic diagram and photograph of Figure 1. The center wire was attached to a coaxial connector on the front plate and was shorted to the grounded outer four wires by the back plate. The front and back plates of the OWL-I probe were cut from copper sheets. All coaxial connectors were silver soldered to the copper sheets. Since the outcome of the results obtained for the sample materials will be primarily used for studying microwave techniques in determining depth to a water table, a system designed to work at L-band frequencies (0.39 GHz to 1.55 GHz) was constructed to measure dielectric constants for various soil materials.

The accompanying test equipment for the OWL-I probe is also shown in Figure 1. The fifth wire or center wire is connected to a Hewlett-Packard model 8620C sweep oscillator capable of covering a frequency range of 0.01 GHz to 2.4 GHz with a leveled power output of 0 to 13 dbm. The center-tapped probe is coaxially connected to a Hewlett-Packard model 423A crystal detector. The detector, which provides a D.C. voltage output proportional to the square of the amplitude of the RF input, is connected to a HewlettPackard model 415E standing-wave meter.

The use of the OWL-I probe is based on standing-wave techniques. Essentially, a nulling procedure is used in the following manner. The frequency of the oscillator is varied over its range of 0.01 GHz to 2.4 GHz and the minimum readings, or voltage, nulls on the standing wave meter connected to the center tap through the crystal detector are noted. These nulls occur whenever there is a minimum in the standing wave on the transmission line. As the frequency is varied, the minimum moves along the line until it coincides with the position of the center tapped probe. If the transmission line is shorted as with the OWL-I probe, then voltage nulls occur at the shorted end and at half wavelength intervals away from the short. The wavelength in the material being tested can be written as:

$$\lambda = L/N \tag{3}$$

where $\lambda$ = wavelength in the dielectric material
$L$ = OWL-I probe length
$N$ = number of half wavelengths between the short and the tap or the number of full wavelengths on the probe.

Then, at the L-band frequencies for the center tapped OWL-I probe, the refractive index (n) is given by:

$$n = \lambda_0/\lambda = \lambda_0 N/L \tag{4}$$

where $\lambda_0$ is the wavelength of the microwaves in a vacuum,

Reproduced from
best available copy.

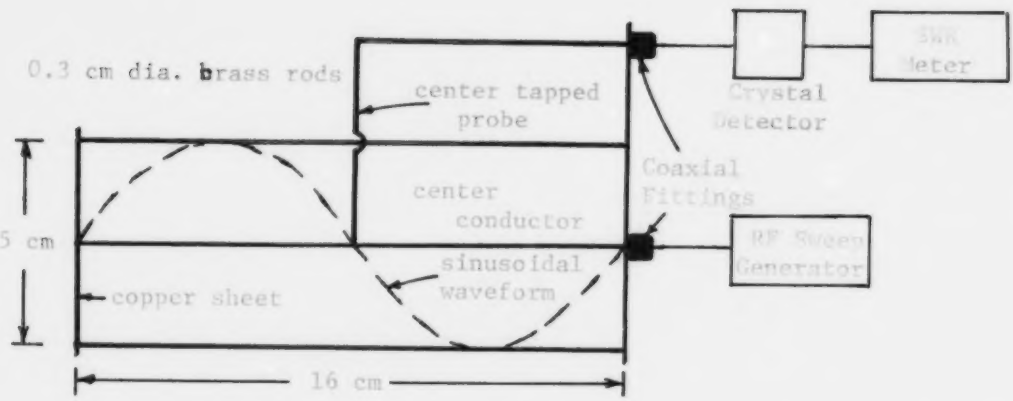


Figure 1. Photograph and schematic diagram of OWL-I.

or in terms of frequencies:

$$n = f_o \, N/f_n \qquad (5)$$

Where $f_o$ = frequency at which one wave length in a vacuum equals the length of the probe, in Hz
$f_n$ = frequency at which one null is found on the OWL-I, in Hz.

The equation for the dielectric value can be written as:

$$\varepsilon = \varepsilon'(1 - i \tan \delta) \qquad (6)$$

The largest values encountered for tan $\delta$, a measure of the dielectric absorption, in this study were less than 0.1, so the tan $\delta$ value is neglected here.

$$\varepsilon \simeq \varepsilon' \qquad (7)$$

and since by definition

$$(n)^2 = \varepsilon \qquad (8)$$

then $$\varepsilon' \simeq (n)^2 \qquad (9)$$

where $\varepsilon'$ = the relative dielectric constant.

It should be pointed out at this time that equation (7) is intended for solid particles in a pure dipolar liquid such as water and that not all solid particle/liquid mediums will yield results in accordance with equation (9), i.e., tan $\delta \neq 0$.

Since sands, silts, and clays form the basic categories of soils, a typical soil for each type was selected for study. Results could then be compared as to the change in relative dielectric constant as the moisture content is slowly increased and the density altered. The specific soils selected were an Atlantic City beach sand, a Delaware River clayey silt, and a commercial variety of Kaolinite clay.

A plastic test tank measuring 24-cm long by 29-cm high by 10.7-cm wide was used to contain the soil samples and the OWL-I probe. The weights of the tank and OWL-I probe were recorded and, then, for each soil type, the following procedure was utilized.

The tank was partially filled with the dry sample soil. Then the OWL-I probe was placed in the tank with the bottom plate resting on the bottom layer of soil. Additional soil was carefully added until the OWL-I probe was completely embedded, and the tank was topped off with the sample soil. The weight was recorded for this entire assembly, and then the coaxial cables were connected to the OWL-I probe. The nulling frequency was found by methods previously described.

The tank was struck from the bottom several times so as to increase

uniformly the density of the soil in the tank. Additional soil was added to assure complete covering of the OWL-I probe and to top off the tank again. The tank assembly was reweighed and the subsequent nulling frequency was found for the new soil density. The soil was then carefully removed along with the probe and distilled water was mixed with the soil. The moist soil along with the probe was placed in the tank again as in the previous test. The testing cycle was repeated as previously stated for the soil at the new water content for at least two different densities. Water content was increased for each soil test sequence until the soil was saturated or the water gradient point, i.e., the point at which soil moisture will not remain homoneneously mixed in the soil medium and will begin to separate gravitiationally was reached.

Using equation (5) to determine n, the refractive index of the material, and substituting the design values for the OWL-I probe presented earlier yields:

$$n = f_o N/f_n = 2x10^9(1)/f_n = 2x10^9/f_n \qquad (10)$$

So the relative dielectric constant of the material is:

$$\varepsilon' = 4x10^{18}/f_n^{\ 2} \qquad (11)$$

Utilizing equations (10) and (11), the data for the beach sand at different moisture contents and densities is shown in Figure 2. Figure 3 shows the graphed data for the second soil tested, the clayey silt, at different moisture contents and densities.

The third and final soil tested in the sequence using the OWL-I was a commercially processed Kaolinite clay. The clay was tested dry and then at varying moisture contents including complete saturation. Figure 4 summarizes the data collected from these tests.

Comparing the data for the three soils tested, the following can be concluded:

1) The open-wire-line (OWL-I) probe is capable of detecting minute changes in relative dielectric constant due to soil density and soil moisture content.

2) Relative dielectric constant values obtained for the three soil samples indicate a behavior following the Beer-Lambert absorption law for electromagnetic energy, namely, the value of the dielectric constant is strongly dependent upon the concentration of dipolar liquid homogeneously dispersed throughout the medium under test.

This last remark can be illustrated by plotting the data for the three soils on a graph where soil moisture in terms of degree of soil saturation (S) times soil porosity (p) is plotted versus relative dielectric constant. This new moisture parameter (S times p) is not a function of soil density,

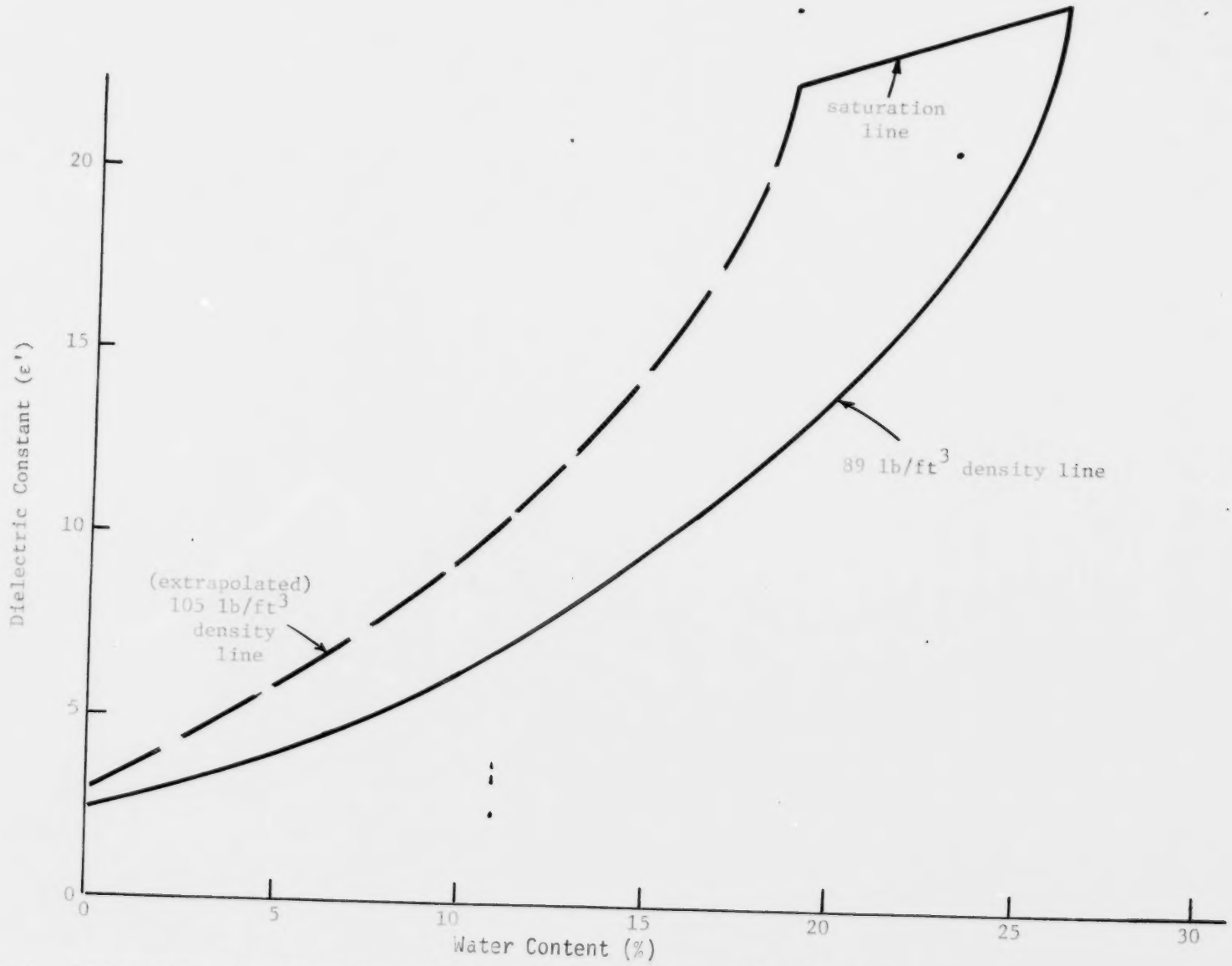


Figure 2. Dielectric constant behavior of Atlantic City beach sand from OWL-1 probe.

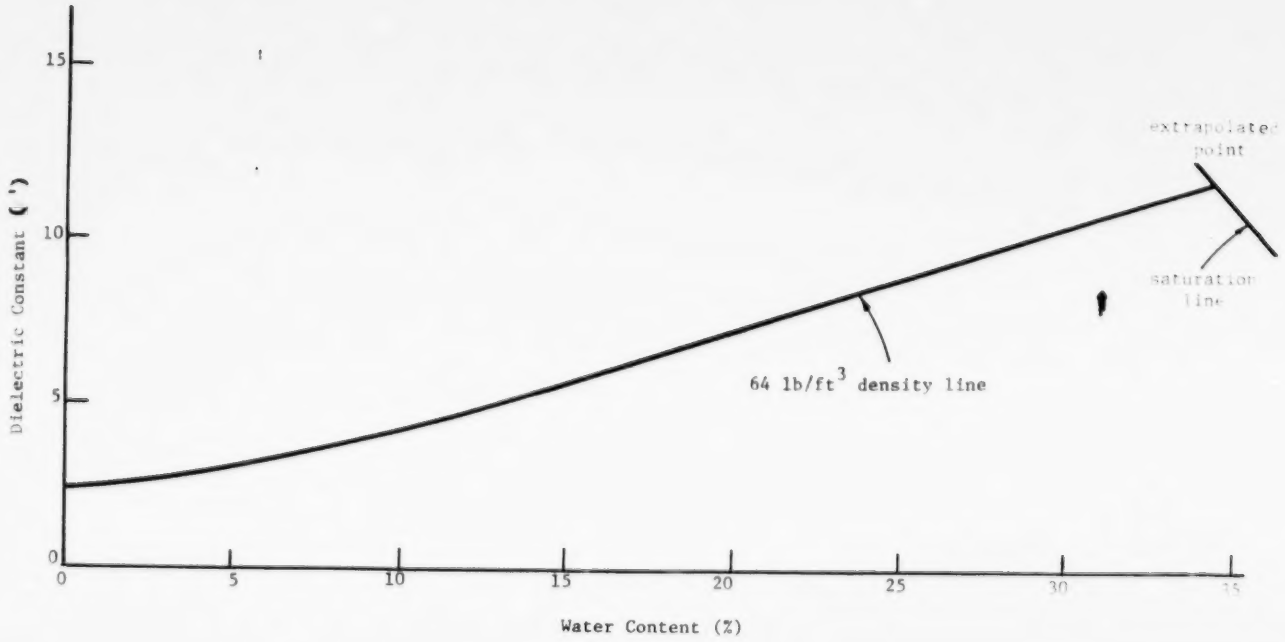


Figure 3. Dielectric constant behavior of Delaware River silt from OWL-I probe.

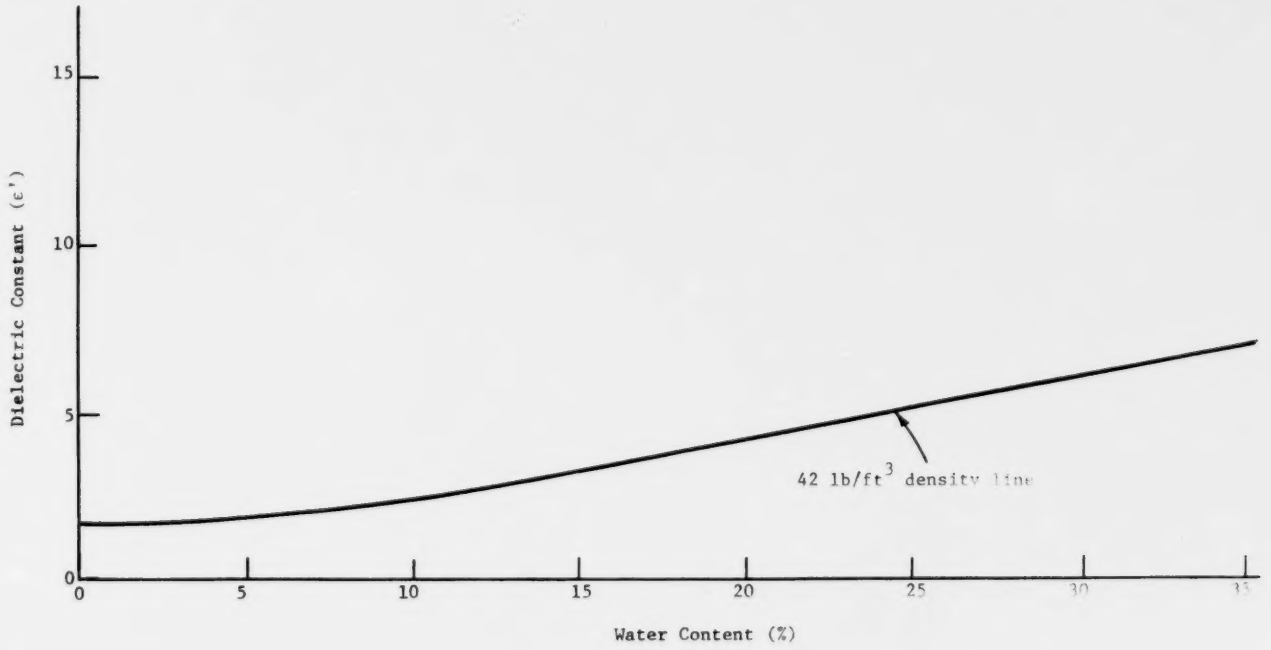


Figure 4. Dielectric constant behavior of Kaolinite clay from OWL-I probe.

and thus shows dielectric changes for varying water contents in soils on a much simpler level, see Figure 5.

Two additional parameters that affect soil dielectric values under field conditions are temperature and electrolyte concentration in the soil moisture. In the modern theory of dielectrics, prediction models must be made at the molecular level. One must picture each molecule as containing elastically bound electrons, ions, and a rigid or semirigid permanent electrical dipole. The presence of these dipoles allows molecular polarization effects when in an alternating electromagnetic field. For dry soils, as was shown previously, few or no permanent electric dipoles exist and relative dielectric constants are consequently of low order (2 to 4). Water, on the other hand, has a high permanent electric dipole count with resonance at 22 GHz. Thus water, at L-band frequencies (0.39 GHz to 1.55 GHz), exhibits a high relative dielectric constant (approximately 80).

As for the permanent dipole, it is sensitive to the temperature of the dielectric material as well as the frequency and, to a lesser extent, the magnitude of the applied field. The effect of a temperature increase is to alter the state of equilibrium and cause the electrical properties to change in an orderly direction. For example, the relative dielectric constant of water shows a decrease with increasing temperature at L-band frequencies. The opposite effect, an increase in the relative dielectric constant with increasing temperature, is exhibited by other materials, for example, ethylene glycol. According to the National Bureau of Standards, water has a relative dielectric constant that is affected by temperature according to the following linear relationship:

$$\varepsilon_r = 79.4\ (1-4.63\ \tau) \qquad (12)$$

where $\tau = (t-25)/1000$
$t$ = temperature, C

Previous data indicate that water is the predominant factor in controlling relative dielectric constant in a soil-water mixture under the Beer-Lambert relationship. Experiments were therefore carried out on dry soil as well as partially and completely saturated soil to see if water produced the majority of the relative dielectric constant change with temperature and if the Beer-Lambert relationship governed in soil-water mixtures for relative dielectric constant changes with temperature, the latter being a linear relationship with increasing water content.

The experiments were conducted in an environmentally controlled room with provisions for temperature control ranging from -25°C to +30°C. Atlantic City beach sand was chosen as the test soil. Soil samples were prepared in the plastic container with the OWL-I probe as previously described. Test monitoring equipment was kept outside the environmental room so temperature effects on the equipment would not complicate or modify the results in any way.

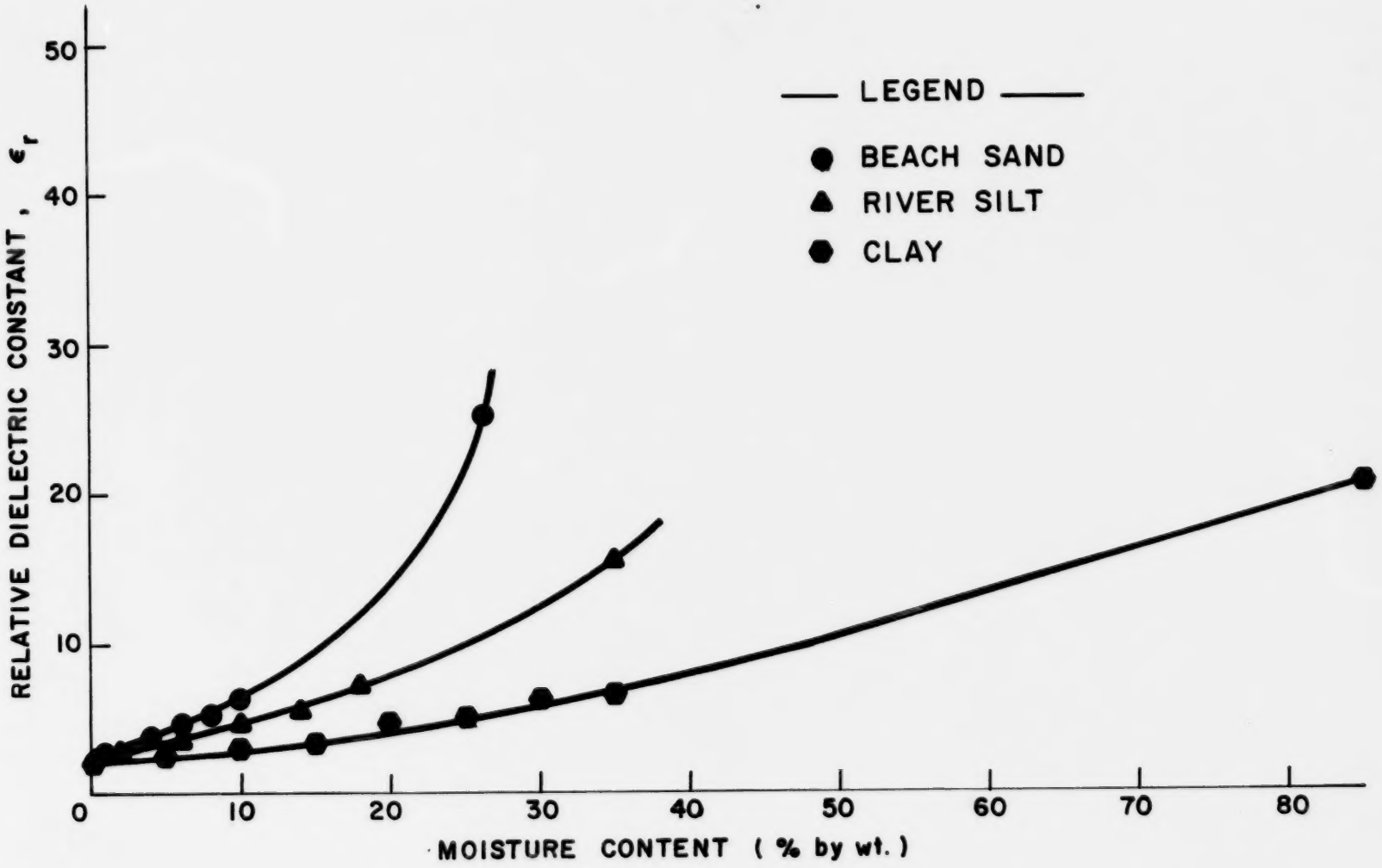


Figure 5. Effect of moisture content on relative dielectric constant for soils at constant density.

In all, six tests were run over a temperature range of 0 C to 25 C. The initial test was on dry beach sand, and four tests were run on sand-water mixtures of 3%, 7%, 10% and 40% moisture content. The sixth test was run with distilled water for comparison with the predicted value from equation (12) for water. Test results had to be corrected for the decrease in length of the OWL-I probe due to temperature effects. Densities in all sand-water tests were kept fairly close together. A plot of the temperature versus relative dielectric constant for the six tests is shown in Figure 6.

Figure 6 indicates that dry sand exhibits a very slight relative dielectric constant decrease as the temperature increases ($\Delta\varepsilon_r = -1.04 \times 10^{-3}$/C rise), and that as the water content increases so does $\Delta\varepsilon_r$ increase. This linear relationship is thus following the Beer-Lambert law for microwave absorption in heterogeneous mixture. The results with distilled water compare very closely with the relative dielectric constant estimated for pure water from equation (12).

The liquid phase of a unit volume of soil is primarily composed of water. Water finds its way into a soil either by percolation of rainwater from the ground surface or by infiltration of groundwater from stored water deposits. Seawater and the processes of percolation, infiltration and capillary action add soluble salts to groundwater in varying amounts. Chemically speaking, soluble salts dissociate in water into cations and anions, forming electrolyte solutions. Table 5 lists some salts typically found in groundwater with their respective relative dielectric constant for the salt in its pure "dry" state.

More recently, a large portion of the soluble salts found in groundwater has been introduced by man. They include pesticides, fertilizers, and sanitary leachates. Levels of these soluble salts vary from area to area and day to day. Soluble salts are more prevalent in desert areas, where groundwater evaporation exceeds percolation, and in large cities, where industry and large populations abound.

Soluble salts ionizing in groundwater will adversely affect the relative dielectric constant of soils saturated or partially saturated with these electrolyte solutions. This is due to the adsorption of these ions into the Gouy-Chapman electric diffuse double layer, which surrounds the soil particles when in a saturated or partially saturated state. Sands and gravels usually have the least electric charge on the particle surface, while clays, being colloids, have strong surface charges. Generally, the surface charge is negative and, when pure water alone surrounds the particle, the positive ends of the dipolar water molecules line up and face the negative particle surface. This electrically-attracted water is called adsorbed water and makes up the electric diffuse double layer.

With the presence of ions from soluble salts in water, the electric diffuse double layer becomes filled with the positive ions or cations, which are attracted to the negatively charged particle surface. These cations now displace adsorbed water, because the cation has a higher electron charge than a water molecule. With the presence of the cations in the diffuse double layer, the relative dielectric constant is no longer solely governed

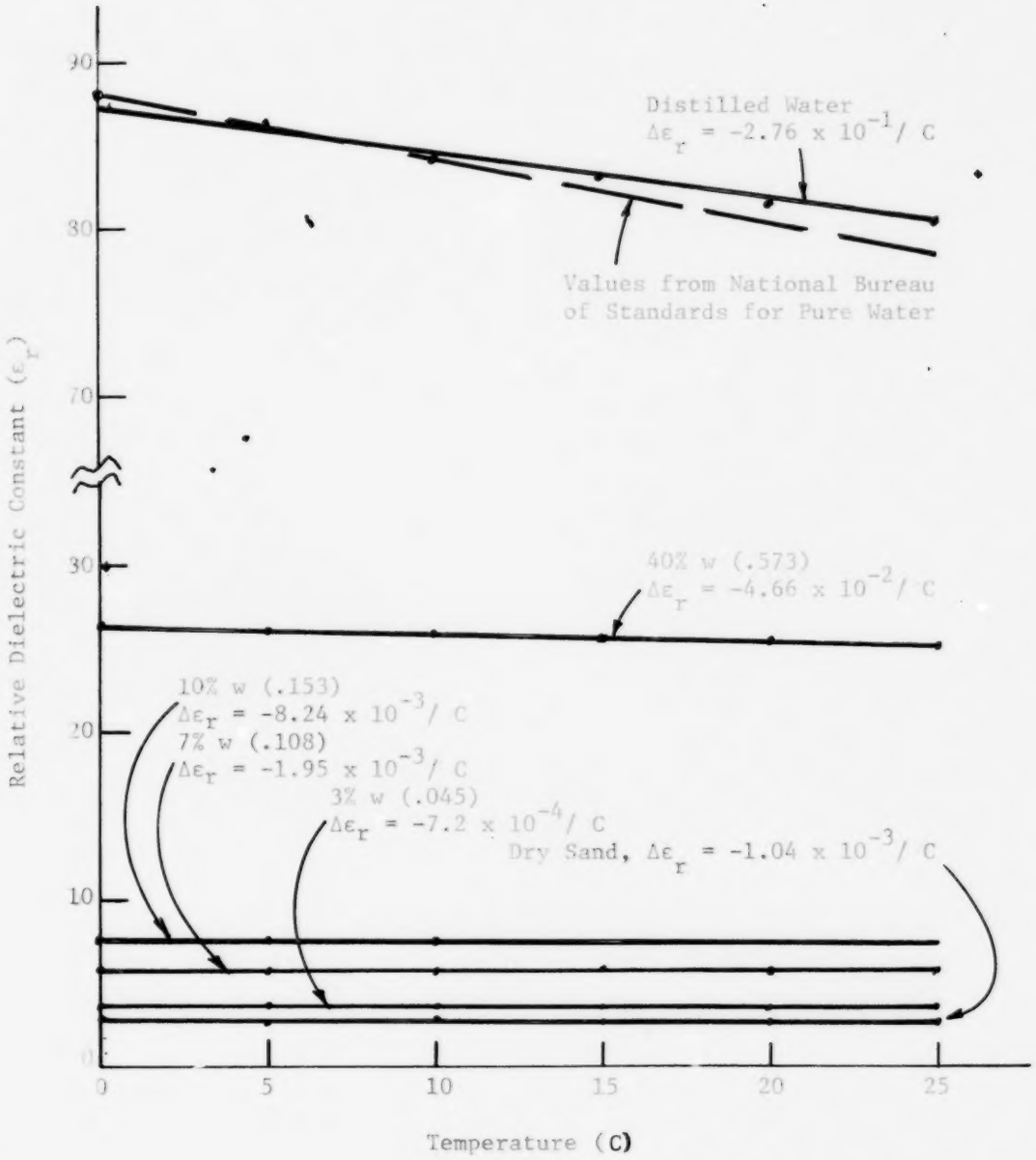


Figure 6. Relative dielectric constant for Atlantic City beach sand at various moisture contents and for water versus temperature. (Values in parentheses are for the volumetric water content of the soil sample.)

TABLE 5. Some Pure "Dry" Salts Typically Found in Groundwater and Their Respective $\varepsilon_r$

| Salt | Formula | Frequency (hertz) | Relative Dielectric Constant* ($\varepsilon_r$) |
|---|---|---|---|
| Ammonium Chloride | $NH_4Cl$ | $10^6$ | 7.0 |
| Calcium Carbonate | $CaCO_3$ | $10^6$ | 6.14 |
| Calcium Fluoride | $CaF_2$ | $10^4$ | 7.36 |
| Calcium Sulfate | $CaSO_4 \cdot 2H_2O$ | $10^4$ | 5.66 |
| Potassium Nitrate | $KNO_3$ | $6 \times 10^7$ | 5.0 |
| Sodium Carbonate | $Na_2CO_3 \cdot 10H_2O$ | $6 \times 10^7$ | 5.3 |
| Sodium Chloride | NaCl | $10^4$ | 6.12 |
| Sodium Nitrate | $NaNO_3$ | ----- | 5.2 |
| Potassium Carbonate | $K_2CO_3$ | $10^8$ | 5.6 (15 C) |
| Potassium Chloride | KCl | $10^4$ | 5.03 |
| Potassium Aluminum Sulfate | $KAl(SO_4)_2 \cdot 12H_2O$ | $10^6$ | 3.8 |

by the dipole polarization effects of the water molecules. These ion-bound particles suspended in water now act as a complex heterogeneous dielectric material to microwaves at L-band frequencies. The relative dielectric constant now becomes a factor of frequency and changes as the frequency changes. Thus, the specific value of $\varepsilon_r$ obtained for a soil/elecrolyte mixture is valid for only that particular frequency at which it was measured. Consequently, swept frequency measurements of the OWL-I probe in such mixtures will yield a series of nulls, since $\varepsilon_r$ is changing with frequency.

To observe these effects, it was decided to measure the relative dielectric constant of Atlantic City beach sand at varying levels of saturation with the saturating medium being seawater collected off Atlantic City, New Jersey. Seawater is a rather complex electrolyte composed of many cations and anions of soluble salts dissolved in water. Table 6 lists the most abundant of these ions in seawater with their average concentrations. Seawater was chosen, despite its complexity in composition, because seawater comprises the largest stored water deposit, namely the oceans, and is consequently a major "contaminant" to groundwater in many areas of the world.

TABLE 6. Cations and Anions Present in Large Quantity in Sea Water, Excluding Dissolved Gases

| Cation or Anion | Concentration (grams/metric ton) |
|---|---|
| $Cl^-$ | 18,980 |
| $Na^+$ | 10,561 |
| $Mg^{++}$ | 1,272 |
| $S^{--}$ (as sulfides) | 884 |
| $Ca^{++}$ | 400 |
| $K^+$ | 380 |
| $Br^-$ (as bromides) | 65 |
| $CO_3$ | 28 |
| $Sr^{++}$ | 13 |
| $B^{---}$ (as borides and borates) | 4.6 |
| $Al^{+++}$ | 1.9 |

These initial tests using seawater were prepared in the same manner as the soil samples were prepared for varying levels of saturation in the previous testing. Samples at each moisture content were prepared at two different densities. Samples were prepared at the following moisture contents: 1%, 5%, 8.8%, 10%, and 26%. In addition, a sample was tested in which pure seawater was the sole dielectric medium. Due to the presence of high signal attenuation by the seawater, a DC amplifier with 40 dB gain was used to increase the signal output from the crystal detector.

On samples where $\varepsilon_r$ remained constant over L-band frequencies, their respective dielectric constants were further measured as a function of temperature. The temperature range used was from 0 C to 25 C and the identical test procedures as outlined previously were used to prepare these test samples.

The results of these tests are shown in Figures 7 and 8. Figure 7 shows the relative dielectric constant as a function of volumetric seawater content in samples of Atlantic City beach sand. Figure 8 shows the relative dielectric constant as a function of temperature for Atlantic City beach sand saturated with seawater and for pure seawater.

Below a volumetric seawater content of 0.065, some constant values of $\varepsilon_r$ were obtained for an L-band frequency sweep, but some smaller nulls were present in the sweep that did not fully produce a zero voltage output. Furthermore, some of these nulls were not found at frequencies coinciding with harmonic frequencies. This latter effect marks the beginning of the "discontinuous" zone.

In continuing this phase of the project, emphasis was placed on the effect of adding small amounts of salts to distilled water to note its effect of $\varepsilon_r$ and then focused on attenuation measurements. It was shown how electrolyte solutions such as seawater alter the relative dielectric

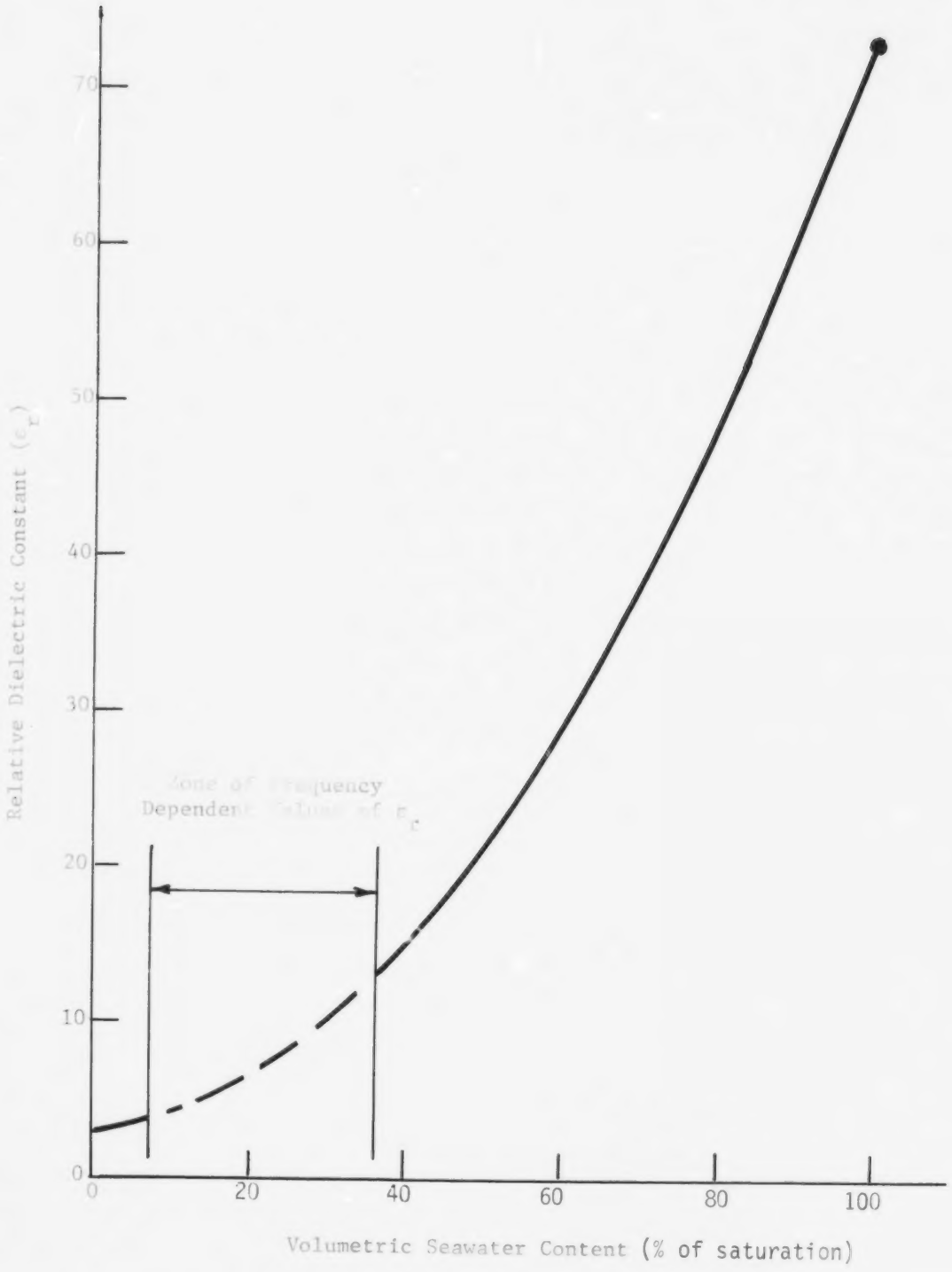


Figure 7. Relative dielectric constant of Atlantic City beach sand at various volumetric seawater contents. (Data taken at 22 C.)

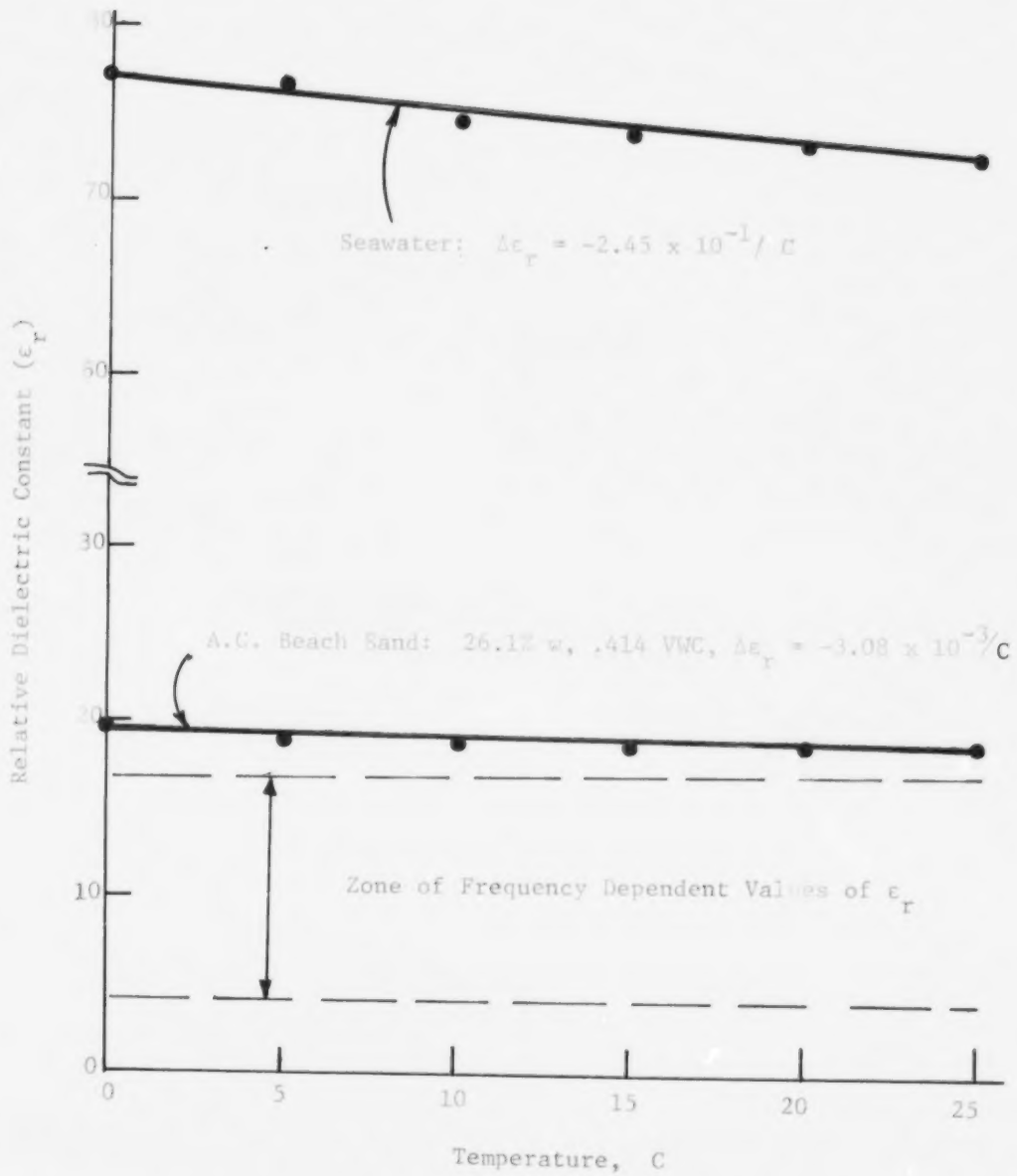


Figure 8. Relative dielectric constant as a function of temperature for Atlantic City beach sand and for seawater.

constant of soils prepared with such mixtures. Stated mathematically, the relative dielectric constant for soils wetted with electrolyte solutions can be expressed as:

$$\varepsilon_r = n^2 - K^2 \tag{13}$$

where $\varepsilon_r$ = relative dielectric constant
n = index of refraction for microwaves in the wetted soil
K = extinction coefficient, a value dependent on the dielectric medium (i.e., electrolyte type), and the frequency.

Attenuation of the microwave signal increases in electrolyte-wetted soils. This can be expressed mathematically as:

$$\varepsilon' = 2nK \tag{14}$$

where $\varepsilon'$ = imaginary part of the dielectric constant.

Dry soils and soils wetted with distilled water have an extinction coefficient that is extremely small, rendering equations (13) and (14) as:

$$\varepsilon_r \simeq n^2 \tag{15}$$

$$\varepsilon' \simeq 0 \tag{16}$$

Furthermore, these values in equations (15) and (16) are nearly constant over the L-band frequency range. Incidentally, since:

$$\varepsilon_r^* = \varepsilon_r - i\varepsilon' \tag{17}$$

where $\varepsilon_r^*$ = complex relative dielectric constant

and $$n^* = n - iK \tag{18}$$

where $n^*$ = complex index of refraction

then $$\varepsilon_r^* = (n^*)^2 \tag{19}$$

Equation (19) is the classical relation between electrical and optical properties of a dielectric in an electromagnetic field.

To observe this expected microwave attenuation of electrolyte solutions, it was decided to examine qualitatively the attenuation of microwaves for samples of pure water with the addition of small amounts of pure salts. Three salts were chosen that differed from each other by a change in cation or anion type. This was done to determine the attenuation of an L-band frequency-range microwave signal by a certain cation-anion combination. The salts selected were sodium chloride (NaCl), potassium chloride (KCl), and sodium bicarbonate ($NaHCO_3$). Molar concentrations of 1/500, 1/250, 1/125, 1/50, and 1/25 were prepared for each salt. All tests were conducted at 22 C using OWL-I and its system components as outlined in previous progress reports.

From the results, it was evident that solutions of potassium chloride (KCl) attenuate microwave signals much more than do sodium chloride (NaCl) and sodium bicarbonate ($NaHCO_3$) solutions at the same molarities. The fact that only small concentrations of a particular salt do produce a moderate decrease in signal strength indicates that electrolytes in water have high values of conductivity as compared with distilled water.

Since OWL-I could only be used here as a qualitative tool in measuring attenuation, then a different device had to be constructed to measure quantitatively microwave attenuations, a value having as much importance as relative dielectric constant itself. This new device, a modified version of OWL-I, is called OWL-II and is described in the next section.

(b) Attenuation Coefficient ($\alpha$)

By a suitable modification to the OWL-I probe, i.e., removing the center tap, and incorporating a standing-wave-ratio (SWR) meter into the circuit, attenuation coefficients of the soil can be measured. See the photographs of Figure 9 for the OWL-II.

For a line of loss d (in nepers per meters) and length $\ell$ (meters), and a short-circuited termination, the reflected voltage wave $V_{ref}$ will be related to the incident voltage wave $V_{inc}$, at the lossy line input terminals by the following equation.

$$|V_{ref}| = |V_{inc}|e^{-2\alpha\ell} \tag{20}$$

In the above equation $2\ell$ is the distance out and back on the OWL-II probe.

Furthermore, use of the relationships:

$$r = \left|\frac{V_{ref}(\ell)}{V_{inc}(\ell)}\right| \tag{21}$$

where r = reflection coefficient, and

$$VSWR = \frac{1 + r}{1 - r}$$

will result in the following relationship:

$$VSWR = \frac{1 + e^{-2\alpha\ell}}{1 - e^{-2\alpha\ell}} \tag{22}$$

Solving equation (22) for $\alpha\ell$, we arrive at:

$$\alpha\ell = 1.1513 \log_{10}\left(\frac{VSWR + 1}{VSWR - 1}\right) \tag{23}$$

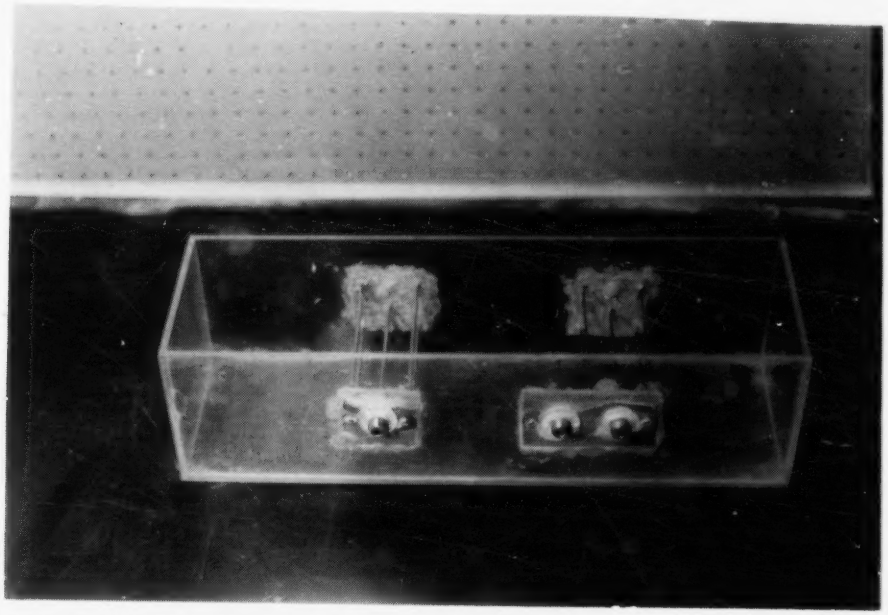

Figure 9. Photographs of OWL-II setup with associated equipment for monitoring attenuation coefficients ($\alpha$).

or

$$\alpha = \frac{1.1513}{\ell} \log_{10} \left( \frac{VSWR + 1}{VSWR - 1} \right) \qquad (24)$$

Thus, by measuring the VSWR and knowing the length $\ell$, the attenuation coefficient ($\alpha$) can be determined.

Preliminary tests were conducted with the OWL-II system on Ottawa sand with different water contents. The basic test procedure began by placing Ottawa sand with a known water content into the plexiglass container (see Figure 9). The density was kept approximately the same for all tests. The VSWR was then measured utilizing the equipment setup previously described and shown in Figure 9. Both the VSWR and the distance of the probe on the slotted-line carriage away from the medium were noted. The type N coaxial connector on the OWL-II probe was then terminated, and the change of position of the probe on the carriage to obtain a new minimum on the VSWR meter was obtained.

Thus, the VSWR and the shift of the probe, given in number of wavelengths either toward or away from the generator are known for a frequency. This information yields one point on a Smith Chart. By varying the frequency, a number of points can be obtained and hence a characteristic curve of the particular material under set conditions can be drawn. These curves are shown in Figures 10, 11 and 12. The curve obtained from each test as plotted on the Smith Chart should be a spiral. A circle would indicate no attenuation of the signal. The tighter the spiraling and the smaller the loops, the greater is the attenuation. Also the frequencies should increase as the spiral proceeds inward.

Tests were conducted first with the box empty (Figure 10), then with dry Ottawa sand (Figure 11), and then with Ottawa sand with 3% water content (Figure 12). The frequencies ranged from one to two GHz. Several trends can be observed from these results that lead to the indication that the system is working properly. The spirals get smaller as the medium changes from air to dry Ottawa sand, then to Ottawa sand with 3% water content. This indicates increased attenuation. The results of the test with the empty box show a curve that is nearly circular. This indicates very little attenuation which would be expected of air. Also, in all cases increasing frequencies follow the inward spiral.

The main points of interest on the Smith Chart for obtaining attenuation values are the points at which the curve crosses the horizontal axis, which represent zero reactance. For each 360° rotation two points can be obtained along the axis. The small value occurrs when the length of the OWL-II probe is a multiple of a half wavelength, and the larger value occurrs when the probe length is an odd multiple of a quarter wave length.

The impedance of a shorted half-wave transmission line is:

$$Z_1 = Z_0 \tanh \alpha\ell \qquad (25)$$

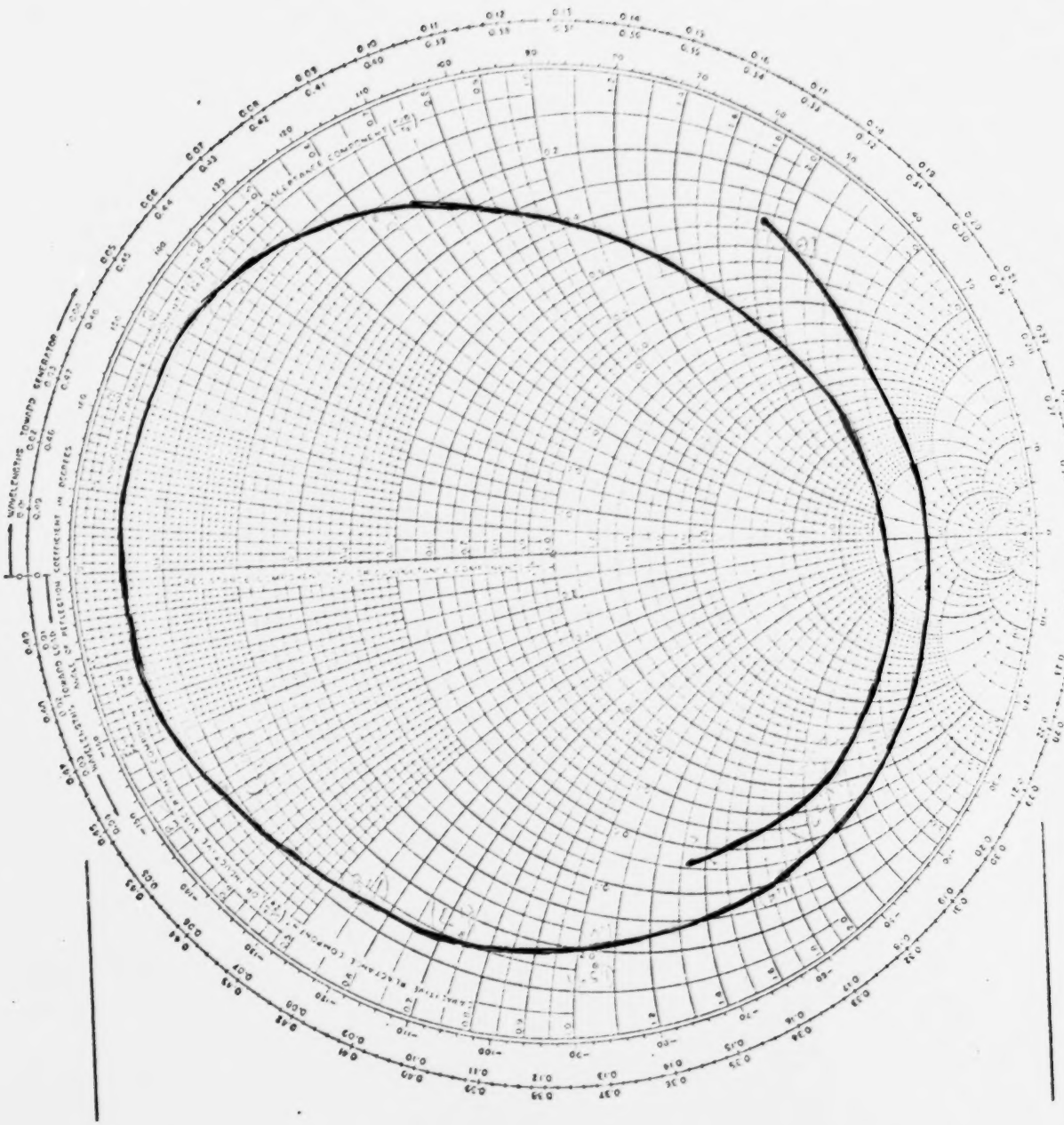

Reproduced from best available copy.

Figure 10. Smith Chart for OWL-II results with container empty, i.e., air.

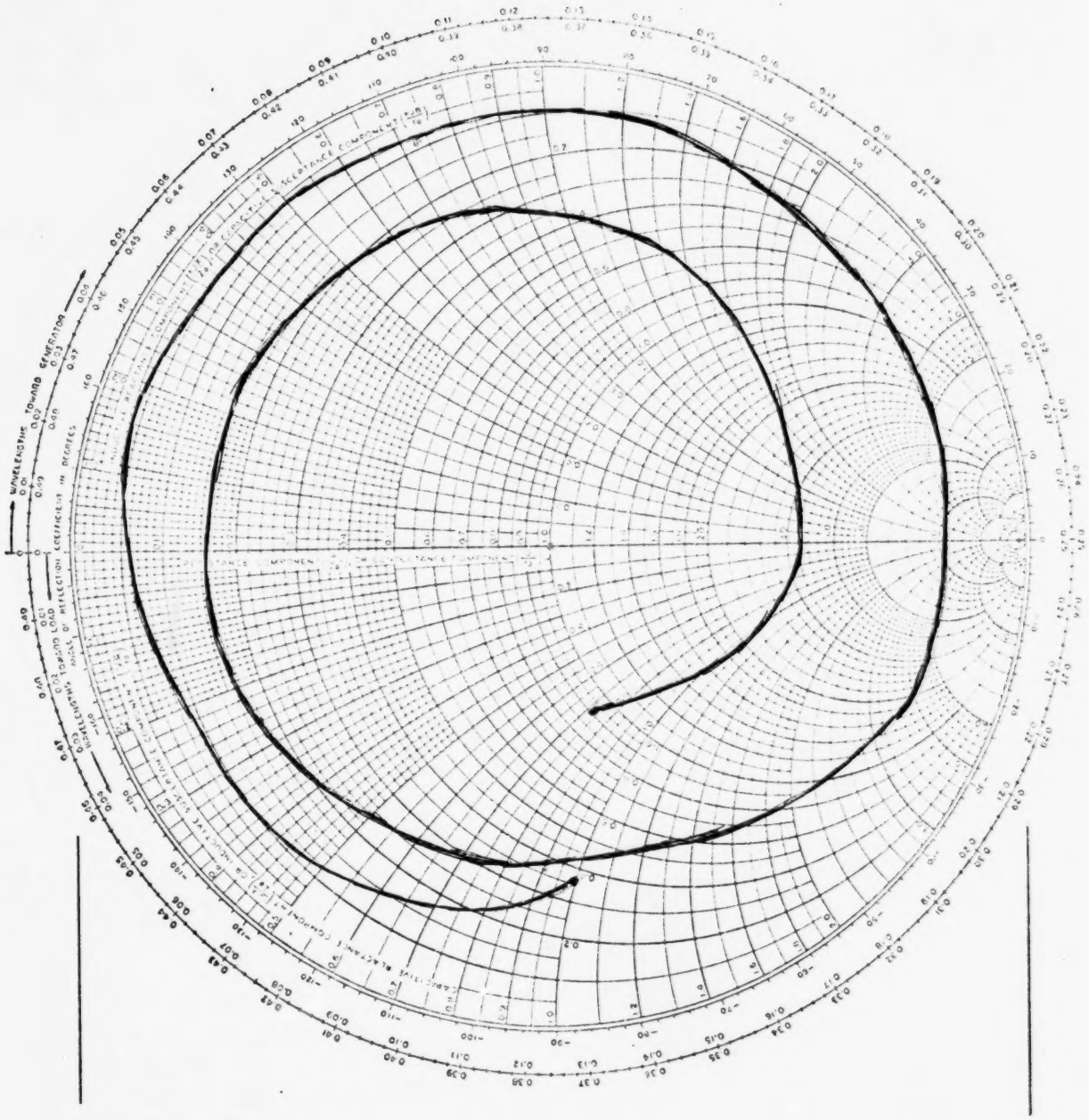

Figure 11. Smith Chart for OWL-II results with container filled with dry Ottawa sand.

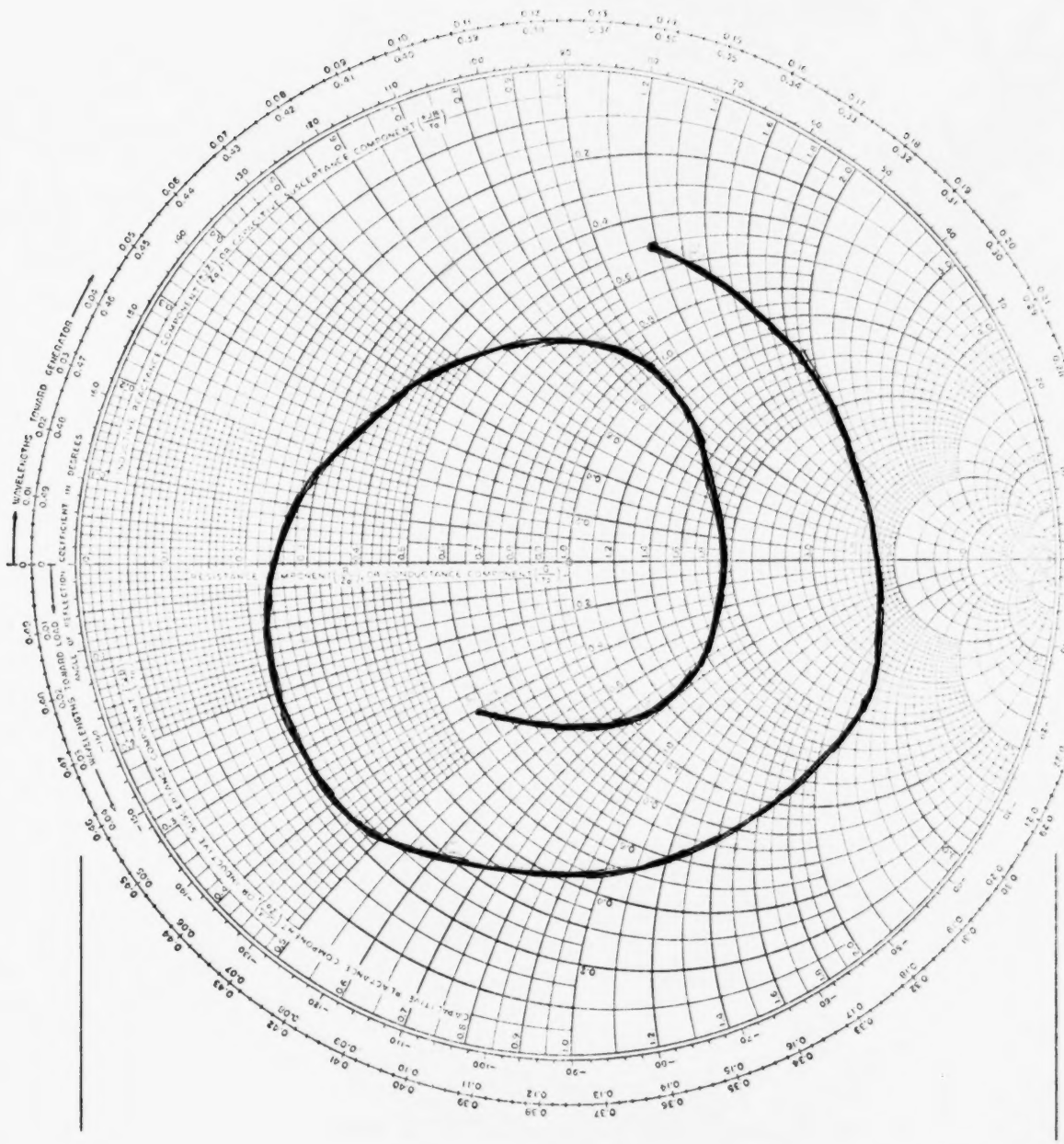

Reproduced from best available copy.

Figure 12. Smith Chart for OWL-II results with container filled with Ottawa sand at 3% water content.

Likewise for a shorted quarter-wave transmission line:

$$Z_2 = Z_0 \coth \alpha \ell \tag{26}$$

From these two equations, a solution for the attenuation coefficient can be obtained as follows:

$$\alpha = \frac{1}{\ell} \tanh^{-1} \sqrt{\frac{Z_1}{Z_2}} \tag{27}$$

where $Z_1$ = impedance of shorted half-wave transmission line, ohms
$Z_2$ = impedance of shorted quarter-wave transmission line, ohms
$Z_0$ = characteristic impedance for line, ohms
$\alpha$ = attenuation coefficient, $m^{-1}$
$\ell$ = transmission line length, m

The attenuation as a function of frequency can be obtained using this method, and a single value appears to work over a range of about 0.15 GHz. Table 7 gives the attenuation coefficients for the preliminary tests on Ottawa sand.

TABLE 7. Attenuation Coefficients Resulting for OWL-II Testing

| Conditions | Frequency Range GHz | Attenuation Coefficient ($\alpha$ in nepers/meter) |
|---|---|---|
| Empty Box | 1.15 - 1.95 | 0.52 |
| Dry Ottawa Sand | 1.83 - 2.00 | 1.47 |
| | 1.38 - 2.22 | 0.52 |
| 3% Water Content Ottawa Sand | 1.22 - 1.60 | 1.56 |
| | 1.60 - 1.78 | 2.22 |

The three basic soil types treated previously were next evaluated to determine their attenuation coefficients. Atlantic City beach sand was tested dry and then at moisture contents from 1% to 15% to determine the attenuation coefficient at each level. The density was also varied at each moisture level to determine its effect on the coefficient. The OWL-II setup was also tested empty to determine if there was any inherent attenuation within the system. The attenuation coefficient obtained for the empty box was 0.12 nepers/meter. This is well below any values obtained for the Atlantic City beach sand, especially when one considers the high frequency range, 1.45-2.10 GHz, where this occurs. For each moisture content and density there is usually more than one coefficient obtained. This is due to the fact that the attenuation coefficient varies with frequency as previously discussed. The results indicate that increasing

attenuation occurs with increasing moisture content and density. The changes in moisture content appear to produce more significant changes in the attenuation than the changes in density.

The attenuation coefficients for two specific frequencies as a function of volumetric water content are given in Figure 13. The volumetric water content is used to account for both moisture and density effects. It is equal to the porosity of the sample times the percent saturation. The attenuation coefficients for the frequencies of 1.30 GHz and 2.10 GHz were interpolated from the results.

As expected, increased water content causes increased attenuation. The two curves are very similar, with the higher frequency curve shifted upward, with the exception of the last point. This point represents the 10% moisture-content test. Very high attenuation values were obtained for this test, with large changes in the coefficient with increasing frequency.

The results for the second soil tested, the Delaware River clayey silt, are given in Figure 14. The soil was tested dry and then at moisture levels from 1% to 16%. Trends similar to those observed for Atlantic City beach sand were obtained. The attenuation increases with increasing moisture content and frequency. The coefficients appear to be slightly higher than those observed for the sand. Samples tested at higher water contents appeared to attenuate the signal completely due to complete saturation of the soil.

Figure 14 shows that the two curves are very similar. The figure also indicates as stated previously that the attenuation increases with increasing frequency and volumetric water content. A comparison of these results and the results presented for Atlantic City beach sand indicates very similar trends. The shapes of the curves are almost identical for the corresponding frequencies. As expected, however, the curves for Delaware River clayey silt are shifted upward compared to the ones for the beach sand indicating increased attenuation.

Kaolinite clay, the third and final soil to be tested, was tested at different densities and with water contents of 0%, 2%, 5%, and 10%. The attenuation coefficients are given in Figure 15. As with the other soils tested, the attenuation increases with increasing water content and frequency. Once again, the increase of attenuation with increasing water content appears to be greater than the increase due to all other factors.

A comparison of these results with the results from the other soils reveals lower attenuation values for Kaolinite clay than for beach sand or clayey silt under like conditions. This result can be attributed to the effects of bound water. Due to the nature of clay particles, water can be visualized as water molecules that are relatively free to move in two directions parallel to the clay particle surface but are restricted in their movement perpendicular to or away from the surface. This is similar to the behavior of ice in which the movement of water molecules is restricted in all three directions. The relative dielectric constant is lowered from

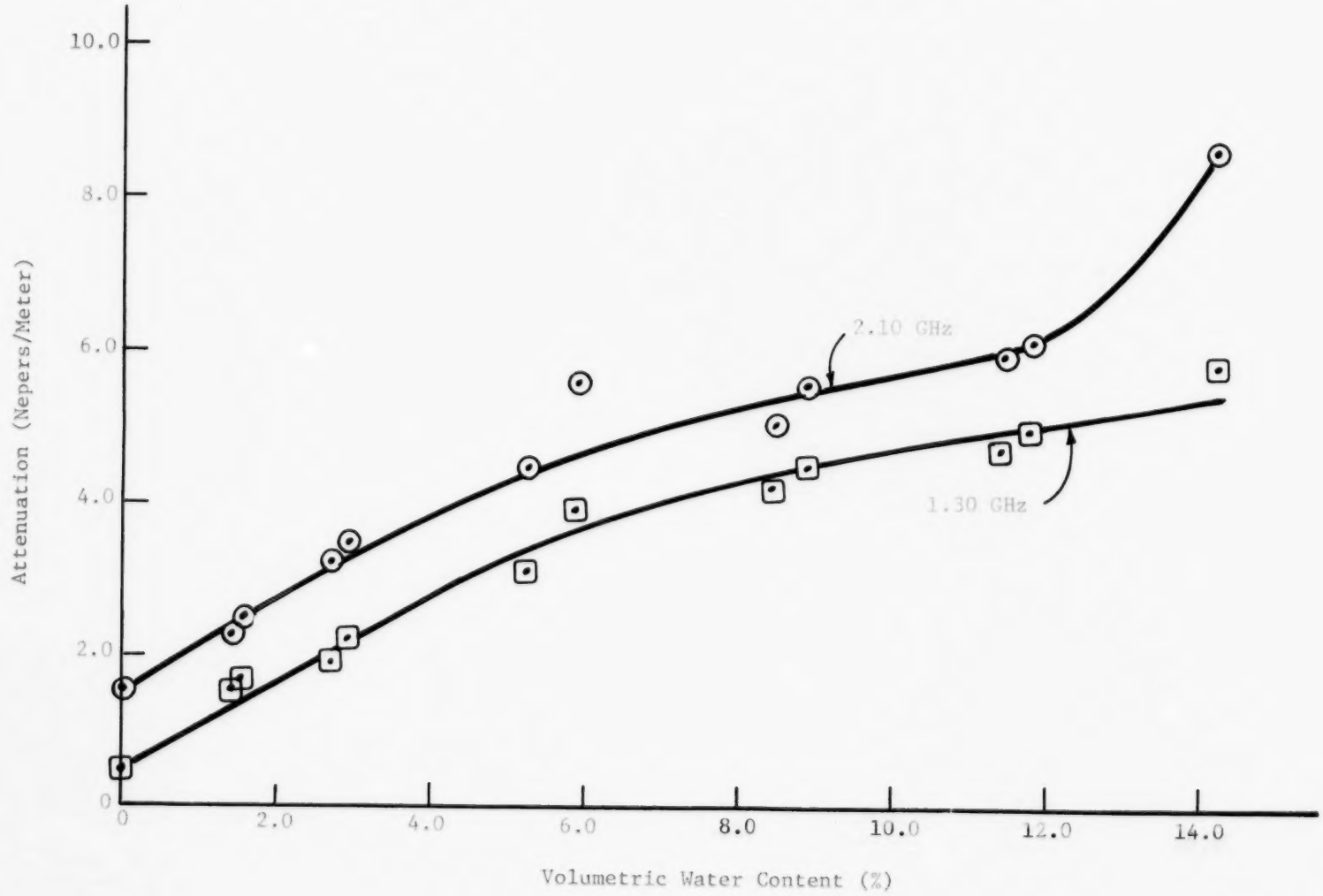


Figure 13. Attenuation results for Atlantic City beach sand with different water contents.

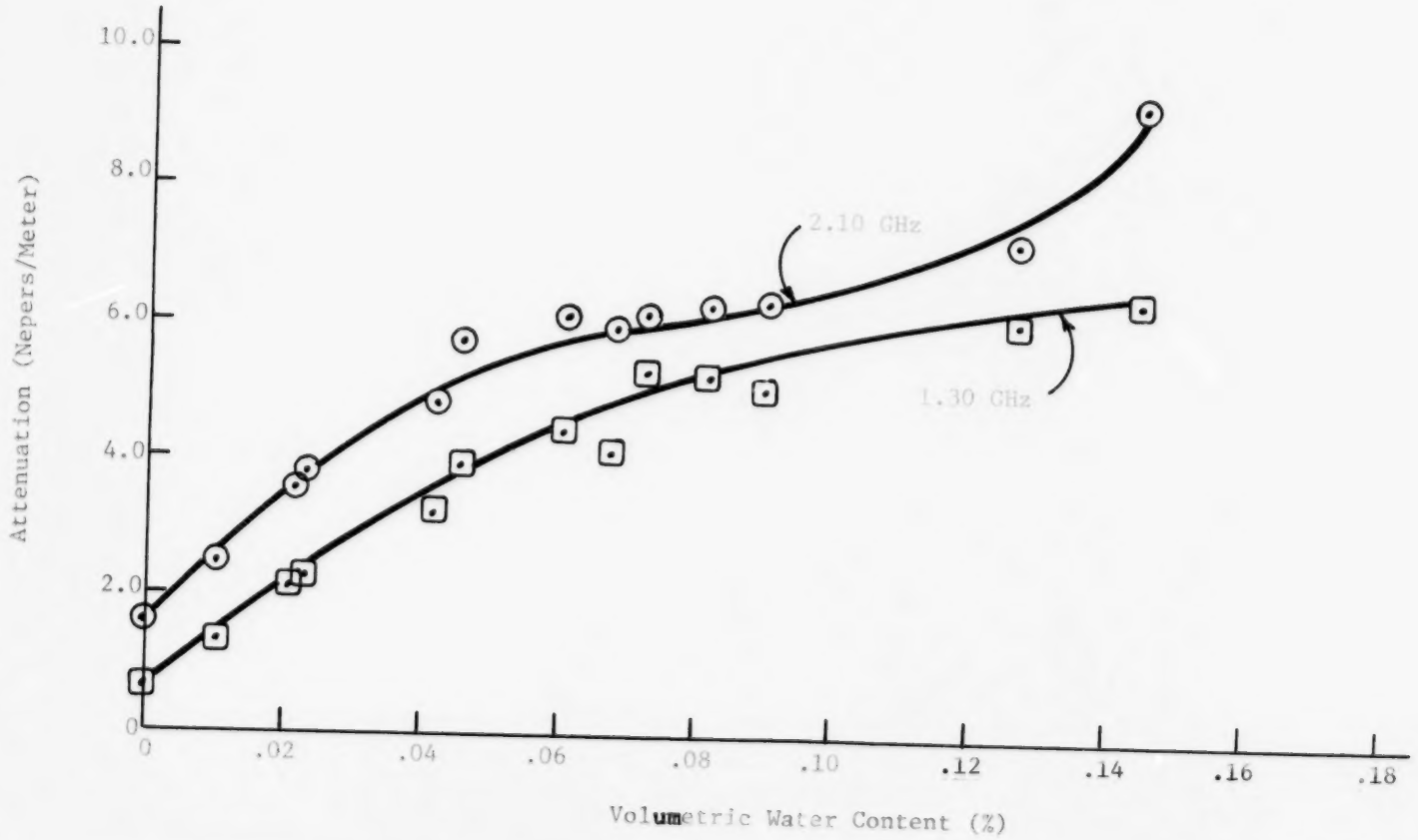


Figure 14. Attenuation results for Delaware River silt with different water contents.

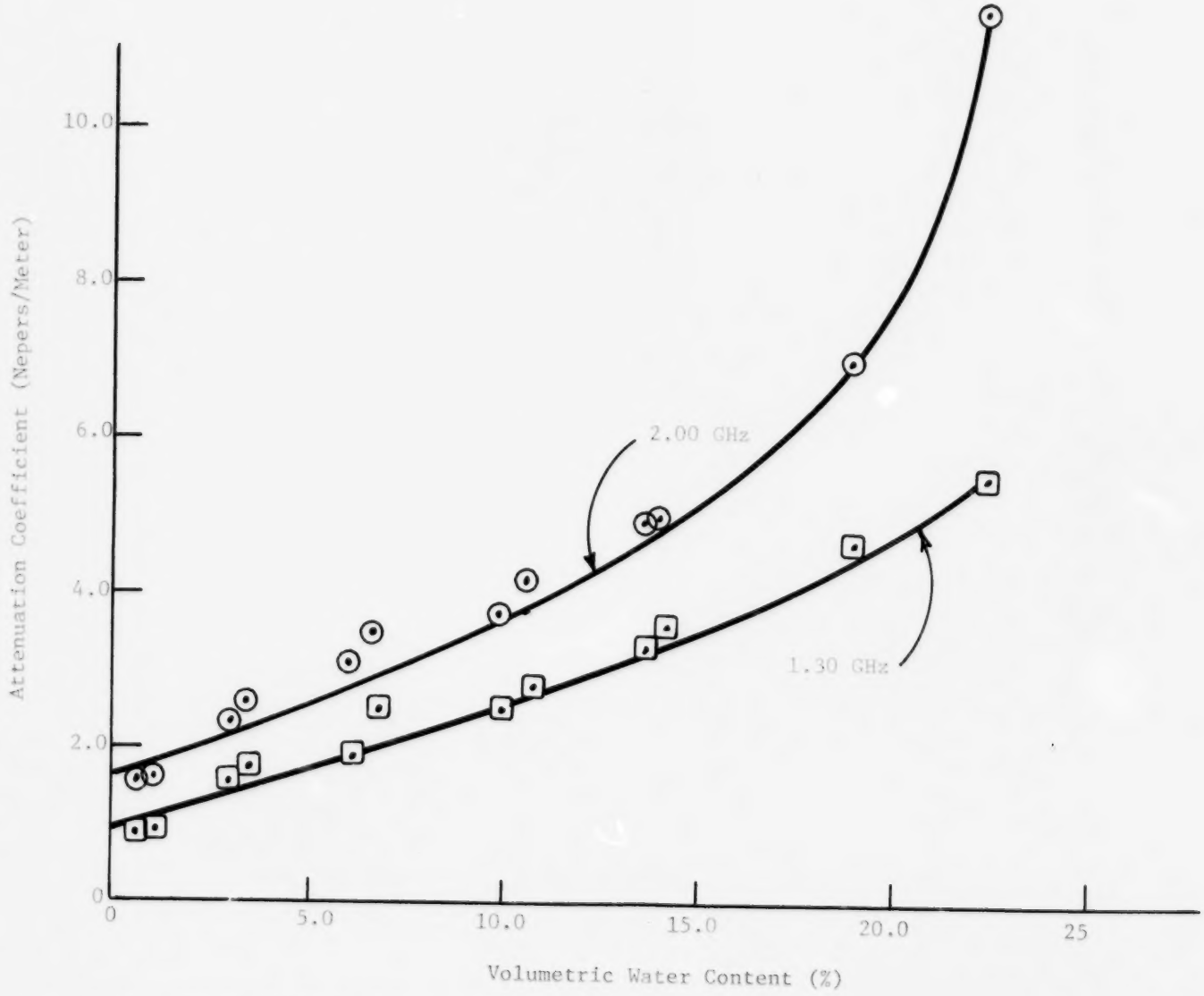


Figure 15. Attenuation coefficients of kaolinite clay with different water contents.

approximately 80 for water to 3 for ice due to this phenomenon. Likewise the attenuation is also reduced. One would expect the attenuation of microwaves in clay to be intermediate to that for water and ice. Beach sand and clayey silt also exhibit this phenomenon but to a lesser degree.

(c) Penetration Depth (d)

It is of great interest to estimate the effective depth of subsurface profiling possible once the microwave dielectric constant and attenuation of the soils are known. A simplified procedure has been used to do this; the ray tracings of the various waves are shown in Figure 16. Microwave power $P_{inc}$ is directed at the air/soil interface. A fraction $P_{gd}$ of the incident power is reflected; the remainder is transmitted into the soil. All of this transmitted power is reflected from the metal surface (a perfect reflector) at a depth d, and a portion of $P_{inc}$, $P_{out}$, ultimately finds its way back into the air (see Figure 16). Using basic theory and neglecting multiple reflections, the radio $P_{out}/P_{gd}$ can be easily calculated by using the following formula:

$$P_{out}/P_{gd} = \frac{16n^2}{(n+1)^2(n-1)^2} e^{-2\alpha d} \qquad (28)$$

where n is the dielectric constant.

For both pulsed and continuous-wave microwave profiling, this ratio will determine to a great extent the depth to which the monitoring system can be used. It is reasonable to assume that this ratio must be at least 0.10 if the instrument is to produce useful information (that is, a good relative return echo strength for the pulsed method and a good interference pattern for the continuous wave system). Equation (28) can be rewritten as follows:

$$d = (1.15/\alpha) \cdot \log \left[ \frac{16n^2}{[n+1]^2[n-1]^2} \cdot P_{gd}/P_{out} \right] \qquad (29)$$

With $P_{gd}/P_{out} = 10$, we obtain

$$d = (1.15/\alpha) \cdot \log \left[ \frac{16n^2}{[n+1]^2[n-1]^2} (10) \right] \qquad (30)$$

Table 8 estimates the penetration depth for some typical soils for given moisture conditions, dielectric constant, and attenuation. These values agree in order of magnitude with experience in the field. It is seen that at 1 GHz one cannot tolerate a great deal of water in the soil, if any reasonable depths are to be probed.

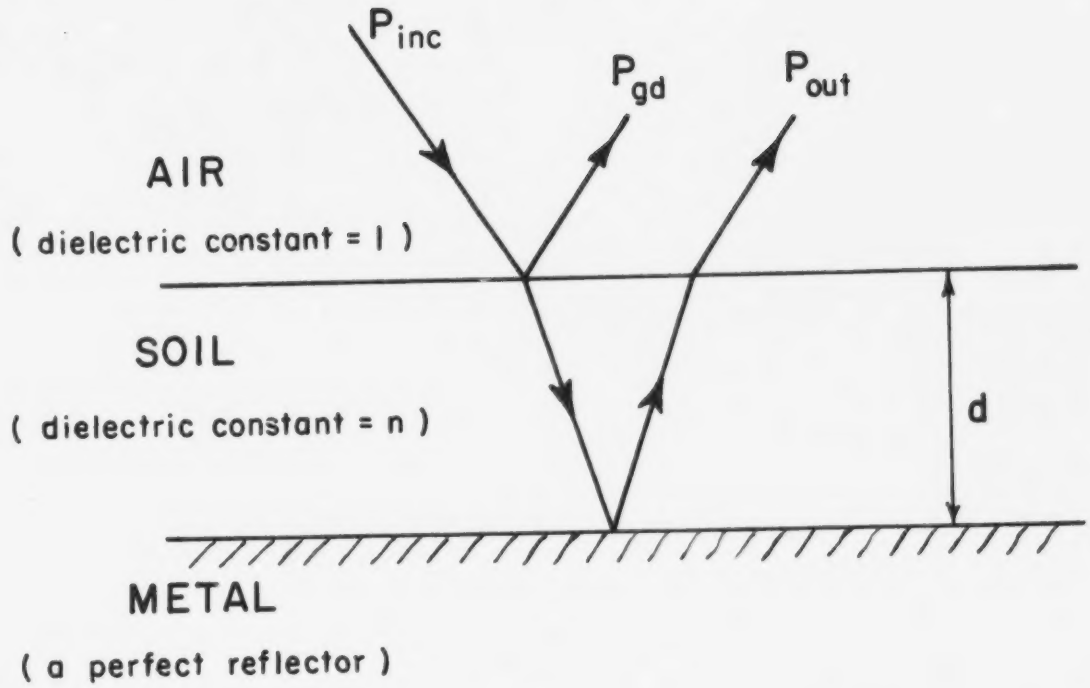


Figure 16. Ray diagram for penetration depth calculation.

TABLE 8. Calculated Penetration Depth for Various Soils at a Microwave Frequency ≈ 1 GHz

| Soil Type | Dielectric Constant n | Attenuation Coefficient α, nepers/m | Penetration Depth d, m |
|---|---|---|---|
| Very dry | 3.0 | 0.5 | 3 |
| Lightly moist | 5.0 | 1.0 | 1 |
| Moderately moist | 6.0 | 2.0 | 0.4 |
| Heavily moist | 8.0 | 6.0 | 0.07 |
| Very wet | 12.0[a] | 10.0 | 0.005 |

[a]For $P_{gd}/P_{out} \leq 10$, n must be $\leq 12$.

Section 7

# CONTINUOUS-WAVE MICROWAVE METHOD

The difficulty in obtaining very-near-surface information in a non-destructive testing manner leads to the use of an electromagnetic method based on generating and directing continuous waves into the material being investigated. At frequencies of about 1 GHz, the method can appropriately be called a continuous-wave microwave method, or simply "CW microwaves". The waves are reflected by a material with different electrical properties, e.g., a void filled with air or water, and, when received back at the surface, form an interference pattern. Using these patterns and a theoretical analysis, the depth to the reflecting surface can be calculated. It is with this method that the following laboratory and field experiments were conducted.

## (a) Laboratory Tests Using The Continuous-Wave Microwave Method

### 1. Water Location

Results from preliminary tests indicated that a microwave system with the capability of frequency variation could produce an interference pattern for a particular location along a scan and compare such interference patterns with the patterns from other scan locations to detect the presence of a buried water pocket.

It was determined that Bragg's Law is the dominant effect in an active transmitter/receiver microwave system and that a variable-frequency microwave system would best utilize this effect in locating a water pocket and determining its depth from the surface.

Since microwaves behave as light waves, Bragg's Law coupled with Snell's Law for an air/soil/water-pocket medium can be mathematically represented as follows:

$$m = \frac{2\,d\,nf}{c}\sqrt{1 - \frac{1}{2}\cos^2\theta} \qquad (31)$$

where m = the order number of reflection peak
d = is the depth of soil to a water pocket or a reflecting layer
c = speed of light in free space
n = index of refraction

$\Theta$ = look angle of the transmitting and receiving antenna relative to the horizontal (angle of incidence)
f = frequency of the generated microwaves.

For the order number (m), the problem arises as to what order number a particular constructive peak represents at a frequency f. This is determined by varying frequency f and thus obtaining two adjacent constructive peaks for two different frequency values. The following formula will yield the value of "m".

$$m = \frac{f_1}{f_2 - f_1} \tag{32}$$

Thus, using n,c, $\Theta$, and f as just described, it is now feasible to locate and determine the depth to a water pocket without chance of overlooking it (as was the problem in the constant frequency system) by using equations (31) and (32) and a variable frequency system, and then applying equation (1) to obtain final result.

A variable frequency system was constructed and is shown schematically in Figure 17. This system has been used in a large-scale laboratory test to determine the degree of accuracy and limitations in locating and measuring depth to a water surface. The results have shown that a subsurface water table can be located to within ±5% of its actual location for depths of up to 46 cm. This is the practical limit for the laboratory setup that was used in this study. It is by no means a limitation of the technique.

For each test, the microwaves were beamed at an angle to the surface of the soil. The responses from the microwaves reflected from air/soil and soil/water interfaces were measured. Figure 18 shows these results for a swept frequency range. The continuous-wave, variable-frequency microwave transmitter was capable of producing an average of 4 mW of power over a frequency bandwidth of 2.1 to 4.2 GHz. This bandwidth was automatically swept by the transmitter at an adjustable sweep rate. The transmitter output was fed to a fixed horn specifically tuned to the 2.1 to 4.2 GHz bandwidth. The receiving antenna had its output fed to a detector, where the RF signal was rectified to produce a voltage output proportional to the amplitude of the incoming microwaves. The detector output was plotted on the Y axis of an X-Y recorder against frequency on the X axis.

The soil system examined was housed in an open-top box constructed of plywood. For the bottom stratum, a moist clayey silt was compacted in place. The clayey silt layer was 8-cm thick and was placed on a layer of Eccosorb-70 microwave absorbent, which rendered the clayey silt layer infinitely thick relative to the microwaves. Above the clayey silt layer was placed 46 cm of dry Ottawa sand which simulated a top soil stratum overlying the clayey silt. A water table was established at several depths in the sand layer for the series of tests conducted. For each test, the water level in the sand was increased in increments of 5.1 cm, starting from zero. Thus, a series of curves was generated showing the microwave response

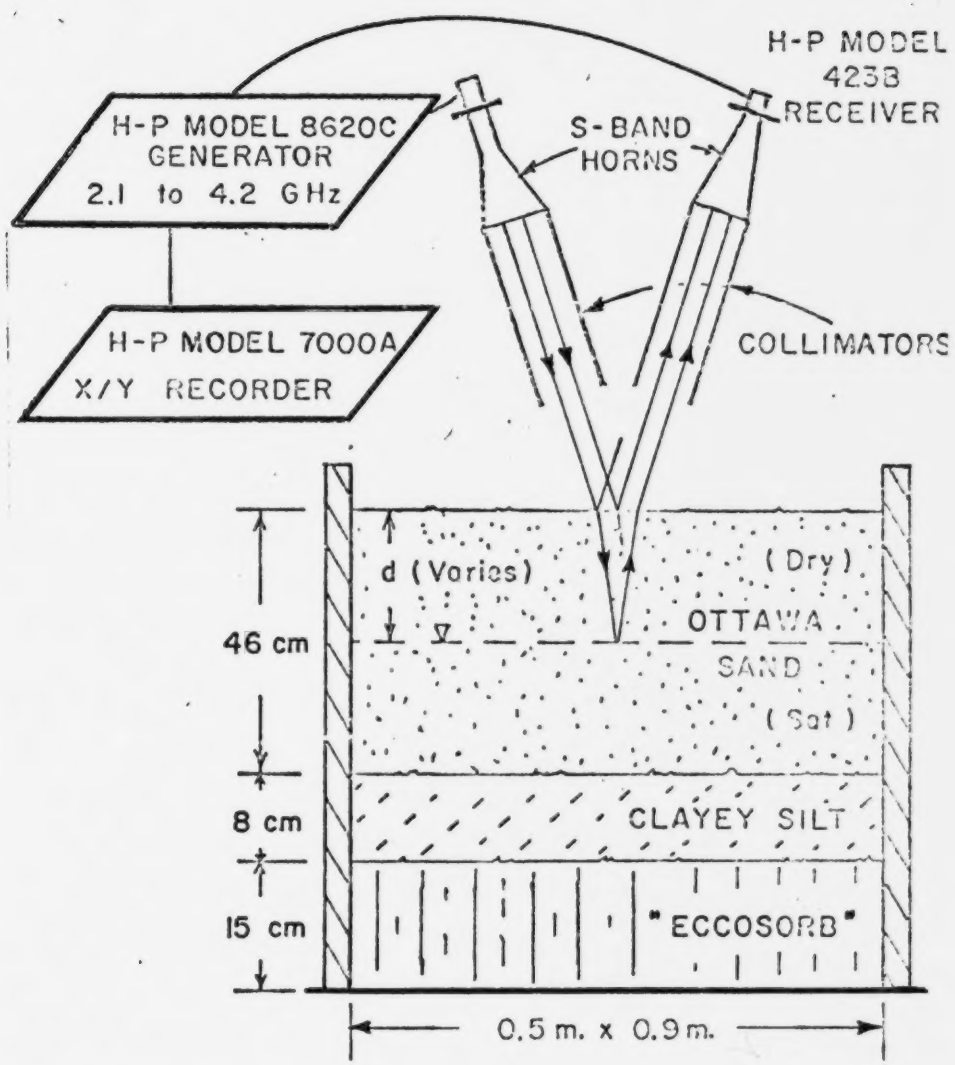


Figure 17. Schematic diagram of variable-frequency microwave system used to determine depth to water surface.

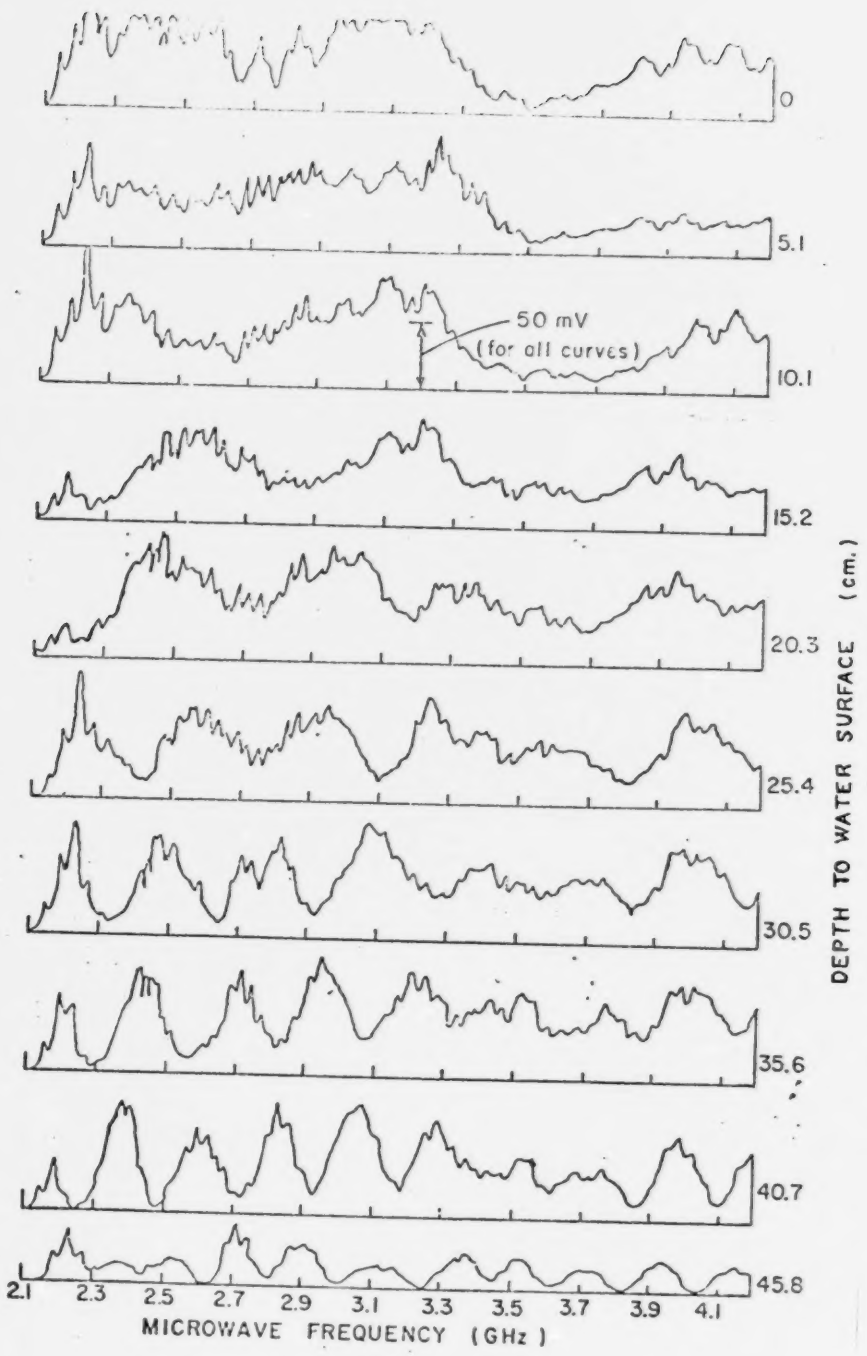


Figure 18. Variation of microwave power received as a function of various depths to water surface over a frequency sweep of 2.1 to 4.2 GHz.

changes from an upper stratum bearing a transient water table.

Figure 18 shows the progressive response from one test to the next. It should be noted that the number of cycles (the order number) increases as the depth from the ground surface to the water table increases. Using this data plus the results of equations 31 and 32 gives the equation presented at the beginning of this report, equation 1.

$$d = \frac{c}{2n}\left[1 - \frac{1}{n^2}\cos^2\Theta\right]^{-1/2} \frac{x}{f_2 - f_1} \qquad (1)$$

For equation (1), $f_1$ and $f_2$ are the frequencies corresponding to two peaks on the graph, and x is the number of peaks plus one between the peak associated with $f_2$ and the peak associated with $f_1$. Also, c is the speed of light ($3 \times 10^{10}$ cm/s), n is 1.64 for the Ottawa sand, and $\Theta$ is 81° (the set angle of the transmit/receive horns relative to the ground surface).

Table 9 summarizes results from such calculations using the data for each graph in figure 18. The results are plotted in figure 19 where the excellent correlation between actual depth and predicted depth to the water table can be seen. It is apparent here that the microwaves never "see" the clayey silt layer due to the high attenuation of the microwaves in the saturated layer at the 2.1 to 4.2 GHz bandwidth. Thus, this attenuation resulted in microwaves reflecting from just two layers (top surface, and surface of the saturated layer). Even in the first graph, where there was no water table present, the microwaves still reflected well from the clayey silt/dry sand interface due to the high moisture content present in the clayey silt.

TABLE 9. Predicted versus Actual Depth to Water Surface

| Actual Water Depth (cm.) | Calculated Order Number* (m) | Calculated Water Depth (cm.) |
|---|---|---|
| 45.8 | 11 | 45.1 |
| 40.7 | 10 | 42.0 |
| 35.6 | 9 | 37.4 |
| 30.5 | 7 | 28.7 |
| 25.4 | 6 | 24.6 |
| 20.3 | 5 | 18.7 |
| 15.2 | 4 | 14.3 |
| 10.1 | 2 | 8.1 |
| 5.1 | No Definable Peaks | -- |

*Order number for the first peak occurring in the frequency sweep (rounded off to the nearest whole number.

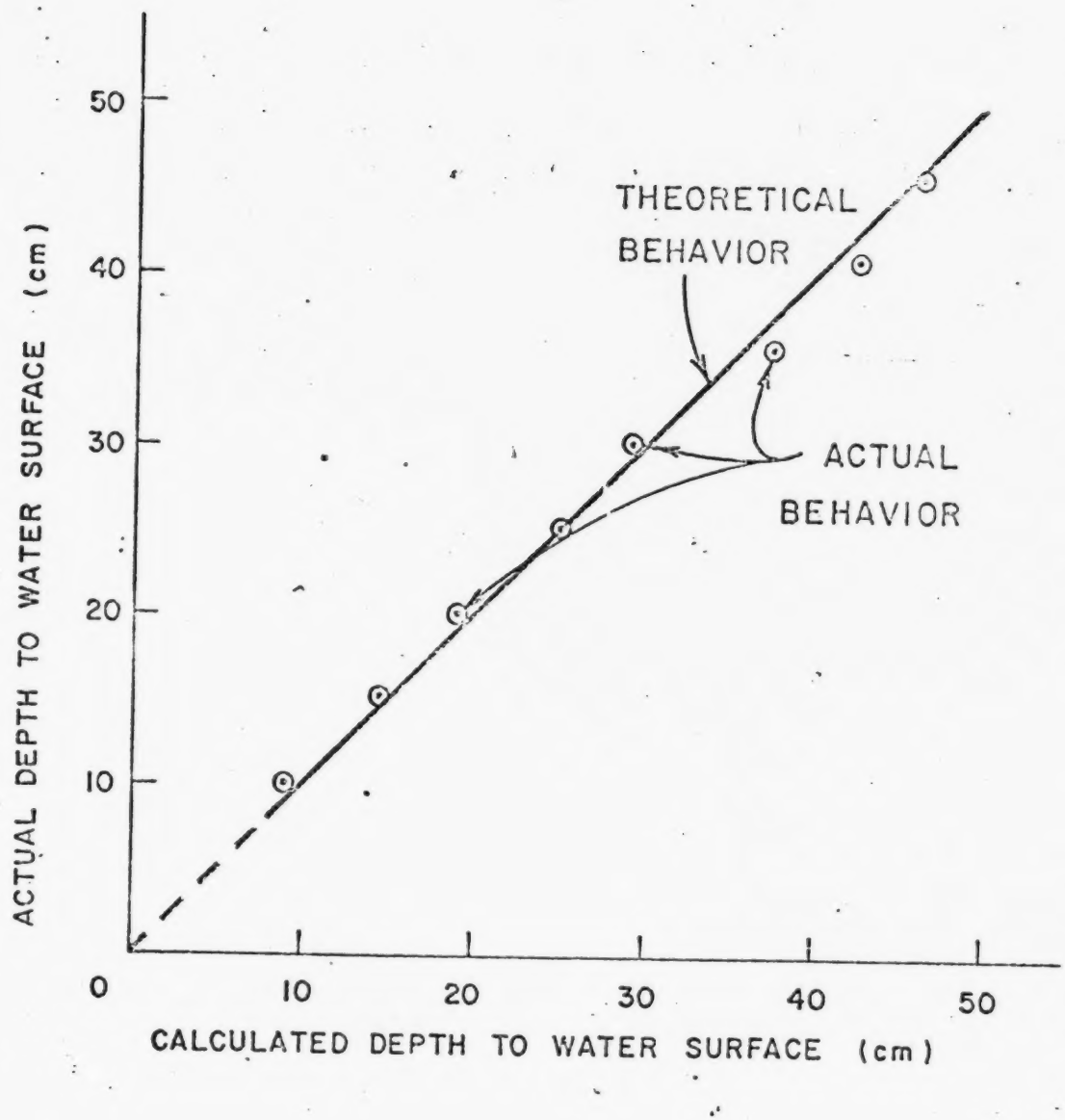


Figure 19. Comparison of calculated and actual depths to water surface for frequency sweep tests shown in Figure 18.

Since this test series used extreme moisture contents in defining the soil strata (partially wet/dry or wet/dry), it was necessary to study the effects of microwave reflections from an interface of two dry or partially saturated soils of different types and microwave attenuation in soils with increasing moisture content. Though the literature indicated that low-frequency microwaves show less attenuation in water and thus better subsurface penetration, low frequencies mean longer wavelengths and less resolution. Further studies were made to determine the bandwidth that yields only small attenuations to microwave signals but still exhibits good resolution. It should also be noted that the determination of depth by equation 1 requires the value of n (index of refraction for the soil under evaluation) to be known. This topic was discussed in Section 6a.

For the next test sequence, the same laboratory equipment setup was used but the dry layer of soil lying above the saturated soil layer was replaced with different soils and with soils of varying saturation conditions. The two soils that were used were Atlantic City beach sand and Delaware River clayey silt. The tests were run for soil depths of 25 cm over the saturated soil layer, and for saturation percentages of 0, 15%, 30%, 45%, etc., or until no recognizable changes in the reflectance patterns were distinguished. It is apparent that for increasing percent saturation, both Atlantic City beach sand and Delaware River clayey silt show no microwave interference patterns for the frequency sweep.

Large-scale tests were performed in the laboratory to obtain more accurate results in locating subsurface anomalies. First, a water pocket was created by filling a plastic container 30.5 cm x 45.7 cm x 10.2 cm (12 in. x 18 in. x 14 in.) with water and burying it under 43.2 cm (17 in.) of dry sand. Smaller antennas were used in this test and the tests that follow. They were held between 8 cm (3 in.) and 15 cm (6 in.) from the surface at an angle of approximately 20° to the vertical. Eccosorb was placed 8 cm (3 in.) above the surface separating the two horns. The frequency range used was 0.8 GHz to 2.4 GHz. The results are shown in the upper graph of Figure 20. The calculated depth to the pocket was 41.7 cm (16.4 in.).

The next test was the detection of a saturated sand layer 45.7 cm. (18 in.) below the surface. The saturated layer was obtained by filling a 76.2 cm x 76.2 cm x 10.2 cm (30 in. x 30 in. x 4 in.) box with saturated sand. Dry sand was then placed over this to a height of 45.7 cm (18 in.). The frequency range was 0.8 to 2.4 GHz. The results are shown in the lower graph of Figure 20. The calculated depth was 49.5 cm (19.5 in.).

Next, a 1.8 m x 1.2 m x .76 m (6 ft x 4 ft x 2.5 ft) box was constructed for the purpose of studying the detection of seepage flow using the continuous-wave microwave system. A channel for the seepage flow was constructed using polyethylene. This kept the seepage within known boundaries. Water was fed into one end of the channel via a hose and a hole in the box. A steady flow is established using this configuration.

The microwave unit was used to determine the difference in depths between the seepage flow and the depth to the concrete underlying the dry

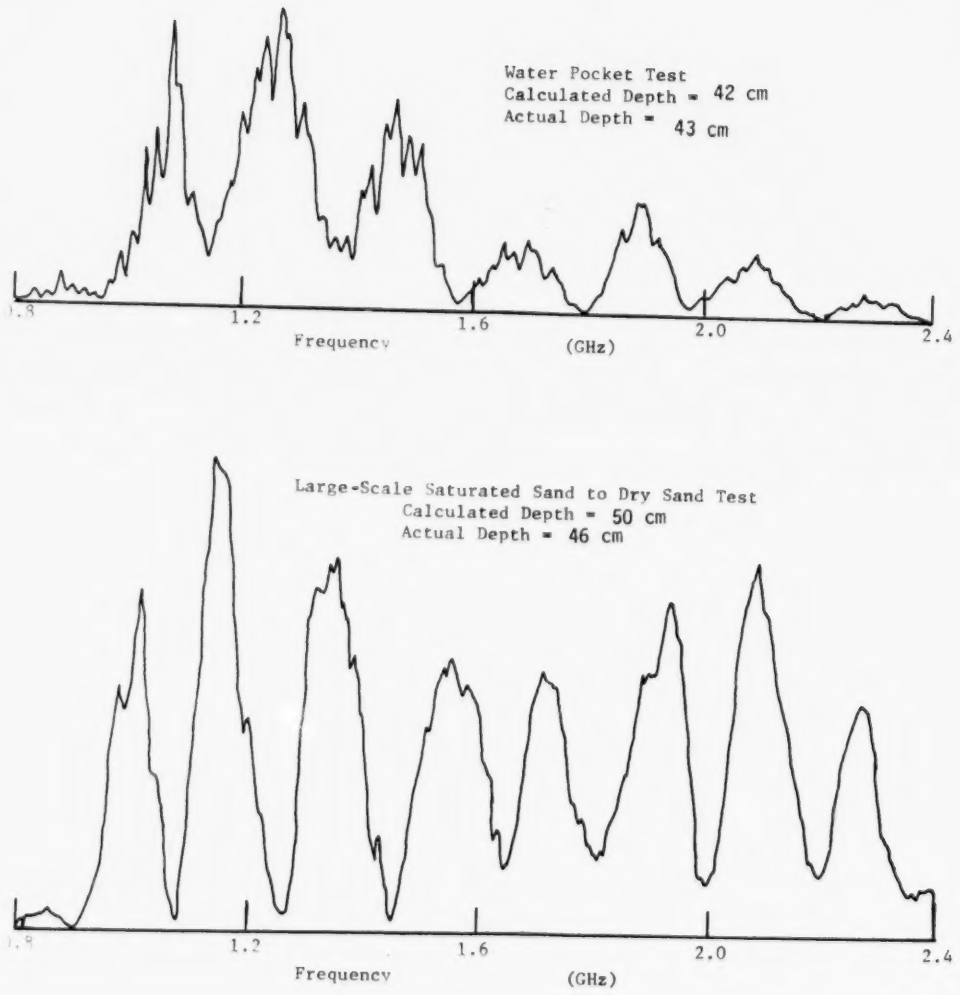


Figure 20. Signal response for buried objects at various indicated depths.

soil surrounding the seepage channel. A well-graded sand was used in the study. Figure 21 is an illustration of the box and the seepage channel. The locations of the test sites within the box are also shown on Figure 21. The results are presented in Table 10. As can be seen, the comparison of predicted versus actual depths to the water surface are quite favorable. There is, however, a marked difference in the depths predicted over the seepage as compared to those predicted over the concrete. There was also a very significant change in the response pattern when the system was moved over the edge of the channel, which was bounded by a plastic barrier. This was encouraging because it was the first time that the system had been used to determine the boundaries of an anomaly in addition to depth. Another interesting observation is that in all cases the predicted depth to the seepage flow was less than the actual. This may have been the result of capillary action wetting the fine sand, creating a false boundary.

TABLE 10. Seepage Test Results

| Station | d | Actual | % Error |
|---|---|---|---|
| 1 | 14.3 cm | 45.7 cm | +19.0 |
| 2 | 32.2 cm | 32.2 cm | -12.0 |
| 3 | 55.9 cm | 45.7 cm | +21.0 |
| 4 | 48.6 cm | 47.0 cm | +4.0 |
| 5 | 14.3 cm | 20.3 cm | -5.0 |
| 6 | 44.2 cm | 44.4 cm | -0.6 |
| 7 | 38.6 cm | 38.1 cm | +1.0 |
| 8 | 26.4 cm | 30.5 cm | -13.0 |
| 9 | 47.5 cm | 44.4 cm | +7.0 |

2. Interface Detection

The purpose of this testing program was to determine what types of soil layer interfaces (and other objects) can be detected by our continuous-wave microwave field unit. Interfaces such as a loose soil layer over a denser layer (density interface), a dry layer over a wetter layer (moisture interface), and an interface between different soil types (soil interface) were created.

The test setup consisted of a 122-cm x 183-cm x 98-cm (4 ft x 6 ft x 3.2 ft)-deep box filled with soil. The box was filled with a uniformly

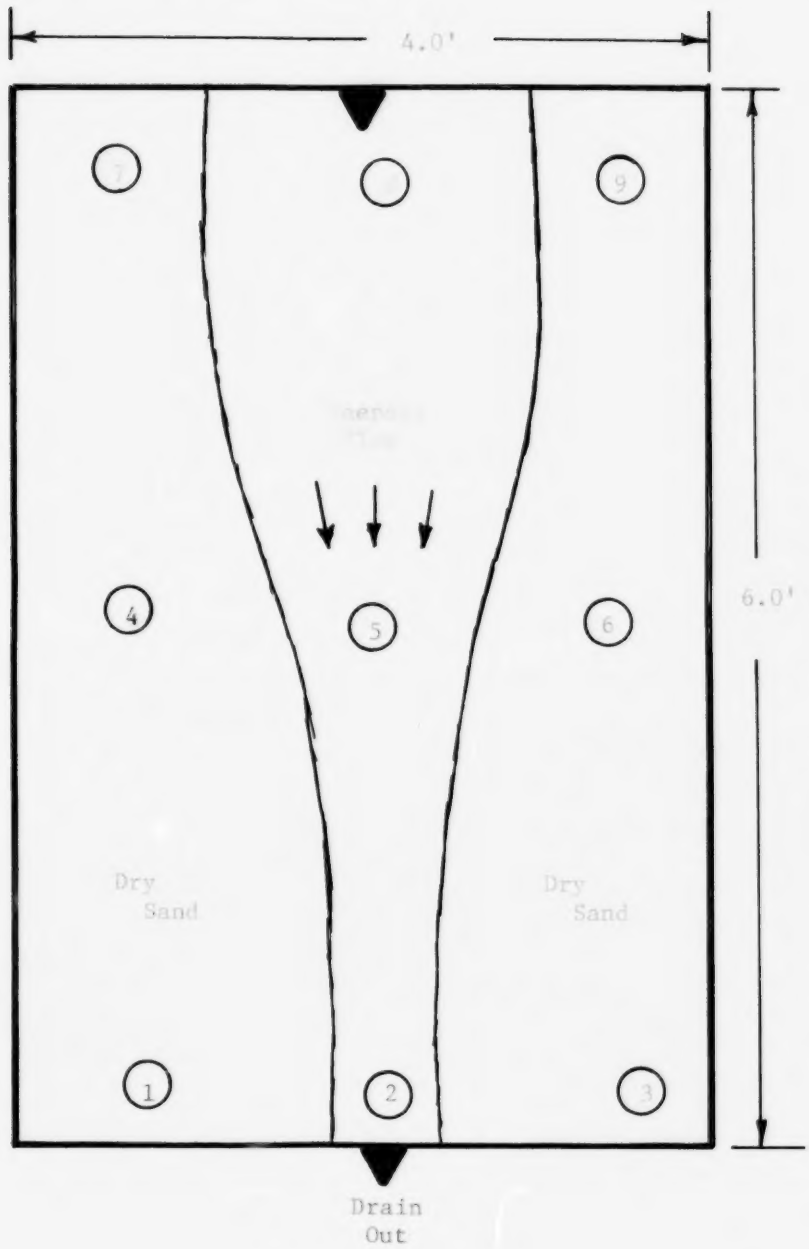


Figure 21. Seepage box and flow channel.

compacted quartz sand having the following characteristics: effective size of 0.21 mm, coefficient of uniformity of 2.8, water content of 0.3% and subrounded shape. When the sand was placed it was compacted in 15 cm (6 in.) layers, giving it a relative density of 70%. Nine microwave stations were established on the sand's surface by a series of evenly spaced strings forming a grid over the soil. Before testing began, the sand surface was leveled and smoothed to eliminate any surface effects. When making initial microwave measurements both microwave antennas were mounted on wooden stands so they remained at a 60° angle to the sand's surface.

After developing the test procedure and recording the basic microwave response of the box, the initial tests were run. First a density interface was created in the box. Twenty-three centimeters (9 in.) of sand was removed from the box so it could be replaced in the loosest state possible. The replaced soil in the upper 23 cm (9 in.) of the box now had a relative density of 40%, whereas the sand below it had a relative density of 70%. Microwave measurements to determine whether the interface is detectable were made at station B-2, (see Figure 22). The microwave interference pattern resulting from the measurement made on the surface of the sand with a 70% relative density throughout can be compared with the waveform resulting from the 40% over the 70% density interface. The depth calculated from the interference peaks for the 40% over the 70% at 23 cm gives d = 75 cm (30 in.), which is approximately the bottom of the box (and not the density interface). A visual comparison of the microwave traces showed no change in the total number of major peaks. However, the relative amplitudes of these peaks had changed. The 40% over 70% trace shows an amplitude increase of 0.5 scope division (0.25 volts) over the uniform density (70%) trace. Peaks in the density interface trace are also less sharp and well defined than those for the uniform density trace.

In the next test, the 40% over density interface was created at a lower depth of 35 cm (14 in.) and the microwave interference pattern was recorded. As with the previous, shallower density interface, no change in the number of major peaks is noted when compared with the uniform density case. However, notable increases in amplitude of some of the peaks, as compared with the uniform density case occurred again. The amount of increase was up to 1.5 scope divisions. Although only three data points are available, the overall trend of increasing amplitude with an increase in interface depth is evident.

Because of the trend described above, density interfaces are detectable, but only in terms of a change in interference pattern amplitude. These amplitude changes increased as more of the soil was made less dense (and the interface became deeper). Since the soil's attenuation determines the amplitude and because attenuation decreases with decreasing density, these results appear logical, and they suggest a new direction for field monitoring.

After our inability to determine the depth to a soil density interface using a number of frequency peak countings, a glass plate (30 cm x 30 cm) was

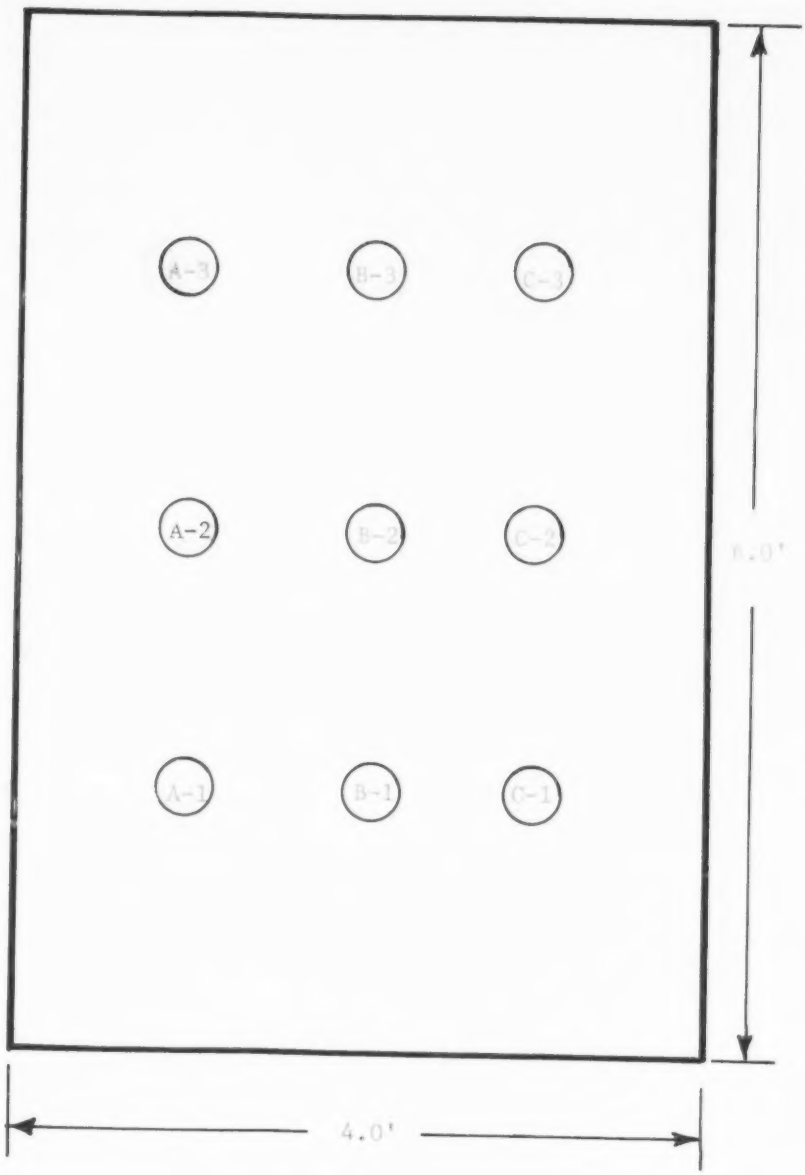


Figure 22. Location of the nine microwave stations.

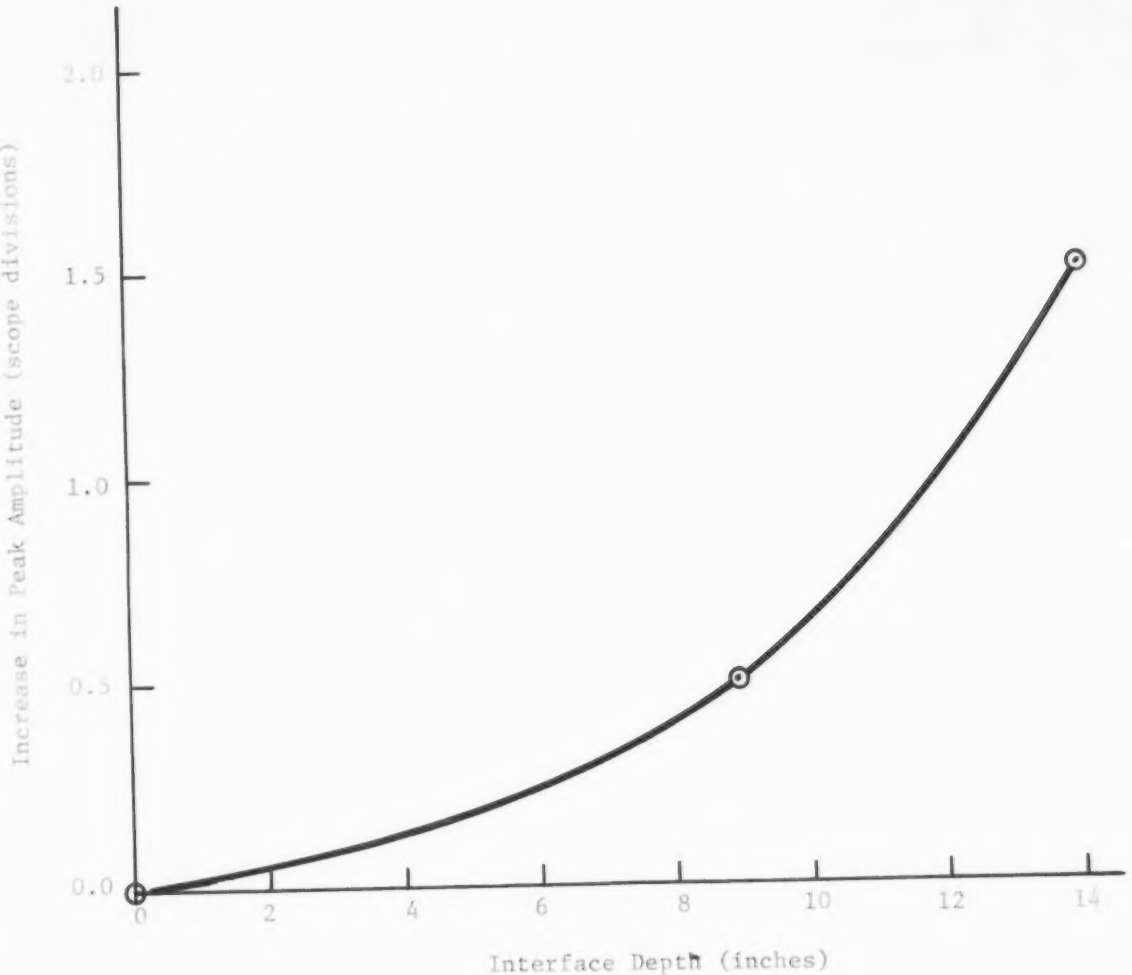


Figure 23. Peak amplitude increase versus interface depth.

buried 15 cm (6 in.) in the quartz sand. Such a test gives a larger density interface than possible by compaction. Microwave reflections for the glass plate test can be compared with the reflections with only uniform sand ($D_R$ = 70%). Again, the depth to the plate was not capable of being calculated as there was no detectable change in the interference peaks except for an increase in their amplitude of 1.25 scope divisions (maximum).

Reflections from the glass plate can be compared with the sharp reflections from a metal plate. To obtain reflections from the plate, it was buried 20 cm (8 in.) in uniform, quartz sand. Two unmistakable peaks were obvious and the depth calculated from them is 15 cm (6 in.). This shows that a metal plate is an excellent microwave reflector.

During testing the clearest and largest amplitude waveforms were obtained with the antennas on the soil surface and with Eccosorb (a microwave attenuating material) between them. As the antennas were raised above the soil surface, the amplitude of the peaks decreased. Various depths can also be calculated from the interference peaks depending on the peaks chosen (there is no single depth given by the pattern). An additional test showed how the calculated depth becomes erroneous as the antennas are raised 10 cm (4 in.) above the surface as compared to resting the antennas on the surface. The antennas must, therefore, be kept on the ground surface and in contact with the soil.

Conclusions from the above series of tests are as follows:

- Soil density interfaces do not affect the spacing or number of peaks in the reflected microwave waveform.
- Soil density interfaces are detectable as a change in interference peak amplitude and clarity, probably due to changes in soil attenuation. Analyses of interference pattern amplitude changes in the field may prove useful in the future. We can conclude that density changes in the soil have no effect on our ability to determine the depth to other subsurface targets, such as a water surface.
- Even a very sharp density interface as produced by a glass plate, does not affect the number of interference peaks therefore its depth cannot be determined. The interference pattern amplitude is greatly increased, however, over the uniform case.
- Antennas should rest on the soil surface for a clear and accurate reading.

Large-scale laboratory tests were next performed to determine if different soil interfaces could be detected using microwaves. Mica schist sand was chosen because its particle size and shape distribution are quite different from those of the quartz sand. The total depth of soil in the box was kept constant at 79 cm (31 in.) while the ratio of the depth of the mica schist to quartz sand, and thus the interface depth, was varied.

The effective size of the mica schist sand was determined to be 0.14 m, with a coefficient of 4.9. Note that the mica schist sand has much finer particles than the quartz sand. Both sands are well graded. Other differences between these sands include water content and shape. The mica schist and quartz sands have water contents of 2.1% and 0.3% respectively. The mica schist sand particles are either flaky or subrounded while the quartz sand has all subrounded particles.

Since we were using two different types of soil, a plastic sheet was laid across the soil interface in order to keep the sands segregated. In order to have a reading when no interface was present in the quartz sand, a separate test was made. A plastic sheet was buried 23 cm (9 in.) under the surface of 79 cm (31 in.) of uniform, quartz sand and a photograph of the resulting waveform was taken. It was then compared to all the following interface tests. A microwave trace was also made with uniform sand and no plastic sheet so that the effect of the plastic could be seen. Although the sheet does not cause any change in the number of peaks or their spacing (its depth cannot be calculated), a change in the peak amplitude of from -0.25 to +1.00 scope divisions (1 scope division = 0.5 volts) was noted when the sheet was present. The relative amplitudes and shapes of the peaks are also different with and without the sheet.

The first soil interface test was run with the interface 23 cm (9 in.) below the sand's surface. When a depth is calculated from the results, one obtains 79 cm (31 in.), which is the bottom of the box, not the interface. If the case with the interface at 23 cm is compared with the case with no interface, one immediately sees that the relative amplitudes and peak shapes are different. Interference pattern changes of -0.5 to +0.5 scope divisions are noted, but no difference in the total number of peaks is observed.

For the next test, the interface was created at a lower depth of 33 cm (13 in.), below the sand's surface. When calculating a depth from the resulting microwave trace, one gets 79 cm (31 in.), which is again the bottom of the box and not the interface. When this case is compared with the uniform, no-interface case, the relative amplitudes and shape of the peaks are changed. Peak amplitudes for the 13-inch-deep interface case are also less than those for the uniform case (no interface) by 0 to -1.0 scope divisions.

Both of these interface tests showed a slight decrease or no decrease in the interference peak amplitude compared with the uniform, no-interface case. The decrease in amplitude was found to be greater when there was more mica schist sand in the box (i.e., at deeper interfaces). Since the mica schist sand has a slightly higher water content than the quartz sand, it can be expected to attenuate the reflected microwaves more, and such an effect does appear to occur. The same type of trend seemed to occur with density interfaces in quartz sand. With a larger water content in both sands, though, a larger dielectric constant difference will occur, and since microwave reflections occur due to a change in dielectric constant, a larger interference change is possible.

Results from these low water content soil interface tests show that these interfaces cannot be detected using of the usual method of observing a

change in the number of interference peaks (none occur), and the depth to the interface cannot be calculated. However, such soil interfaces can be detected, when the overlying soil thickens or thins, by subtle changes in the interference peak amplitudes. The overlying soil can be discerned as thickening or thinning once its attenuation with respect to the lower soil's attenuation is known. Monitoring amplitude changes may prove to be an aid for future field work.

A summary of the past work presented in this subsection is given in Table 11. The table provides the type of test, soil depths in the box, interface depths, changes in peak amplitudes, changes in the number of peaks, the depth calculated from the waveforms, and miscellaneous comments on the interference patterns with respect to the patterns from the box when filled with uniform, quartz sand.

The final series of large-scale lab tests conducted were carried out to determine the minumum difference in soil/water content detectable with the continuous microwave system.

The water interface tests were performed in the large rectangular box described previously. The box was kept filled with a constant 79 cm (31 in.) of quartz sand throughout the tests. After waterproofing the box, it was partially filled with saturated sand having a volumetric water content (VWC) of 0.256. Volumetric water content was used to describe the soil because it includes the effects of both porosity (n) and the degree of saturation (s) and is in fact the product of the two; VWC = $V_W/V$ where $V_W$ volume of water and V = total soil volume. When the box was filled with saturated sand to the desired level, a layer of plastic (which does not interfere with microwave measurements) was placed over it, and the remainder of the box was filled with dry sand.

Our microwave field unit was used to determine the depth to the dry sand/saturated sand interface (at the location of the sheet of plastic) for various water contents of the upper soil layer. For the first tests the volumetric water content (VWC) of the upper soil layer was kept as low as possible (VWC = 0.0235). After determining the dielectric constant of the upper soil layer from both water content tests and a previously developed graph of VWC versus dielectric constant, the depth to the interface could be determined. For this first test the "microwave depth" was 42 cm (16.8 in.), as compared with the actual depth of 50 cm (20 in.).

The calculated depths are reasonably accurate up to a VWC = 0.1004 of the upper soil layer. For the next higher water-content test (VWC = 0.1116), the calculated depth is greatly in error. Therefore, it is reasonable to say that for lower VWC's, the depth to the interface is detectable, but for higher VWC's the depth cannot be determined. Although all calculated depths are slightly in error up to a VWC = 0.1116, they are not as much in error as those at or above this VWC. The smaller error is thought to be due to the inability to mix properly the large volume of soil in the upper soil layer with the water added to it.

TABLE 11. Summary of Measurement Reproducibility Tests (A and C) and Density and Soil Interface Tests (B and D). (Measurements for A, B, and C compared with the case with uniform quartz sand ($D_R$ = 70%) filling the soil box, Eccosorb between antennas, antennas on the soil surface. $D_R$ refers to relative density. Measurements for D are compared to case C.)

| Test | Soil Depth (cm) | Interface Depth (cm) | Change in Peak Amplitude (scope divisions) | Calc. Depth (cm) | Comments on the Waveform |
|---|---|---|---|---|---|
| A) Uniform Quartz Sand | 84 | 84 | | | Only one test location showed a change in peak amplitude of +1.00. All others were about +0.50. |
| 1)Reproduce the same reading | | | 0 to +1.00 | 86 | |
| 2)Remove Eccosorb between the antennas | | | 0 to +1.50 | 86 | Peaks are slightly less sharp without Eccosorb. The change in peak number may be due to amplitude changes bringing out hidden peaks. |
| 3)Raise antennas 4 in. above surface | | | See comments | | Depending on the height the antennas are raised, almost any number of peaks can be created. Amplitudes are also varied from a maximum on the surface to zero when the antennae are about 30 cm above the surface. |
| B) Density Interface in the Quartz Sand ($D_R$ ratios given below) | 84 | | | | |
| 1) 40% over 70% | | 23 | 0 to +0.50 | 76 | Some peaks much less well defined and sharp. |
| 2) 40% over 70% | | 36 | 0 to +1.50 | 84 | Same as above but less distinct. |
| 3) Glass plate buried in sand $D_R$ = 70% | | 15 | 0 to +1.25 | 79 | Peaks are very sharp and appear to increase with amplitude. |
| C) Plastic Sheet in Quartz Sand $D_R$ + 70% | 79 | 23 | -0.25 to +1.00 | 89 | Relative amplitudes and shapes of peaks change. |
| D) Soil Interface Mica Schist Sand over Quartz Sand | 79 | | | | With a larger water content in both sands, a larger dielectric constant difference will occur and a larger waveform change is possible. |
| 1) Test 1 | | 23 | -0.50 to +0.50 | 79 | Relative amplitudes and peak shapes are greatly changed. |
| 2) Test 2 | | 33 | 0 to -1.00 | 79 | Same as above. |

A series of tests was conducted that resulted in two VWC's, between which a limiting VWC occurs where the depth to the water-content interface is no longer detectable. Such a unique, singular point may not exist, but there probably is an "uncertain zone" (see Figure 24) where only a trained observer can determine the depth to the interface. Results from this series of tests for the soil/water-content interface at 50 cm (20 in.) below the soil surface are combined with past results where the depth to the interface was 25 cm (10 in.) and 31 cm (16 in.), respectively. These results are also plotted in Figure 24. The vertical axis of the plot is the dependent variable, the depth to the interface. The horizontal axis is the independent variable, the range in VWC of the upper soil layer beyond which the depth to the soil interface can no longer be determined. The horizontal axis units are normalized by dividing them by the VWC of the lower or saturated soil layer (i.e., if there were a point at 1.0, it would mean that the upper layer is totally saturated and if there were a point at 0.0, the upper layer would be completely dry).

Figure 24 shows a linear trend in the ability to calculate the depth to saturated soil when a sandy soil having a certain VWC overlies it. Between the curves in Figure 24 lies an uncertain zone having the interpretation described previously. At interface depths below (and, thus, smaller), there is no problem detecting the water table for any corresponding VWC. For any interface depth and VWC of the upper soil layer, above the uncertain zone it is not possible to determine the depth to the water-table interface. The figure also shows it is impossible to detect any interface at 15 cm (6 in.) or less below the soil surface due to the resolution limits of our particular microwave field unit. Resolution limits may result from the inability of the antennae to respond to the higher sweep frequencies needed to resolve a water table at a depth of 15 cm (6 in.).

Figure 24 summarizes the results of the detectability of soil/water-content interfaces and shows the limits of the microwave unit in a totally empirical way and, probably, more accurately than theoretical consideration would have allowed. These tests concluded the large-scale laboratory testing to detect natural interfaces in soil.

3. Void Detection

Voids may frequently form beneath paved areas. The occurrence of such voids is usually associated with water-generated erosion, but is also caused by subsidence, compaction, consolidation, freeze/thaw movements, vibratory action, and a number of other phenomena. The problem is most pronounced beneath paved areas but is also present in a number of other construction related situations. Typical examples are:

- beneath paved areas (concrete and asphalt pavements, parking lots, driveways, sidewalks, etc.)
- beneath footings
- around tunnels and utilities (bottom, sides, and top)
- behind retaining walls and abutments.

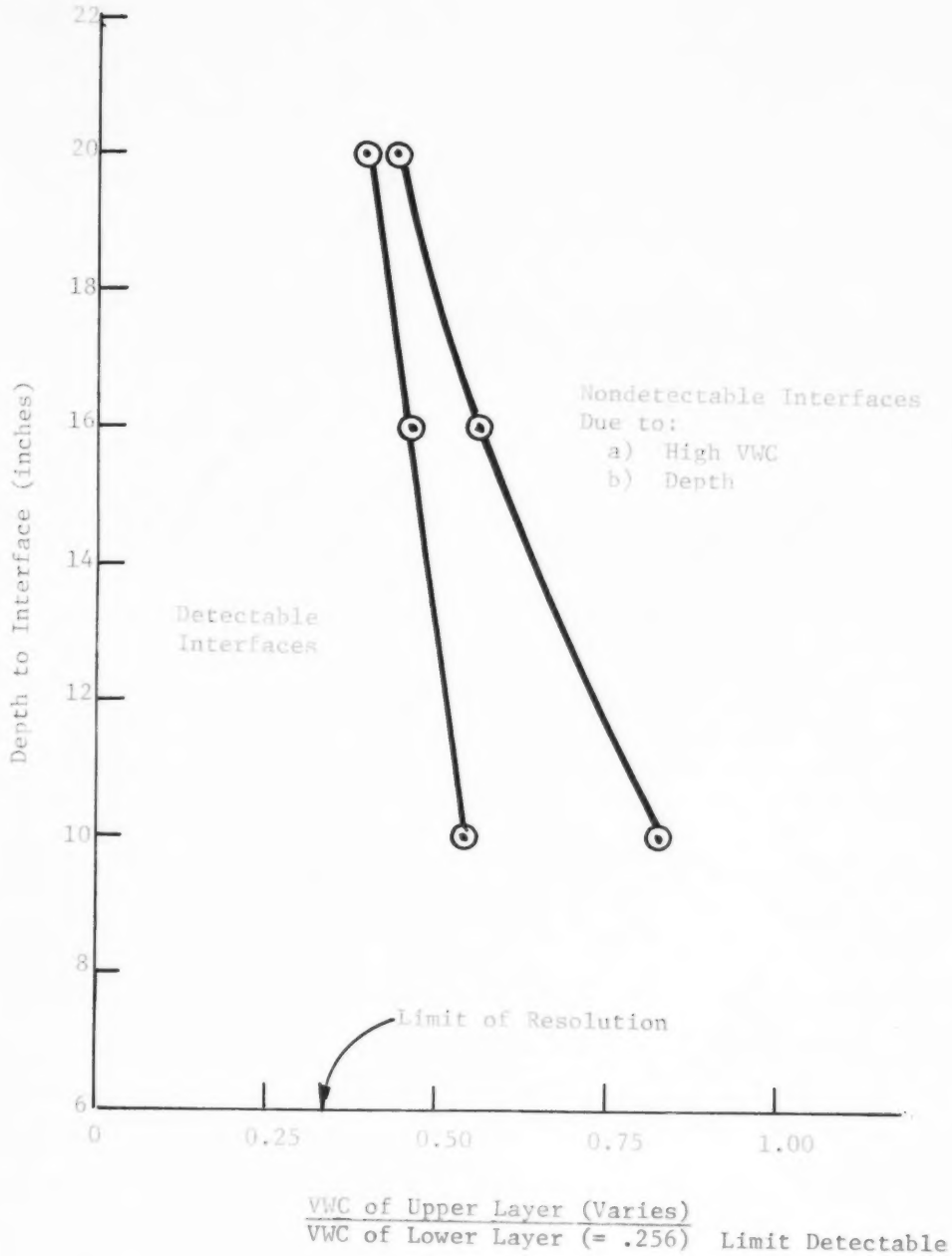


Figure 24. Soil water-content interface test results for quartz sand. (Total sand depth 79 cm for all tests.)

Problems in these areas can arise any time after construction and, when left uncorrected, can completely destroy (or severely limit) the useful lifetime of the structure involved. Furthermore, the apparently random nature of the location of the voids leads to an agonizing and often fruitless search. This search often requires excavation or selective test borings of the paved area to check phycisally for the existence and extent of the voids. Such an approach is often unsuccessful, destructive in its deployment, disruptive to the system, time consuming, and expensive.

A nondestructive testing method is needed to provide a preliminary assessment of the situation without adding damage to the structure. To this end, a laboratory study on the use of continuous-wave microwaves to distinguish between soil, air, or water lying beneath a surface of concrete, asphalt, or stone was conducted.

In this study, the microwave transmitting and receiving antennas were mounted on a wooden frame constructed over the top of a test box that provided control over the angle of microwave incidence on the upper material's surface. The transmitter and receiver components were capable of sweeping through a frequency range from 0.01 GHz to 2.4 GHz. The microwave generator was a Hewlett-Packard Sweep Oscillator model No. 8620C capable of sweeping with continuous-wave output at the previously-mentioned bandwidth and with a power output of approximately 4 mW. The generator output was connected to the transmitting antenna using coaxial cable. The receiving antenna was coupled to a Hewlett-Packard model No. 423B crystal detector using coaxial cable. The transmitting and receiving antennas were identical and specifically tuned for the above range of frequencies. The detector output was observed on an oscilloscope and then recorded on a Hewlett-Packard Moseley model No. 7000A X-Y recorder. The recorder plotted frequency on the X-axis and the corresponding detector voltage output on the Y-axis. The transmitting and receiving antennas were mechanically focused on an imaginary focal point located at the bottom of the test box and set to a constant angle of 60° to the horizontal (Figure 25).

The wooden test box was 0.6 m (2 ft) square and of varying height. This test box was placed in a larger soil-filled wooden box measuring 1.8 m x 1.8 m x 1.2 m (6 ft x 6 ft x 4 ft) so that spurious boundary reflections would be lessened, and the larger box also contained a microwave attenuating material, "Eccosorb", in its base. The soil was placed in a dense state at a water content of about 10%. It was classified as a well graded medium sand (SW) by the Unified Soil Classification system.

The test program was conducted in two separate phases. The first was a single-layer test program consisting of concrete, asphalt, or crushed stone placed over sand, air, or water (Figure 26a). The upper material varied in thickness between 76 and 305 mm (3 and 12 in.). It was placed on a 25-mm (1-in.) plastic sheet, which was required for support during the air and water tests and, for consistency, was used in the sand tests also. (Some preliminary tests were made to see if the plastic sheet would distort the microwave reflections. It was found that when the sheet was buried in the sand, no reflections were produced. Furthermore, when depth measurements

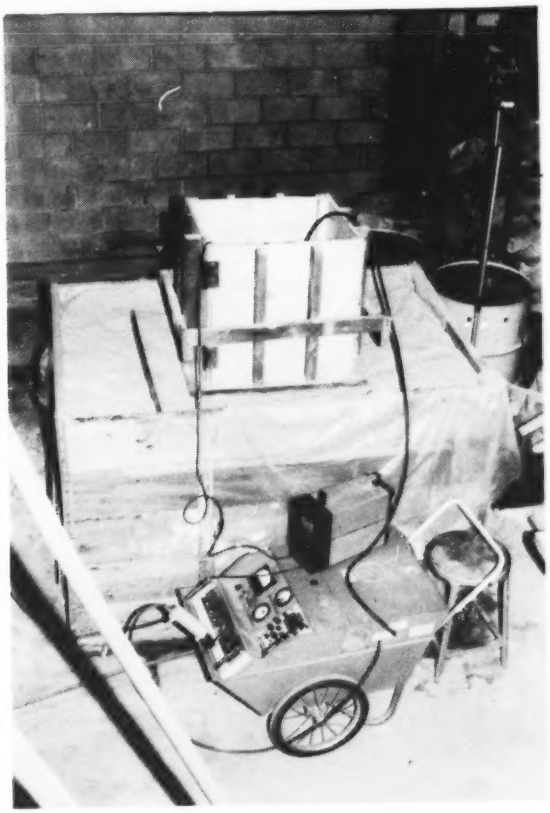

Figure 25. Photographs of continuous-wave microwave experimental test setup used to detect voids under paved areas.

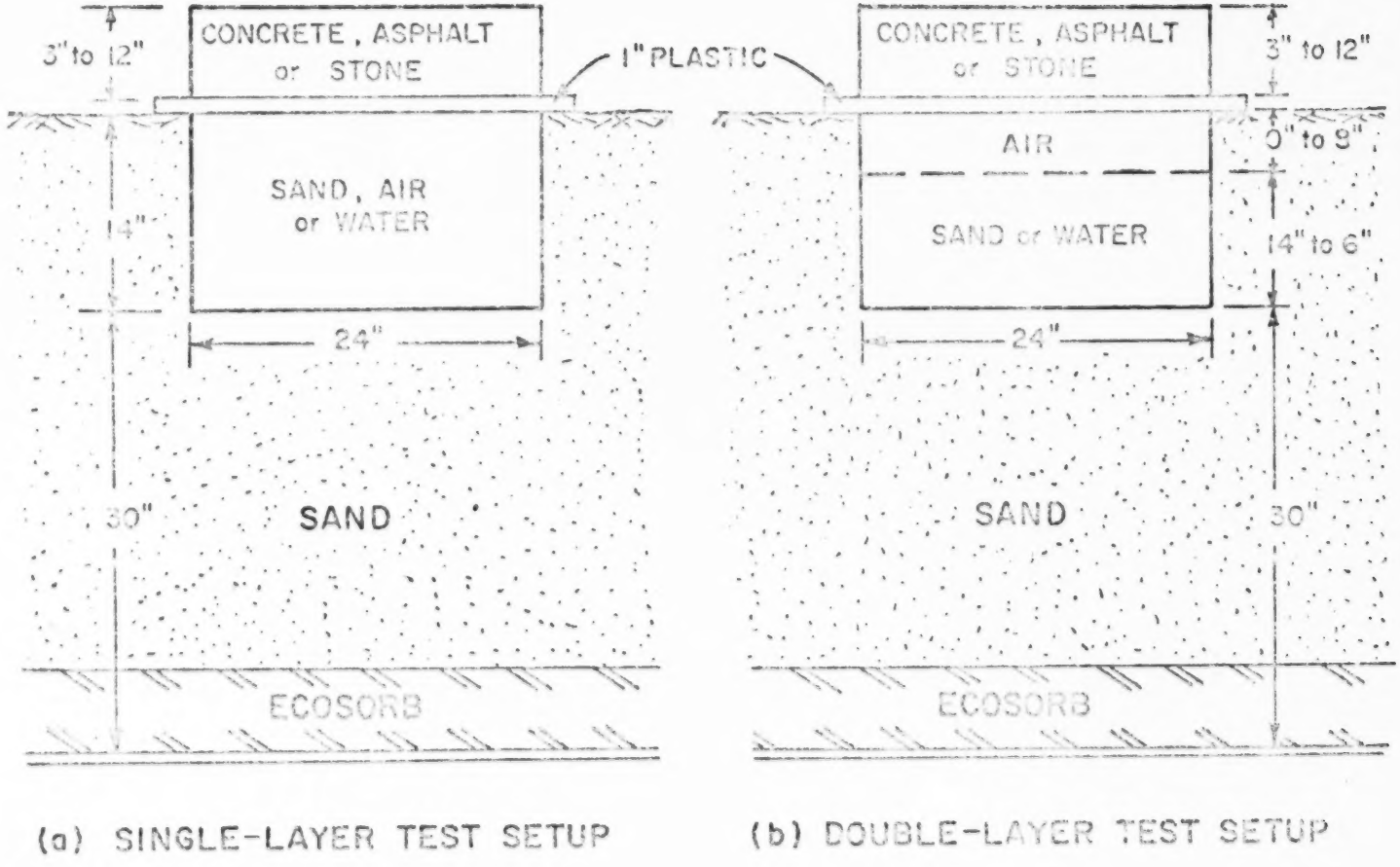


Figure 26. Schematic diagrams of single-layer and double-layer test setups.

were made through the plastic sheet to a metal plate buried in the sand, no errors for the measured depth to the metal plate occurred. These results, together with the fact that the plastic thickness was only a small fraction of a wavelength, suggested that the plastic sheet had little, if any, effect on the main test results. The results of these single-layer tests are listed in Table 12 (on the basis of known upper-layer thickness and then calculating n from one set of data and calculating the other two). The following general trends can be seen in this tabulated test data.

1. Whenever a test parameter was varied (upper material, lower material, or thickness of either), there was a noticeable change in the return pattern (from oscilloscope patterns).

2. The thicker the upper-layer material, the lower the n values of the system (Table 12).

3. In general, the n values for tests using concrete were greater than those for tests using asphalt or stone, which produced approximately equal results (Table 12).

4. For a given upper material, the n values for sand tests appear to be somewhat greater than for air tests and much greater than for water tests (Table 12).

5. Using the known n value calculated from the sand tests, reasonable predicted depths of the upper layer for the air and water tests (Table 13) were calculated.

6. This same comment can be offered for the air test data, which was used to calculate depths for sand and water tests (Table 13).

7. Results were poorer using n values from water test data and then calculating the sand and air test depths (Table 13).

TABLE 12. Results of Single Layer Tests on Calculated "n" Values Using Known Thickness of Upper Material

| Upper material | Thickness of upper material, (cm) | Calculated n for Underlying Material | | |
|---|---|---|---|---|
| | | Sand | Air | Water |
| Concrete | 7.5 | 8.0 | 7.3 | 11.2 |
| | 15 | 3.5 | 3.6 | 3.7 |
| | 23 | 2.6 | 2.7 | 2.5 |
| Asphalt | 15 | 5.5 | 5.0 | 1.7 |
| | 23 | 3.8 | 3.2 | 2.3 |
| | 28 | 2.9 | 3.1 | 2.7 |
| Stone | 15 | 7.1 | 5.0 | 1.8 |
| | 23 | 3.1 | 3.2 | 1.9 |
| | 30 | 1.9 | 2.0 | 1.7 |

TABLE 13. Results of Single Layer Tests on Calculated Thickness of Upper Material Based on n Value of Sand, Air, and Water, Respectively

| Upper Material | Nominal Thickness (cm) | n | Data base | Calculated d for Underlying Material | | |
|---|---|---|---|---|---|---|
| | | | | Sand, (cm) | Air (cm) | Water, (cm) |
| Concrete | 7.5 | 8.0 | Sand | 7.6 | 6.9 | 11.4 |
| | 15 | 3.5 | Sand | 15.2 | 15.7 | 16.3 |
| | 23 | 2.6 | Sand | 22.9 | 23.6 | 21.8 |
| Asphalt | 15 | 5.5 | Sand | 15.0 | 14.0 | 4.8 |
| | 23 | 3.8 | Sand | 22.9 | 19.1 | 13.7 |
| | 28 | 2.9 | Sand | 27.9 | 29.7 | 25.9 |
| Stone | 15 | 7.1 | Sand | 15.2 | 10.9 | 3.8 |
| | 23 | 3.1 | Sand | 22.9 | 23.4 | 14.2 |
| | 30 | 1.9 | Sand | 30.5 | 33.5 | 27.9 |
| Concrete | 7.5 | 7.3 | Air | 8.4 | 7.5 | 12.7 |
| | 15 | 3.6 | Air | 14.7 | 15.2 | 15.7 |
| | 23 | 2.7 | Air | 22.4 | 22.9 | 21.1 |
| Asphalt | 15 | 5.0 | Air | 16.5 | 15.2 | 5.3 |
| | 23 | 3.2 | Air | 27.7 | 22.9 | 16.8 |
| | 28 | 3.1 | Air | 26.2 | 27.9 | 24.1 |
| Stone | 15 | 5.0 | Air | 21.3 | 15.2 | 5.3 |
| | 23 | 3.2 | Air | 22.4 | 22.9 | 13.7 |
| | 30 | 2.0 | Air | 28.7 | 30.5 | 31.0 |
| Concrete | 7.5 | 11.2 | Water | 5.3 | 5.1 | 7.6 |
| | 15 | 3.7 | Water | 14.2 | 14.7 | 15.2 |
| | 23 | 2.5 | Water | 24.1 | 24.6 | 22.9 |
| Asphalt | 15 | 1.7 | Water | 47.5 | 43.7 | 15.2 |
| | 23 | 2.3 | Water | 37.8 | 31.5 | 22.9 |
| | 28 | 2.7 | Water | 30.5 | 32.5 | 27.9 |
| Stone | 15 | 1.8 | Water | 60.2 | 42.7 | 15.2 |
| | 23 | 1.9 | Water | 37.1 | 38.1 | 22.9 |
| | 30 | 1.7 | Water | 34.3 | 37.1 | 30.5 |

These tests using a single layer (to predict the existence of a void) were followed by a second test series of double-layer tests aimed at predicting the thickness of the void between an upper and lower layer. The upper layer again consisted of concrete, asphalt, or stone (in varying thickness); the lower layer was either sand or water; and the intermediate layer (the void) was air (thickness from 0-20 cm (0-8 in.)) The test schematic is shown in Figure 26b. The theory of interface patterns for the double-layer case is tedious, but straightforward, and can be found in most texts on optics. Much effort was devoted to seeking trends in the resulting test data and in attempting to correlate it with theory, but these efforts were relatively unsuccessful. The only test results found that appear to be significant are presented in Table 14, which was generated on the basis of return signal strength at minimum frequency. The following trends in the data of Table 14 can be noted:

- Return signal strengths increase as the thickness of the upper layer increases.
- Return signal strengths are strongest for the asphalt tests, weakest in the concrete tests, and intermediate for the stone tests.
- Return signal strengths do not appear to be influenced strongly by air void thickness.

The generalized results of this laboratory test program using a CW microwave method to locate voids beneath paved areas as presented in this section can be summarized as follows:

- The first test series (i.e., the single-layer tests) showed marked differences in n values or predicted thicknesses for the upper layer between sand, air, and water trials. This led to the basis of the field measurement technique where one would traverse a part of the paved surface to see if changes in return pattern are obtained from other areas. If so, a void would be indicated. In either the air- or the water-filled condition, the void then could be traced to see how far it extends.
- The second test series (i.e., the double-layer tests) showed very little difference in return signal strength for increasing void thickness. Therefore, it appears as though the microwaves could not propagate through the void and return with sufficient signal strength to be measured. In other words, void depth cannot be determined by the method, at least for the equipment we used.

In conclusion, we feel that the CW microwave method can be used to locate voids beneath unreinforced paved areas (reinforcement effects have not yet been evaluated) and is a useable NDT method for mapping out the two-dimensional extent of voids. For cases where the pavement thickness varies, additional care must be exercised so that changes in the reflected patterns are not incorrectly interpreted as voids. If the variation is gradual, this should be recognizable.

TABLE 14. Results of Double-Layer Tests of Effect of Void Thickness on Signal Strength at Minimum Frequency

| Layer composition | Thickness of upper layer, cm | Signal Strength (volts) at Void Thickness (cm) | | | | | |
|---|---|---|---|---|---|---|---|
| | | 20 | 15 | 10 | 5 | 2.5 | 0 |
| Concrete/air/sand | 7.5 | 0.07 | 0.06 | 0.07 | 0.08 | 0.19 | 0.05 |
| | 15 | 0.17 | 0.24 | 0.24 | 0.36 | 0.30 | 0.25 |
| | 23 | 0.40 | 0.40 | 0.32 | 0.30 | 0.33 | 0.35 |
| Concrete/air/water | 7.5 | 0.42 | 0.26 | 0.40 | 0.15 | 0.31 | 0.20 |
| | 15 | 0.32 | 0.33 | 0.32 | 0.17 | 0.27 | 0.24 |
| | 23 | 0.34 | 0.32 | 0.34 | 0.41 | 0.50 | 0.42 |
| Asphalt/air/sand | 15 | 1.40 | 1.00 | 1.50 | 1.80 | 2.10 | 2.25 |
| | 23 | 2.30 | 2.40 | 2.30 | 2.10 | 2.00 | 2.40 |
| | 28 | 1.50 | 1.50 | 1.90 | 1.90 | 1.90 | 1.80 |
| Asphalt/air/water | 15 | 1.30 | 1.10 | 1.55 | 1.50 | 2.15 | 2.40 |
| | 23 | 2.20 | 2.40 | 2.30 | 2.20 | 2.10 | 2.00 |
| | 28 | 2.40 | 2.50 | 2.50 | 2.40 | 2.40 | 2.40 |
| Stone/air/sand | 15 | 0.28 | 0.26 | 0.24 | 0.26 | 0.28 | 0.30 |
| | 23 | 0.44 | 0.38 | 0.44 | 0.46 | 0.34 | 0.37 |
| | 30 | 0.37 | 0.41 | 0.39 | 0.37 | 0.30 | 0.38 |
| Stone/air/water | 15 | 0.21 | 0.20 | 0.23 | 0.30 | 0.37 | 0.50 |
| | 23 | 0.42 | 0.40 | 0.40 | 0.26 | 0.72 | 0.32 |
| | 30 | 0.82 | 0.82 | 0.84 | 0.62 | 0.64 | 0.60 |

(b) Field Tests Using Continuous-Wave Microwave Method

1. Steel-Plate Detection

The objective of this first field test series was to evaluate the modified continuous wave microwave system in locating a steel plate suspended in an open hole at different depths below ground level.

The tests were conducted as follows. A local contractor provided the equipment and manpower for the excavation of two holes. Both holes had a two-meter-square surface opening. One hole was excavated to a depth of one meter; the second hole was excavated to a depth of two meters. A 1.3 x 1.3 m, 16-gauge, stainless-steel plate was then installed in the 1-m-deep hole. The hole was left open. The antennas were then placed over the hole. Microwave reflection responses were then recorded on an X-Y plotter for the frequency range of .01 GHz to 2.4 GHz. The metal plate was then placed at the bottom of the 2-m-deep hole, with the hole kept open as in the previous test. Microwave reflections were then recorded on an X-Y plotter for the frequency range of .01 GHz to 2.4 GHz.

Results of this experiment showed that the microwave interference patterns accurately predicted the depth to the plate when no backfill was in place. It was also found that the edges of the steel plate could be observed so that location monitoring as well as depth monitoring can be obtained using the method. However, when moist backfill was placed on top of the plate, the system had insufficient power to penetrate to the plate.

2. Water-Table Detection

A field study was conducted to detect subsurface seepage using continuous-wave microwaves. Two 55-gallon drums of water equipped with a valve and hose at the bottom were situated on the sites in Bellmawr, New Jersey. By burying the hose at the top of a hill and pointing it downhill, the water was made to run close to the surface and to fan out. Microwave measurements were taken before and after the seepage was established. Holes were then made to find the actual depth to the saturated soil after the drum of water had emptied.

The first seepage study was performed on a 45° slope with microwave stations positioned as shown in Figure 27. Microwave measurements made after draining the water into the soil show anomalous shallow reflections at stations #1, #2, and #5 when compared with the deeper reflections at stations #3, #4, #6, and #7. These shallow reflections are apparently coming off the seepage. Microwave measurements at stations #8, #9, and #10 are about the same, indicating that the seepage did not reach these stations.

Holes were then bored to verify the microwave depths. Saturated soil was located only at stations #1, #2, and #5, just as predicted by the microwaves. The holes at all other stations were dry. A difference was found between the microwave and actual depths to the water. The microwaves appear to be reflecting from within the seepage stream, not from its actual surface. Microwave measurements, therefore, were more useful at locating the boundary of the wetted area than the depth to the water. Reflections from the dry holes (#3, #4, #6, #7, #8, #9, #10) are thought to be coming from a change in soil type, because borings showed the soil to change with depth.

Seepage study #2 yielded the results shown in Figure 28. Microwave measurements were made both before and after the seepage began. These depths differ, although not in the right direction, since the reflections from the seepage stream are deeper than the reflections before the seepage was started. Next, holes were dug to determine the actual depth to the seepage stream (marked "extent of wetted area" in Figure 28). In all cases the microwaves predicted greater depths to the saturated soil just as they did in the prior seepage study. Reflections appear to be coming from inside the seepage stream and not its surface. A certain "skin depth" of penetration appears to be associated with these relatively shallow probes. Microwave depths before seepage and after the seepage began, outside of the wetted area, are believed to be the depths to differences in soil type.

Continuing with these seepage studies, a third field study was per-

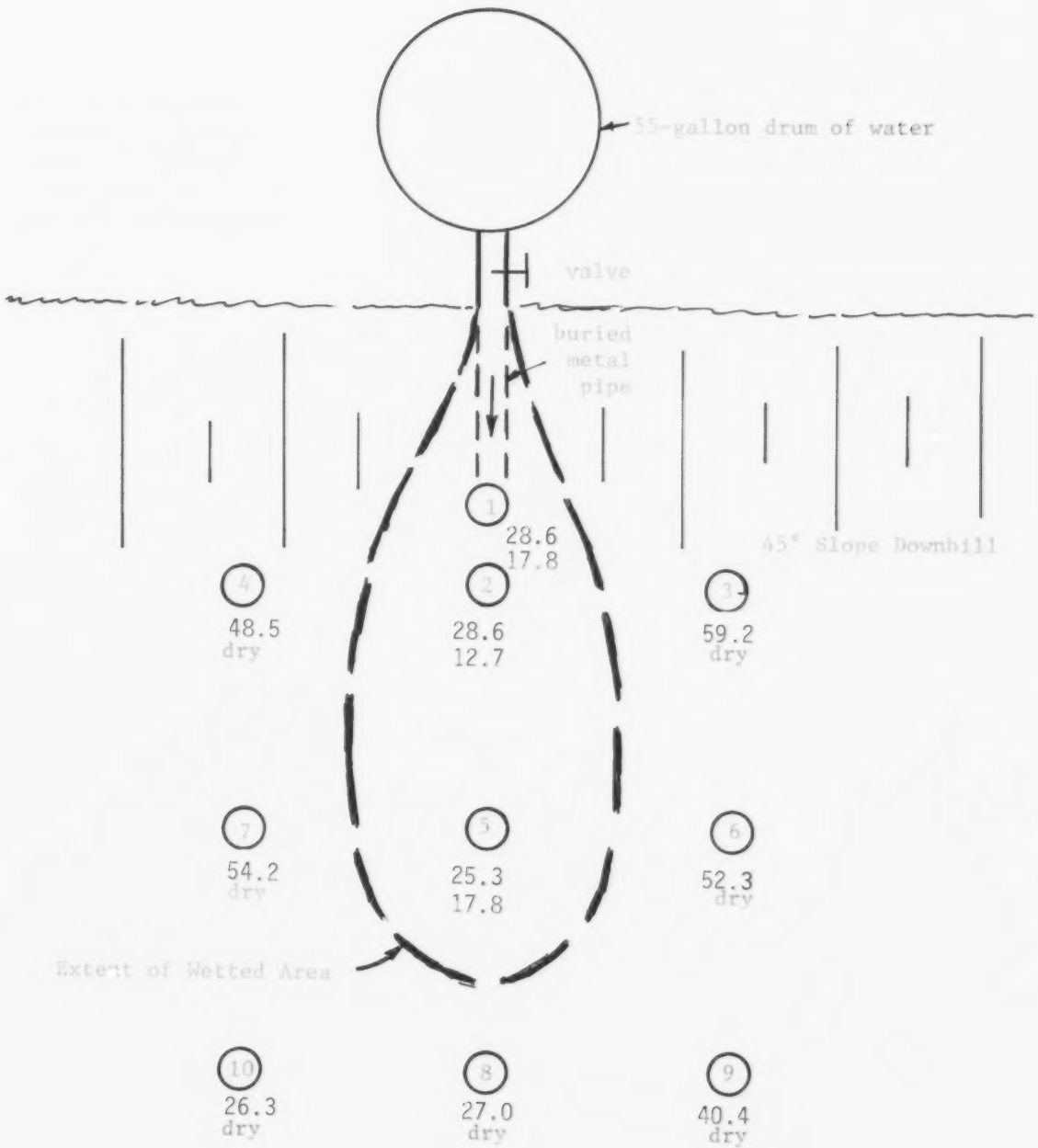


Figure 27. Seepage Study #1 at Bellmawr, New Jersey. The circled numbers identify the measurement stations. The top number under each circle is the interface depth in centimeters measured with the microwave system. The lower number is the depth to water measured in the bored holes.

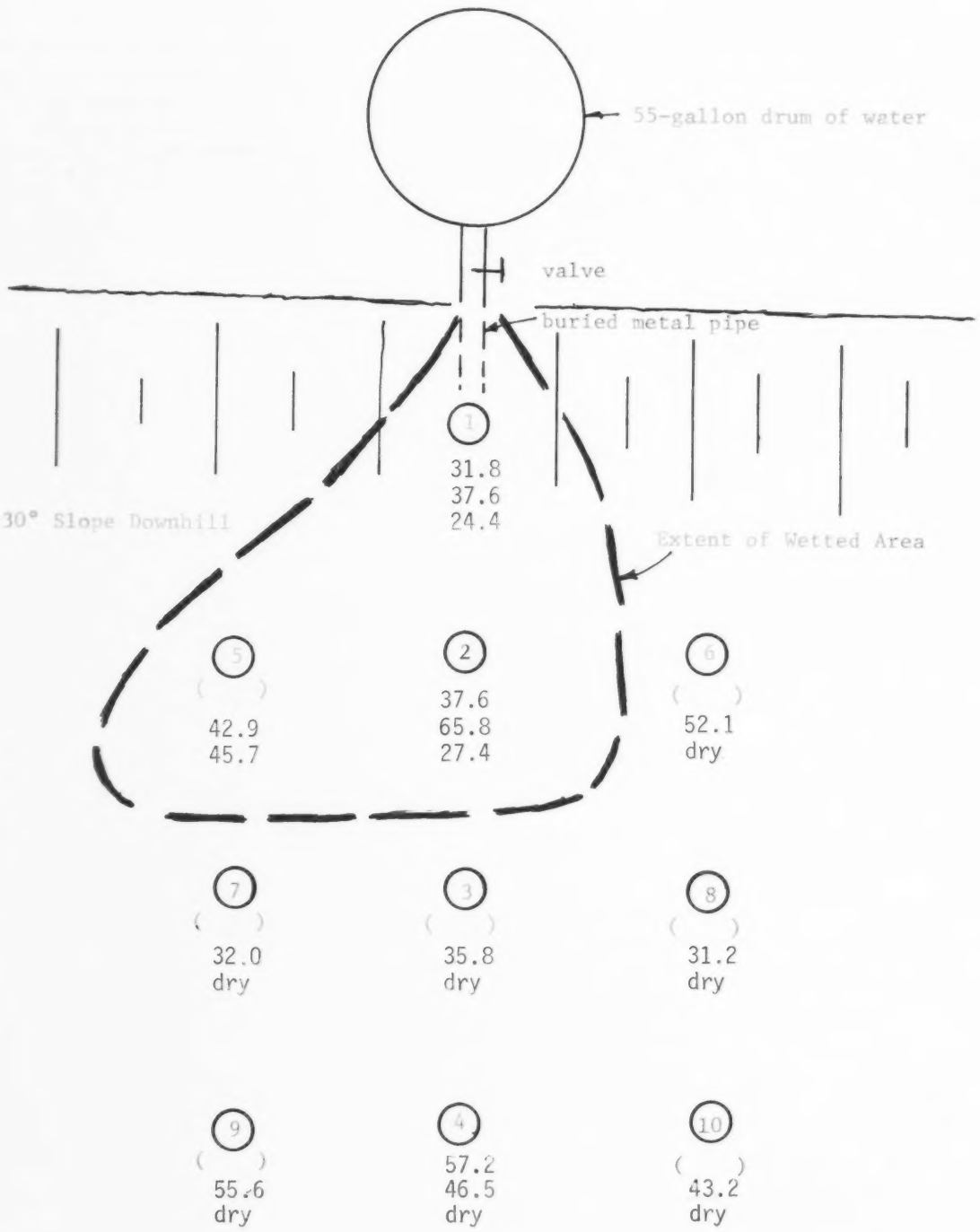


Figure 28. Seepage study #2 at Bellmawr, New Jersey. The circled numbers identify the measurement stations. The top number under each circle is the interface depth in centimeters measured with the microwave system before seepage was begun. The lower number is the depth to water measured in bored holes.

formed at the Bellmawr, New Jersey, site. A 55-gallon drum of water was drained through a hose into the top of a 45° slope. All the water was allowed to drain into the hill and a seepage stream was established before microwave measurements were made. The slope was marked with stakes on 0.6 m (2 ft) centers where the microwave measurements were to be made. Microwave measurements were made both before and after the seepage stream was started in order to observe any change in the microwave reflections. After all measurements were made, a post-hole auger was used to bore down to water at each station. These measurements were used to verify the microwave depths to the seepage stream.

All measurements made during the study are collected in Figure 29. No obvious trend in the data is noticeable except that, at most of the stations, all depths seem to be about the same (within several centimeters). At stations #1, #2, #6, #8, #9, and #11, though, there is a large difference between the measured depths and the actual depths. Possibly, the soil may have had a high enough water content to reflect microwaves at the same depth the water hose was buried in the ground. Thus, when the seepage stream was created it had no additional effect on the microwaves. When holes were dug at each microwave station, the sandy soil was found to have more clay fines and be wetter with greater depth. It was difficult to determine an exact depth to water with the auger. Often only the depth to completely saturated soil could be determined.

3. Top of Rock Detection

A field survey was made at a site in King of Prussia, Pennsylvania, in order to locate the surface of limestone rock beneath the overlying soil. This site is located about 32 km north of Philadelphia and was chosen because of a shallow blanket of grouted soil underlying a level-surfaced upper soil layer. Beneath the area is a limestone bedrock that is subject to solution by groundwater. As a result, its surface is very irregular, with localized zones where the rock was dissolved away to great depths. Many sinkholes exist. Such an area is properly called Karst topography and is prevalent in the King of Prussia area. Building on such a site is dangerous, because the structure may be founded on a sinkhole or one may form under the structure after it is built. In fact, a structure was built on this particular site, and it settled, resulting in large cracks in its walls. Borings were taken and cement grout was pumped into them in order to fill any air-filled sinkholes near the building. The result was a shallow layer of grouted soil formed around the building.

Depths to rock vary from about 4 m to 11 m, as determined from borings. The grout blanket, however, started about a 0.3 m or less under ground surface.

Microwave stations were set up around two sides of the building in an attempt to locate any sinkholes near the structure's foundation. The microwave method showed its unique ability to "see through concrete and asphalt surfaces" in addition to "seeing through the soil."

The first survey line was run several feet from the side of the building,

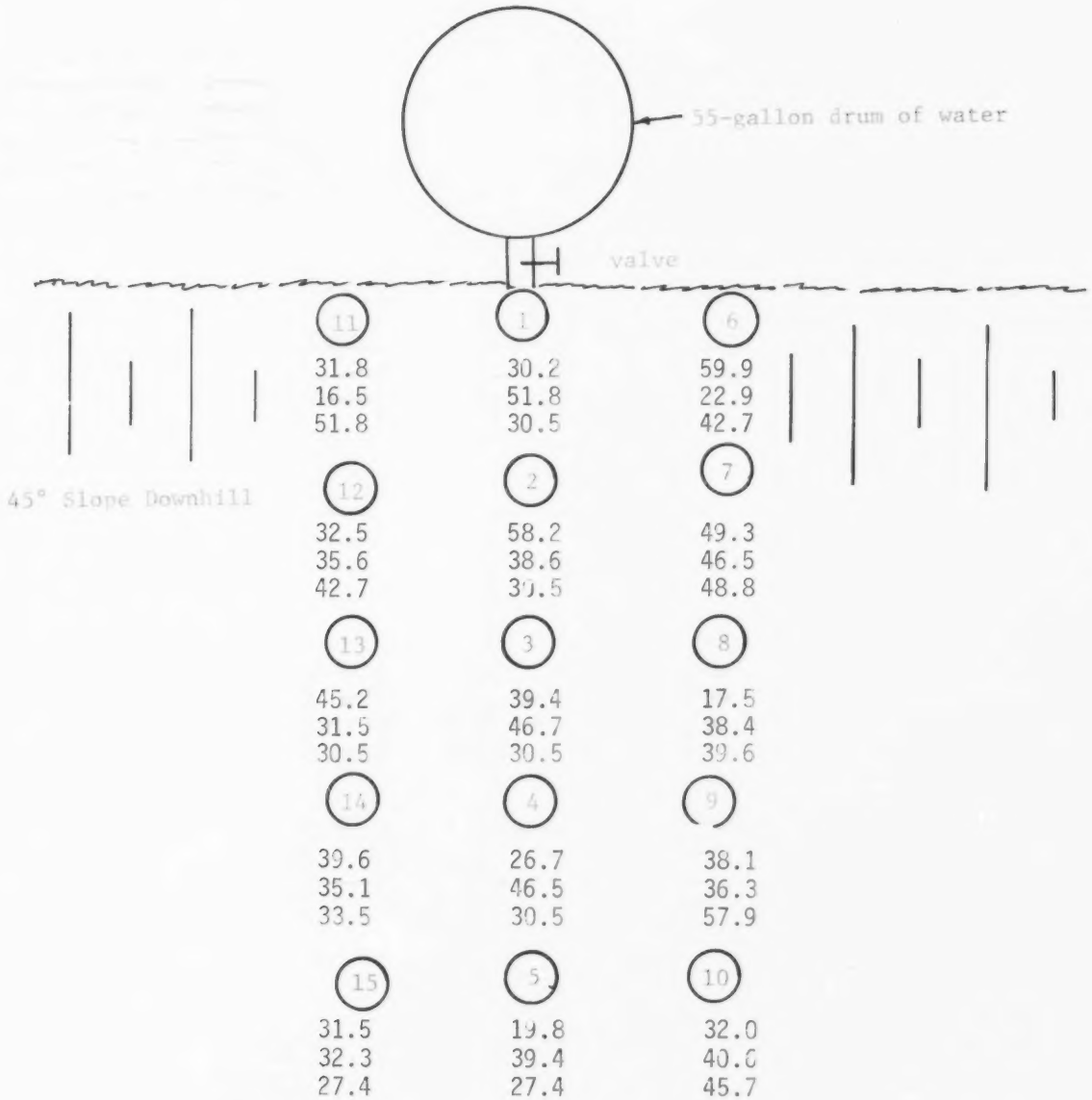


Figure 29. Seepage study #3 at Bellmawr, New Jersey. The circled numbers identify the measurement stations. The top number under each circle is the interface depth in centimeters measured with the microwave system before seepage was begun. The lower number is the depth to water measured in bored holes.

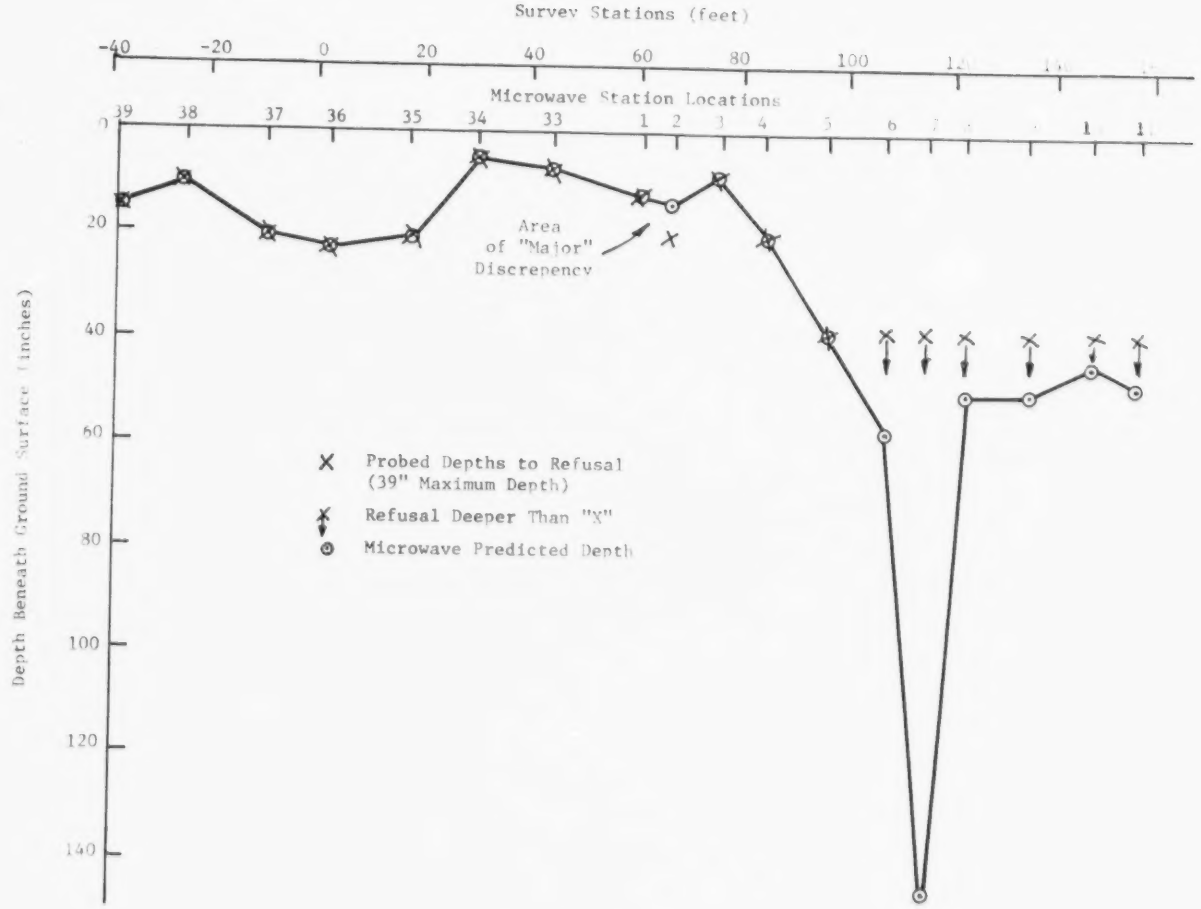


Figure 30. Results of microwave survey at King of Prussia, Pennsylvania, site.

and its results are shown in Figure 30. A dielectric constant of 4 was used to calculate all depths and was found to be correct by back-calculating it once the depth to rock was determined by a sounding rod. Depths to the limestone as determined by the continuous-wave microwave unit were substantiated by driving a rod through the overburden to the rock for microwave stations 39 to 5. In all cases but three, the microwave and the actual depths agreed to within 5 cm. For one case, at station #2, the difference was 10 cm. At the other stations the depth to rock as determined by the microwave survey correlated exactly with the soundings. For example, between stations #35 and #36 there was a drainage pipe carrying water out of the subsoil. The grout surface was determined by microwaves to be deeper under these stations than under neighboring stations. Since the relatively large amounts of water flowing from the drainage pipe between these stations could have dissolved some of the limestone away, the microwave measurements seem logical in indicating a depression in the grout blanket's surface. A reading at station #7 predicted the depth to rock as 3.7 cm and was the deepest microwave reading obtained in any of these studies. The deep sinkhole region at station #7 is precisely the type of information that is desired in this type of building foundation survey. The grout blanket appears to be discontinuous here and the microwaves appear to be reflecting from the underlying rock. The width of the sinkhole is only 3 m and could be easily missed by a boring survey. With this information, the sinkhole's location is known and a boring can be made or grout can be injected to help stabilize the foundation.

Depths to a blanket of grout a 30 cm or so under the ground surface were determined to within several centimeters using the microwave unit. The shallowest and deepest penetrations at any site were also observed here. The depth to the grout 8 cm under the surface was verified, and the depth to rock at 3.7 m (12 ft) was also determined. The microwave's high resolution allowed the depth to rock to be determined at exact points (within a 30 cm radius) and the degree of averaging out of the subsurface contours was negligible.

Owing to the success of this effort, an adjacent area (5 m x 3.7 m) was mapped out to provide a "ground truth" test site. Shown on Figure 31 is a three-dimensional sketch of predicted and actual depths to the top of rock. (The actual depths were obtained by probing with a steel rod.) The results are seen to be excellent.

4. Void Detection

Past laboratory studies showed it is possible to detect air or water through 30-45 cm (12 in. to 18 in.) of concrete or brick with the microwave field unit. Only a weak and uncertain response occurred when trying to detect a concrete-to-soil interface. In order to see if the same effect occurs in the field, the antennas, on 30-m cables, were lowered into a storm sewer tunnel in Reading, Pennsylvania. It was proposed to locate air- or water-filled voids on the outside of the tunnel lining from within by beaming microwaves through the tunnel lining and observing the reflections. If reflections occurred and were sharp, then a void should exist on the outside of the tunnel lining.

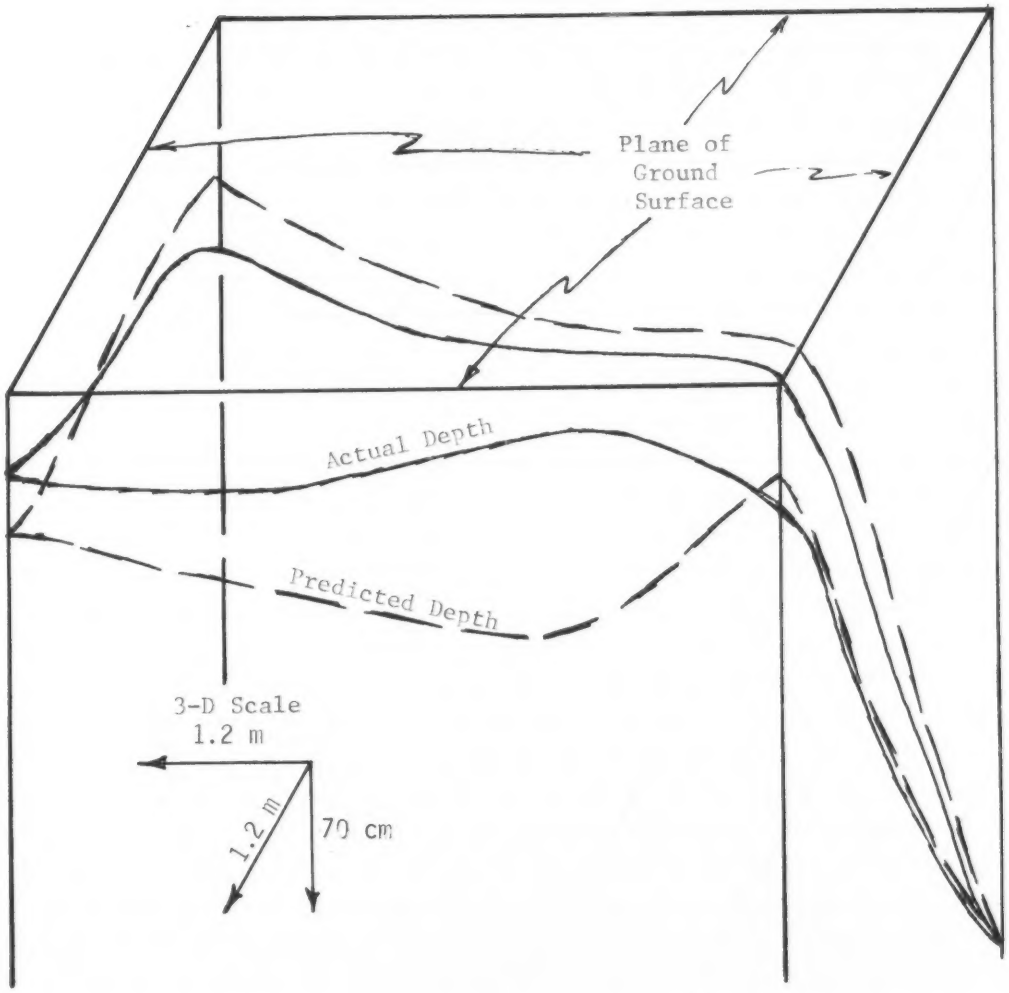


Figure 31. Three-dimensional plot of area surveyed showing ground surface, microwave-predicted depth to rock, and actual probed depth to rock.

Two different sections of storm drain were roughly surveyed in order to see if the technique was feasible. The tunnel lining was wet and in some areas the bottom was completely eroded away, exposing the soil. The microwave antennas were moved around the circumference of the tunnel while someone topside, with the generator equipment, watched the change in waveform. In one section, good reflections were obtained from 4 o'clock to 8 o'clock, in the lower portion of the tunnel, possibly indicating the presence of air or water behind the tunnel lining. In the upper portion of the tunnel, between 8 and 4 o'clock, no reflections occurred (the waveforms had only one peak) possibly indicating a good contact between the tunnel lining and the soil. Other tunnel sections gave good reflections from 1 to 10 o'clock, in the lower part, and some reflections, in one small area, persisted for 360° around the lining. The size of the void areas behind the tunnel, producing the reflections, could not be determined since the microwaves reflect from the first interface they encounter.

Besides running circumferential surveys, surveys along the tunnel's length were also performed on various lines on the tunnel's circumference, such as 8 or 10 o'clock. Both tunnel sections examined gave good reflections all the way along the survey at 8 o'clock and no reflections for the 10 o'clock survey.

Results were presented to the town's Engineering Office and the results were enthusiastically accepted. To this date, however, no ground truth measurements were made to confirm or deny our predicted void areas.

A surface microwave survey was also performed to detect voids under the street. Several cave-ins of the street had occurred in the past. Only air voids directly under the asphalt or concrete seemed to be detected. The tunnel itself was too deep to be detected from the surface. Voids beneath several concrete slabs were detected and could be visually observed through cracks in the pavement. Along the curb line, hollow zones were detected under the asphalt. Rainwater had probably eroded away the soil under the curb. No definite voids under the center of any of the streets were detected but some sporadic microwave reflections occurred in some streets more than others. No reflections occurred under a surveyed street that did not have the tunnel under it.

## Section 8

## PULSED RADIO-FREQUENCY METHOD

As noted in the overview section, section 2(c), a pulsed system differs greatly from a continuous system. Pulsed methods are based on time of travel of a wave penetrating the soil, then reflecting back to the ground surface. The signal is sensed and displayed on an Alden-type recorder for a visual image, in black and white, of subsurface conditions.

Since a few systems are commercially available, we purchased one for this portion of the project. The system was a GSSI-SIR System 7 from Geophysical Survey Systems, Inc., of Hudson, New Hampshire. Details will be described as we present the laboratory and field tests conducted using this system.

### (a) Laboratory Tests

#### 1. Sensitivity Study

Much of the supporting data acquired for the previously presented continuous-wave microwave system is applicable to the pulsed RF system, including dielectric constants and attenuation coefficients. However, data interpretation is somewhat different for the two systems. The continuous-wave microwave system merely involves recognizing peaks due to interference patterns but the pulsed RF system requires much interpretation between true reflections and background "noise". Therefore, a sensitivity study of the pulsed system was performed.

The objective of this study was to determine the minimum amount of power that can be reflected and printed. These reflections often cause difficulties in the interpretation of the signal. Along with this determination, the dielectric discontinuity needed to produce this minimal power reflection was determined.

To accomplish these goals, a review of the literature concerning electromagnetic (EM) properties was undertaken. Table 15a, b and c shows relative dielectric constant ($\varepsilon'$), conductivity ($\sigma$), and index of refraction (n) at several frequencies for different soils under various conditions. With these values and using equation 33, the percent reflected power for several situations was calculated (Table 16).

$$R_n = \left[\frac{n_1 - n_2}{n_1 + n_2}\right]^2 \times 100 \qquad (33)$$

where $R_n$ = percent of power reflected
$n_1$ = index of refraction of upper stratum
$n_2$ = index of refraction of lower stratum

Examination of Table 16 shows that the reflective power generally is a low percentage (less than 10%) of the total power, and density variations cause minimal power reflection (< 7%).

Having determined from the literature that density changes reflect a minimal amount of power, a laboratory experiment was carried out to interpret the signal visually using a GSSI-SIR Model No. 7 and a 900-MHz transceiver. The transceiver was passed horizontally (left to right) over a uniformly-filled and compacted box of sand (Figure 32b). This resulted in a trace shown in Figure 33a. Examination of this trace (Figure 33a) reveals that for an range of approximately 30 cm, (surface to depth of 30 cm), the direct coupling of the transmitted signal to the receiver eliminates all reflected signals. Below a depth of 30 cm, the trace shows relatively uniform layers of soil. At this point, a trench with sloping sides was excavated in the center of the sand. The trench was then backfilled with loose sand, as shown in Figure 32c. Using the same GPR equipment, the transceiver was passed over this setup, which resulted in the trace shown in Figure 33b. Again the first 30 cm of depth is darkened due to direct transmission. Beginning at a depth of 45 cm the sloping sides of the trench become evident. Thus a minimal density variation can be readily detected using this particular system.

Comparison of these experimental results with those found in the literature brings forth several noteworthy conclusions. First, Rosenfarb et al. (22) showed that the minimum detectable density contrasts correspond to dielectric differences of less than 1 (recall Table 15c). This small change will cause less than 1% of the signal power to be reflected. Second, the experimental evidence proved that this small amount of reflected power will be detectable. Recalling that in the field non-homogeneous situations prevail, and minor density changes abound, one can conclude that GPR traces will often be cluttered. This can and has been a major obstacle in the interpretation of return patterns using pulsed-RF monitoring systems. It strongly suggests that signal enhancement techniques should be considered for interpretation of GPR signals. This might be approached in one of two ways:

- Using computer methods, as in signal-enhanced seismology.
- Using an empirical approach, as in electrical resistivity methods.

Knowledge of the extreme sensitivity of the GPR system will at least provide some relative basis for ranking the received signals to the individuals charged with interpreting the data . At the present, most interpretation of the signals is based on prior experience. However, for GPR to achieve a high reliability status, either a method of signal enhancement (as previously noted) or other techniques should be developed and employed.

TABLE 15a Electrical Parameters of Gray San Antonio Clay Loam, after Hipp (20)

| Parameters | Frequency (MHz) | $\sigma$ (Mho/m) | $\varepsilon'$ | $n = \sqrt{\varepsilon'}$ |
|---|---|---|---|---|
| w = 20% | 30 | 0.08 | 25 | 5 |
| | 120 | 0.1 | 20 | 4.47 |
| | 480 | 0.2 | 15 | 3.87 |
| | 960 | 0.3 | 13 | 3.60 |
| | 3840 | 0.5 | 13 | 3.60 |
| w = 5% | 30 | 0.01 | 9 | 3 |
| | 120 | 0.02 | 7 | 2.64 |
| | 480 | 0.05 | 6 | 2.45 |
| | 960 | 0.07 | 5 | 2.24 |
| | 3840 | 0.1 | 5 | 2.24 |
| w = 0% | 30 | -- | 3.5 | 1.87 |
| | 120 | -- | 3.5 | 1.87 |
| | 480 | 0.003 | 3.5 | 1.87 |
| | 960 | 0.006 | 3.5 | 1.87 |
| | 3840 | 0.02 | 3.0 | 1.73 |

TABLE 15b Electrical Parameters of Goodrich Clay and Suffield Silty Clay, after Hoekstra and Delancy (21)

| Soil | Parameters | Frequency | $\varepsilon'$ | $n = \sqrt{\varepsilon'}$ |
|---|---|---|---|---|
| Goodrich Clay | w = 10%<br>temp = +24 C | 100 MHz | 7 | 2.64 |
| Suffield Silty Clay | w = 10%<br>temp = +24 C | 100 MHz | 15 | 3.87 |
| | | 1 GHz | 12 | 3.46 |
| | | 10 GHz | 6 | 2.45 |

TABLE 15c Electrical Parameters of Kaolin Clay, after Rosenfarb et al. (22)

| Compaction | Frequency (MHz) | $\varepsilon'$ | $n = \sqrt{\varepsilon'}$ |
|---|---|---|---|
| loose | 20 | 1.3 | 1.14 |
| | 40 | 1.9 | 1.38 |
| | 60 | 2.5 | 1.58 |
| medium | 20 | 1.6 | 1.26 |
| | 40 | 2.5 | 1.58 |
| | 60 | 3.5 | 1.87 |
| dense | 20 | 2.4 | 1.55 |
| | 40 | 3.3 | 1.82 |
| | 60 | 4.4 | 2.10 |

TABLE 16 Calculated Powers of Reflection

| Soil | Frequency | $R_A$ | $R_B$ | Situation |
|---|---|---|---|---|
| Grey San Antonio Clay Loam | 30 MHz | 5.4 | 6.2 | 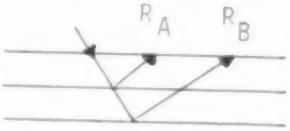 w = 0% |
| | 130 MHz | 2.0 | 6.6 | w = 5% |
| | 480 MHz | 1.8 | 5.0 | w = 20% |
| | 960 MHz | 1.6 | 5.4 | |
| | 3840 MHz | 1.6 | 5.4 | |
| Goodrich Clay Suffield Clay | 100 MHz | 3.5 | - | Goodrich |
| | 1 GHz | 1.8 | - | Suffield |
| | 10 GHz | 1.8 | - | |
| Kaolin Clay | 20 MHz | 0.25 | 1.1 | 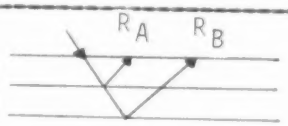 Loose |
| | 40 MHz | 0.46 | 0.50 | Medium |
| | 60 MHz | 0.71 | 0.33 | Dense |

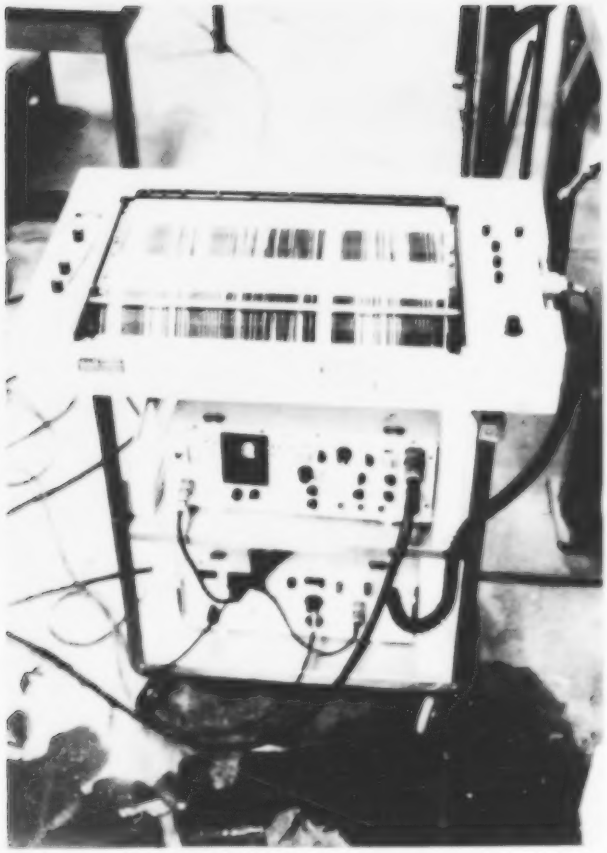

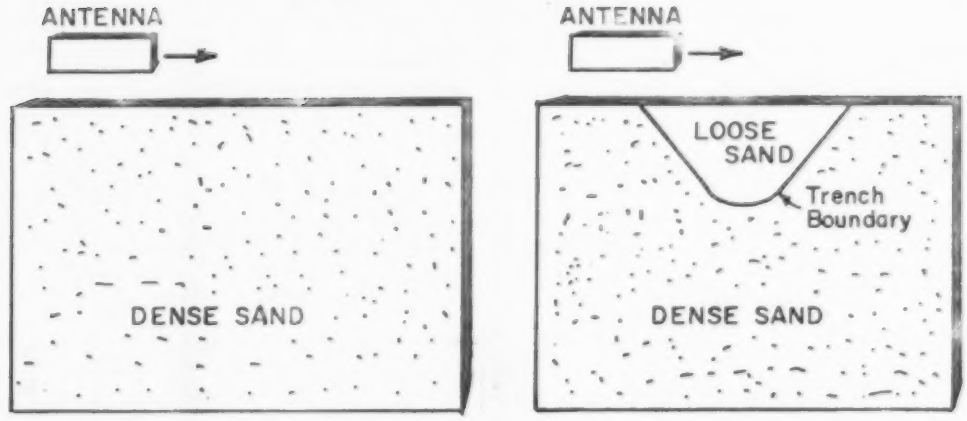


(b) Schematic Diagram of Box Filled with Uniform Dense Sand

(c) Schematic Diagram of Box with Excavated Trench Filled with Loose Sand

Figure 32. Photograph and schematic diagrams of Ground-Probing Radar (GPR) equipment and test setup.

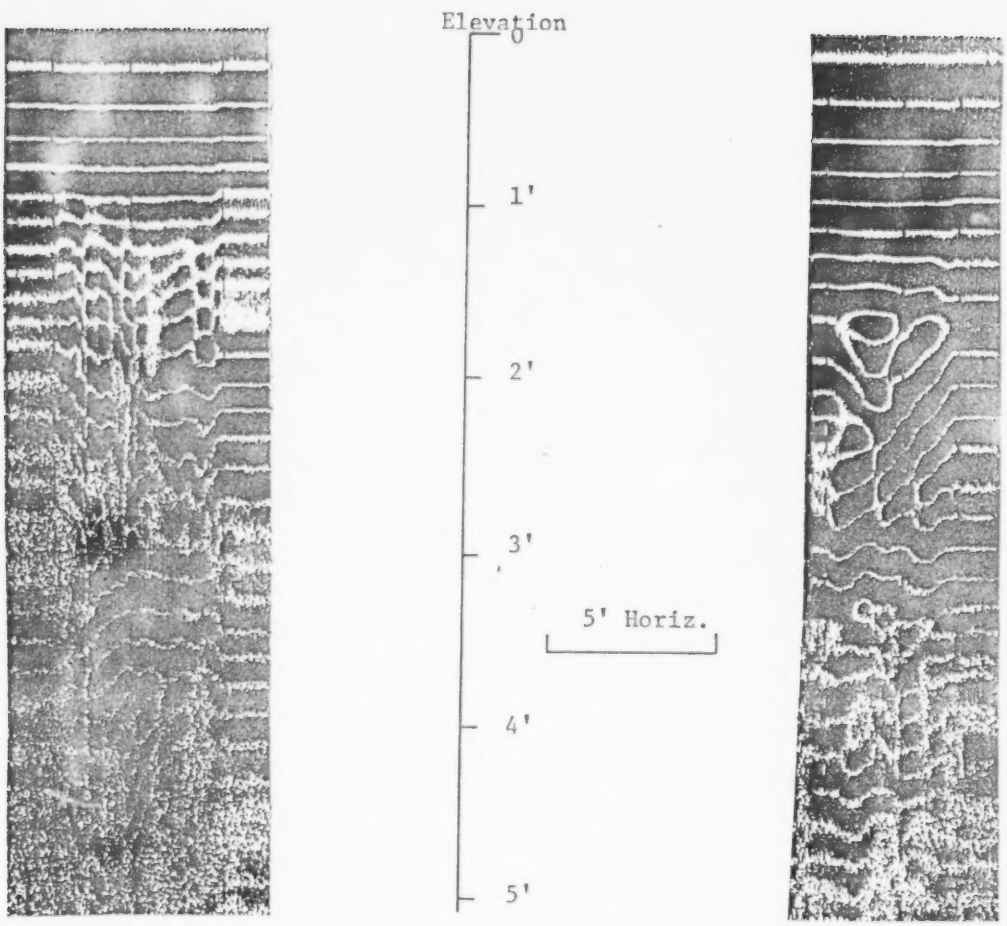


(a) Uniform Dense Sand Trace

(b) Trench Backfilled with Loose Sand

Figure 33. GPR traces of two different test setups showing the differences that density variation causes.

2. Polluted-Water Detection

Owing to the great sensitivity of the GPR technique, and coupled with the well-established fact that high ion content pore fluids severely attenuate EM waves, it can be hypothesized that the method can be used to distinguish soils containing hazardous wastes from soils containing non-polluted (at least with regard to conductivity) pore water. Using these features of the technique in an inverse manner, it is felt that GPR systems might identify subsurface liquid pollutants by virtue of the strength and nature of the return signals. The confirmation of this premise was the goal of this part of the laboratory test program.

A wooden box, measuring approximately 1 m x 1 m x 1 m was filled with a well graded, uniform density sand in the dry state. A 900-MHz transceiver was placed on the surface of the sand in the center of the box and a GPR trace was made. The system was described previously.

The next test was conducted in the same manner, but now the soil was partially saturated (at 33% saturation), and a GPR trace was made. Succeeding tests were performed at 67% and 100% saturation, thus making four separate tests in each series. To assure a well-defined reflecting surface, the bottom of the box in this first fresh water test series had a steel plate beneath it. The results of these four tests are shown in Figure 34. Note that these traces are time traces and that the time for the signal to travel from the soil surface to the bottom of the box increases as the percent saturation increases. Thus, to the signal, it appears as though the depth "d" increases as percent saturation increases. The ringing pattern on the traces is due to the individual pulses that were transmitted and their subsequent reflections.

This first test series was repeated in a similar manner except that the pore fluid was now a highly-concentrated salt solution, i.e., a 6.14-Molar sodium chloride solution that contained 36 g NaCl per 100 g water. The results for the four tests at 0%, 33%, 66% and 100% saturations are shown in Figure 35. In comparing this behavior with the behavior in the first test series, the severely attenuating nature of the high-ion-content pore fluid is easily seen. Furthermore, the number of bands present between the soils' surface and the steel plate has been significantly decreased. Thus both qualitative and quantitative distinctions can easily be seen.

To simulate field conditions more reasonably, the steel plate beneath the box was removed and replaced with "Eccosorb", a microwave attenuating material. Both of the previous test series were repeated (with fresh water and with the highly concentrated salt solution) with the Eccosorb material beneath the box containing the soil. Similar patterns to those with the steel plate were seen, with the major features being that the high-salt-concentration pore fluid significantly lightens the GPR trace, i.e., it attenuates the signal, and the number of pulse/reflection rings is again reduced.

On a qualitative basis it is easily seen that high salt concentrations in soil pore fluid significantly attenuate GPR signals. Furthermore, this

Reproduced from
best available copy.

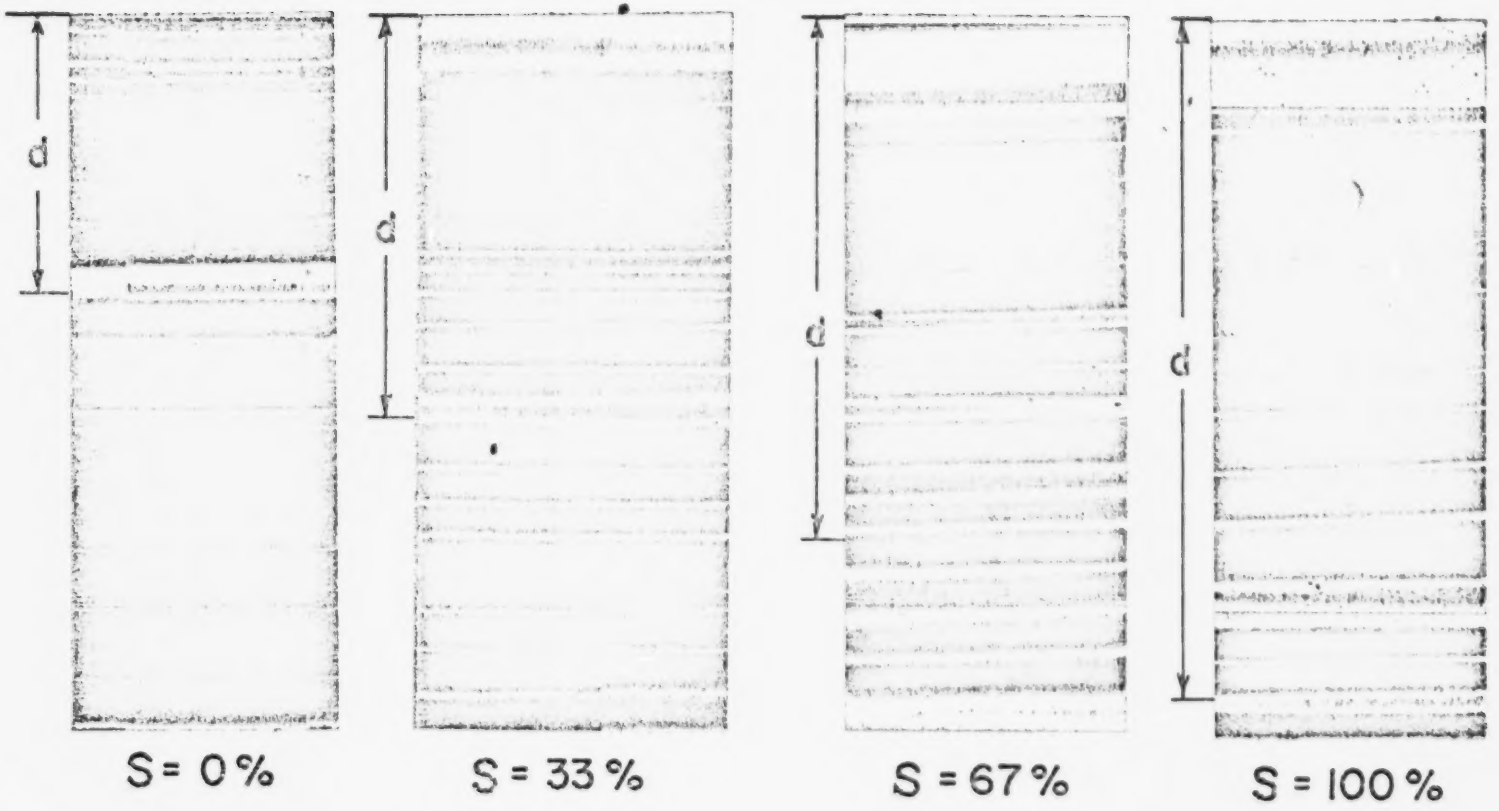


Figure 34. GPR traces of well-graded sand at varying water contents using fresh water with steel plate beneath box.

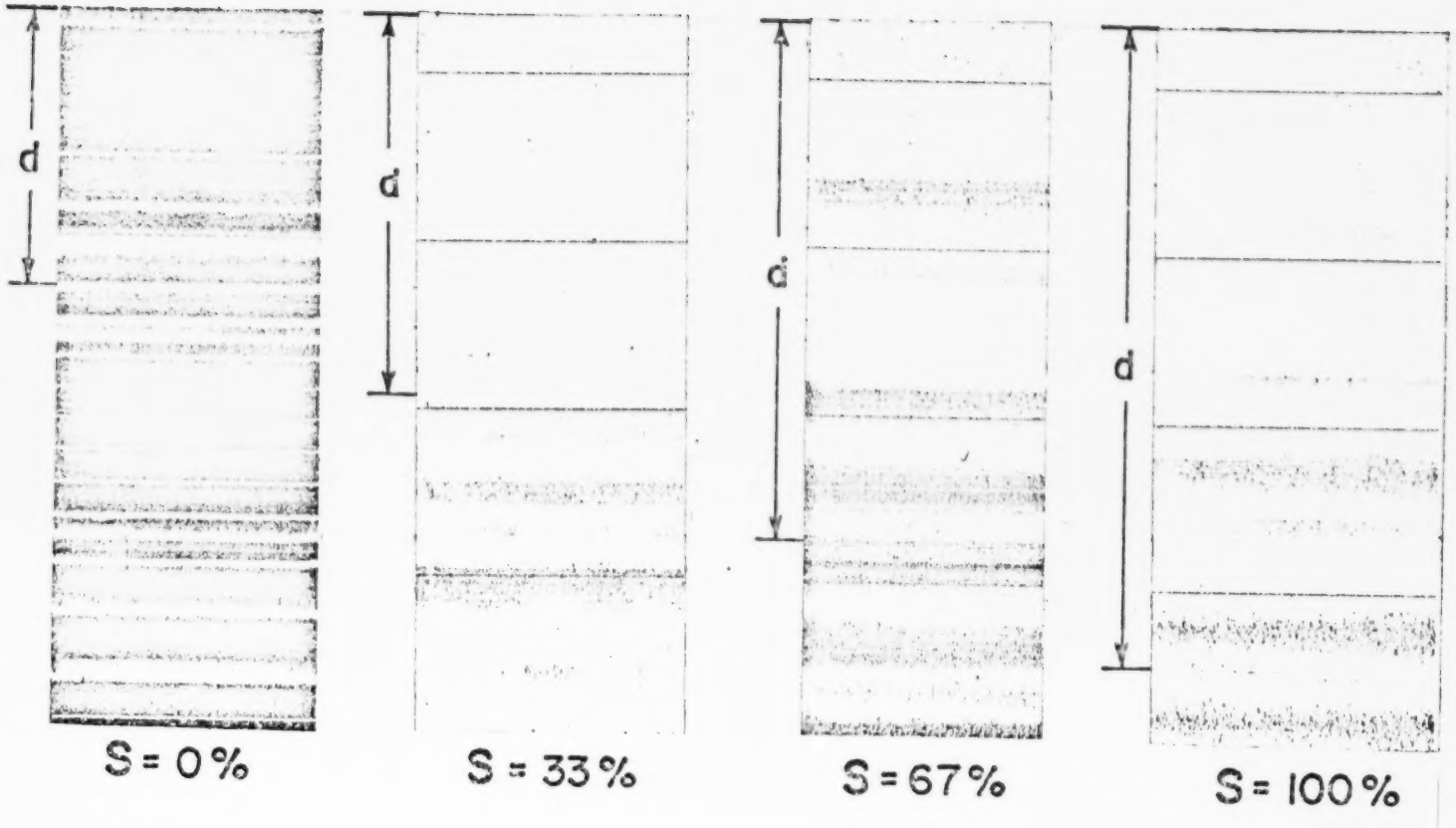


Figure 35. GPR traces of well-graded sand at varying water contents using salt saturated water with steel plate beneath box.

attenuation, as evidenced by the lightness of the GPR traces, increases with increasing degree of saturation.

In an attempt to quantify the process, the bands between the soils' surface and the bottom of the box have been counted and plotted in Figure 36. These bands, which are due to the transmitted pulses and their reflections, might be a tool that can be used to determine the presence of high-ion-content pollutants in soil pore water at various degrees of saturation, including the fully saturated case. Such a sweeping statement, however, must be further explored beyond the limits of this feasibility study. Our current ideas are listed in the following section.

Use of a pulsed RF method, as in the GPR system used in this study, to assess groundwater pollution in partially and fully saturated soils, needs additional work in the following areas:

- Pore-fluids with less than fully concentrated salt solutions need evaluation. Hopefully, the responses will fall within the limits shown in Figure 36.
- The detection of a salt-water layer beneath a fresh-water layer is important, and an attempt was made at its detection with the result shown in Figure 37a. The interface can be distinguished but it is not easily interpretable. It is, therefore, a limiting factor.
- Other pore-fluid pollutants than the sodium chloride used here should be evaluated and their effects compared with the results of this study. In this regard, acetone was used as a pore-fluid contaminant, with the results shown in Figure 37b for the 100% saturation case. Only minor attenuation of the signal is observed, so the technique is not at all responsive in this case.
- The effect of nonhomogeneous soil conditions must be evaluated. For example, a dry soil layer overlying the contaminated stratum must be evaluated to see if the stratigraphy masks out the response from the lower layer, which is the layer of interest.
- Other soil types, e.g., silts and clays, need investigation.
- Penetration depths must be determined before the practical utility of the method can be suggested. The maximum limit of the system used in this study is about 10 m in dry soil and 2 to 3 m in saturated soil. When the pore-fluid is more attenuating than fresh water, the combination could be severely limiting. Perhaps a lower-frequency transmitted pulse would be helpful in this regard.
- As with all exploratory research projects of this type where instrumentation is involved, "ground truth" measurements are essential. Actual sites of polluted ground water are attractive, but carefully controlled conditions are needed to determine the advantages and limitations of the procedure.

3. Small Void Detection

A laboratory study was carried out to determine if the pulsed RF system

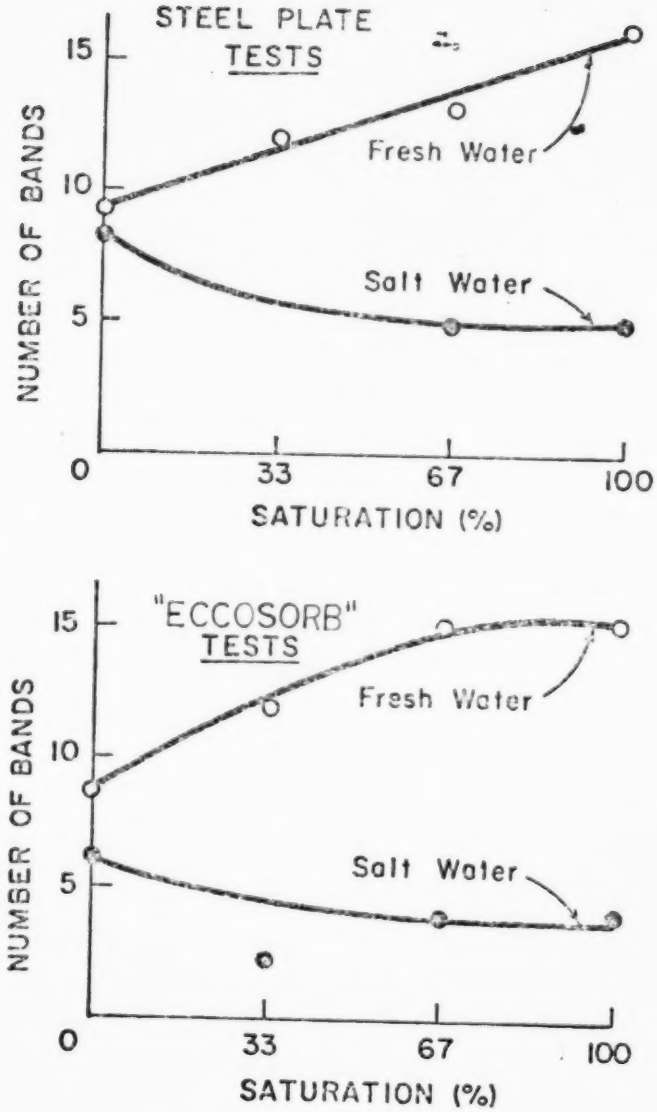


Figure 36. Pulse/reflection bands showing differences between fresh water and salt water tests at all saturation states from dry to saturated.

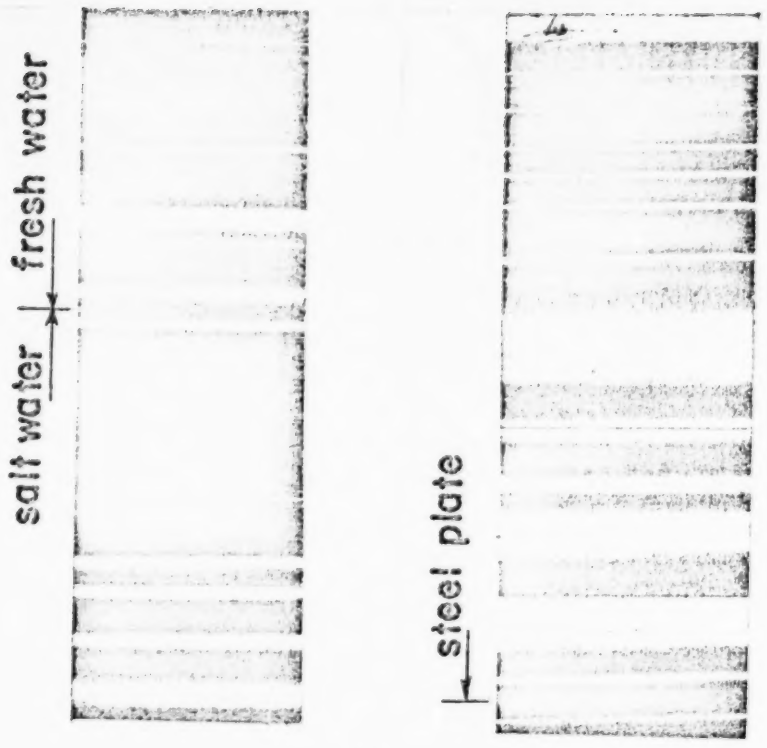


(a) 30 cm Sand Saturated with Fresh Water Above 30 cm Sand Saturated with Salt Water

(b) Uniform Sand Saturated with Acetone as a Pore Fluid Contaminant

Figure 37. GPR traces of uniform well-graded sand in other possible situations.

could detect small voids (7-cm diameter) in soil. Figure 38 shows the general test setup of the wooden soil box used for these tests. The soil was a dense clayey silt, placed in approximately 3-cm layers at 15 to 20% water content (near its optimum) to a total unit weight of approximately 2.1 g/cm$^3$ (130 PCF). A 3-inch (7-cm) steel pipe was placed near the bottom of the box and the soil placed around it.

Pulsed radar scans were then made with the pipe in place, with it removed (resulting in a smooth-side void), and with a void with artificially roughened sides. The scans were repeated for various depths of soil cover over the void: 23 cm, 18 cm, 6.4 cm of soil cover. Also, two complete sets of tests were conducted. In the first test series, the soil box was placed on Eccosorb (a microwave attenuating material).

Table 17 summarizes the results. The results fall short of the crystal-clear image originally anticipated. Moisture content, pieces of gravel, limitations due to the size of the box, background influence of other laboratory equipment, etc. are possible reasons. Nevertheless, the traces obviously show the location of the hole and the proper depth. Thus, the experiment was partially successful.

We conclude that these results show moderate promise for the use of pulsed RF methods in locating subsurface holes from depths near the ground surface down to at least 40 cm.

TABLE 17 Summary of GPR Test Results Used to Detect Voids in Clayey Silt Soil

| Base of Box | Cover cm | Steel Pipe | Smooth Hole | Rough Hole |
|---|---|---|---|---|
| On concrete | 33 | good | good | good |
| On concrete | 23 | marginal | marginal | marginal |
| On concrete | 12 | marginal | marginal | marginal |
| On Eccosorb | 33 | good | good | good |
| On Eccosorb | 23 | good | good | marginal |
| On Eccosorb | 12 | good | good | marginal |

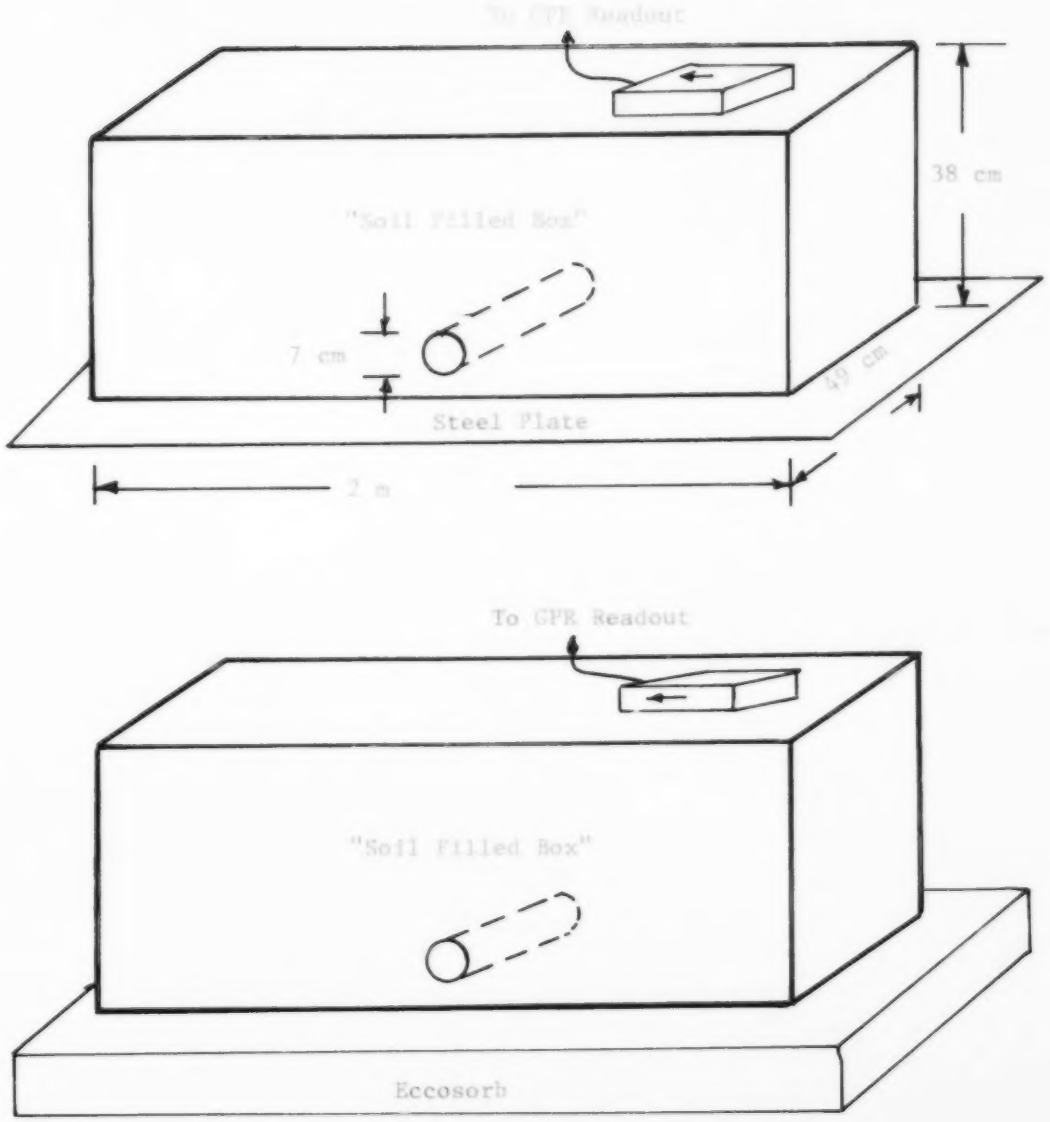


Figure 38. Two types of test configurations used in this study to detect the presence and location of small voids.

(b) Field Tests

1. Defining Water Table and Stratigraphy

Each of the three sites selected for monitoring were unpaved and originally thought to be relatively homogeneous within the upper 3 m. To guarantee the existence of a near-surface water table, sites were selected that began at a creek or river at one end of the traverse and proceeded inland. One site went from exposed creek to exposed creek (Figure 39).

Wharton Site Details

The Wharton site extends from the bank of a 2-m-deep creek over the land for a distance of 100 m. The ground surface rises 3 m within this length. Nine water observation wells were placed in the ground, each deep enough to intercept the water table. The observation wells were 2.5-cm diameter open-ended pipes with removable surface caps to prevent damage or vandalism during time of non-use. The spacing varied from 3 m to 15 m.

Subsurface sampling from the site showed that the soil beneath the upper 15 cm was a poorly-graded sand that contained a well-defined water table, below which the soil was saturated and above which the soil was dry or partially saturated depending on the recent weather conditions. The physical properties of the soil are given in Table 18. Geotechnical properties calculated from the data of Table 18 show an *in situ* porosity of 0.38 and a moisture content equal to 97% of saturation for the soil above the water table.

Springfield Site Details

The Springfield site extends between two shallow fresh-water creeks spaced 90 m apart. Between these two creeks the land surface rises approximately 1.5 m. The ground surface is an asphalt-paved parking lot with a crushed stone base. Total pavement thickness is approximately 145 cm. Eleven observation wells of the type previously described were placed along the traverse at intervals of 4 to 15 m.

Soil samples contained two different soil types. The upper soil (i.e., beneath the asphalt/stone base pavement) is a well-graded silty sand,and the lower soil is an organic clay of high plasticity. Physical properties of the soils are given in Table 18. Calculated values from these properties show the upper sand to have a porosity of 0.39 and is fully saturated.

Penrose Site Details

The Penrose site extends from the edge of a major river (brackish water) up a relatively sharp ridge to gradually upward-sloping land. The traverse selected was 50-m long and four observation pipes were placed at spacings from 5 to 10 m along its length. Soil samples contained two different soil types. Closest to the river is a random fill consisting of cobbles, gravel and miscellaneous fines. It was too coarse to obtain an undisturbed sample. Away from the river the soil abruptly changed due to past construction

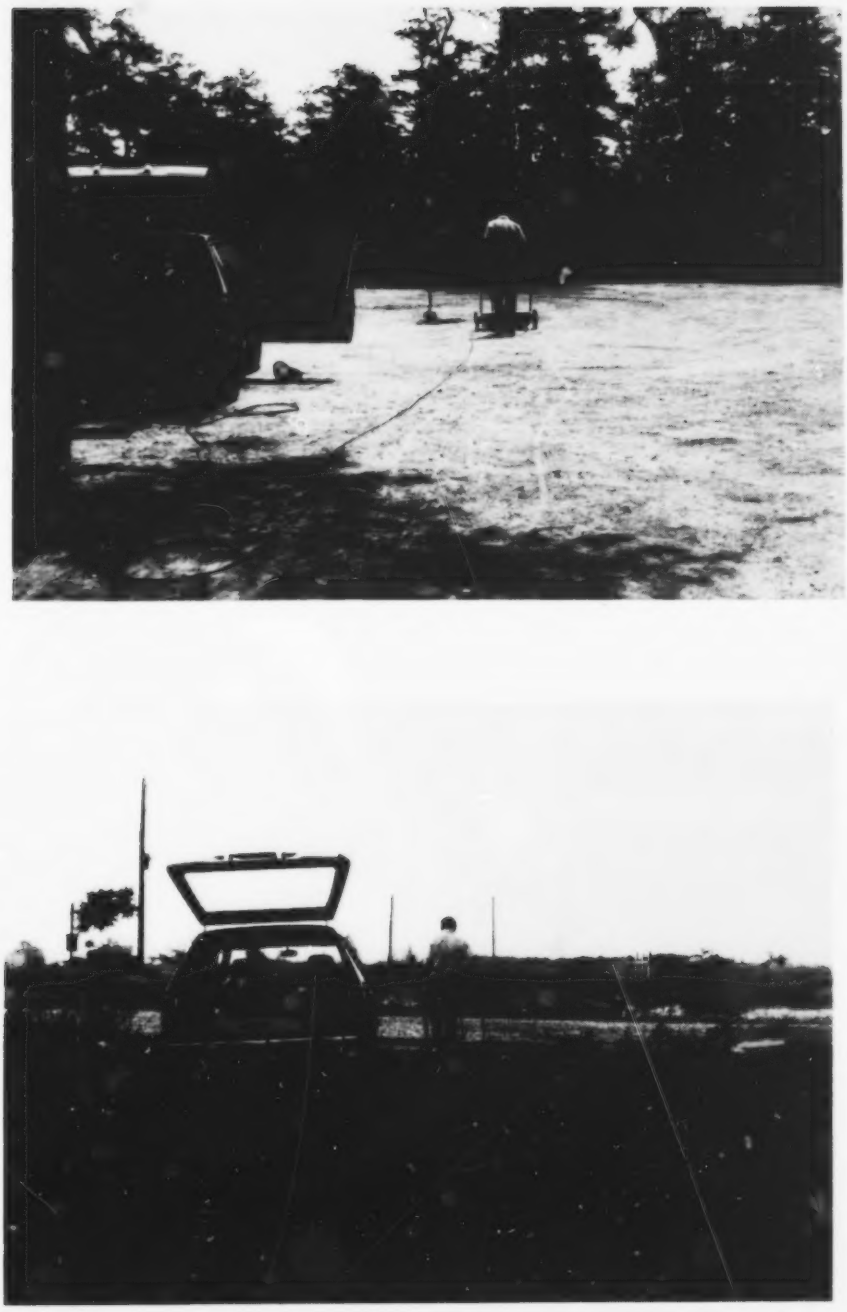

Figure 39. Photographs of pulsed-RF monitoring to detect water table and/or subsurface stratigraphy.

TABLE 18 Physical Properties of Soils Encountered at Various Test Sites

| Location | $\gamma_w$ (g/cm$^3$) | w % | $G_s$ (g/cm$^3$) | $d_{10}$ (mm) | CU | $w_\ell$ | $w_p$ | PI | Classification |
|---|---|---|---|---|---|---|---|---|---|
| Wharton Site | | | | | | | | | |
| Upper Portion | 1.78 | 2 | 2.68 | 0.25 | 18 | N/A | N/A | N/A | SW-GP |
| Lower Portion | 1.68 | 2 | 2.68 | 0.10 | 5 | N/A | N/A | N/A | SP |
| Springfield Site | | | | | | | | | |
| Upper Soil | 1.72 | 13 | 2.70 | 0.065 | 11 | N/A | N/A | N/A | SW |
| Lower Soil | 2.00 | 23 | 2.67 | N/A | N/A | 56 | 36 | 20 | OH |
| Penrose Site | | | | | | | | | |
| Riverside | - | - | - | 0.19 | 130 | N/A | N/A | N/A | GW/SW |
| Landside | 1.73 | 29 | 2.20 | 0.15 | 20 | 51 | 51 | 0 | MH |

where

$\gamma_w$ = wet unit weight
w = water content
$G_s$ = specific gravity
$d_{10}$ = effective size
CU = coefficient of uniformity
$w_\ell$ = liquid limit
$w_p$ = plastic limit
PI = plasticity index
N/A = not applicable

activity. The soil here was identified as a high plasticity silt whose physical properties are given in Table 18. The resulting *in situ* properties of the landside silt were a porosity of 0.39 and 100% saturation. It was observed that the riverside random fill was also high in water content and obviously close to complete saturation.

During the course of this 12-month study, 20 separate scans were taken of each test site. Temperatures ranged from a summer high of 29 C to winter lows of -6 C. Surface conditions varied from dry to wet to snow-covered and included varying amounts of frost penetration. Time of monitoring varied from morning to noon to late afternoon.

Actual water table elevations were taken by placing a stiff coaxial cable down the observation well until it came into contact with the water within the pipe. The shielding of the wire was drawn back from the central lead about 2 mm so that an open circuit existed until contact was made with the water within the well. The cable was connected to an ohm-meter at the ground surface that clearly registered a completed circuit. The length of wire was then measured to determine the actual elevation below the top of the observation well.

Pulsed-RF traces of the various sites were made immediately after water-table measurements. The entire process at each site took less than one hour, so changes in water-table elevation between the two sets of readings were not considered significant.

## Wharton Site Results

A typical pulsed-RF trace at the Wharton site is shown in Figure 40. As with all of the traces it appears as though the ground surface is level, though in reality it rises from left (the creek) to right (landside). Also noted is a heavy black band immediately beneath the ground surface where no data can be obtained. This "main bang" effect is due to the interaction of the three pulses traveling directly across the transceiver. Its thickness depends upon the frequency of the pulses and varies from 20 to 49 cm.

Seen reasonably clearly on the trace is a separation from light (above) to dark (below), which indicates the location of the water table. Superimposed on the figure are the locations of the water surfaces within the water observation pipes. Correlation has generally been good, with an accuracy of 14% during dry ground conditions and 27% during conditions of high surface moisture. This latter situation occurred usually during winter readings when the ground was frozen in the upper 20 to 50 cm. Interestingly, a ground surface having a snow or ice covering did not seriously influence the readings. Taking readings during different times of the day and at temperatures above freezing did not appear to influence results.

## Springfield Site Results

A typical pulsed-RF trace of the Springfield site is shown in Figure 41. Here a very different situation is seen to occur: no correlation exists between the RF trace and the actual water table elevation. This is undoubtedly due to the capillary zone, which draws moisture above the water table in fine-grained soils. Since the moisture level in this zone is very high, e.g., completely saturated in the lower soil, no distinct boundary exists for the pulsed RF system to define a distinct water-table elevation. However, within the water observation well, the capillary zone does not exist, so the acutal water table surface can be located.

What is dominant on the pulsed-RF trace of Figure 41 is an undulating discontinuity showing two well-defined areas. This discontinuity matches the boundary between the upper granular soil and the lower fine-grained soil. It was present in this exact location every time that a traverse was made. The only difference noted from time to time was in contrast, which was probably due to varying performance of the printer.

## Penrose Site Results

A typical pulsed-RF trace of the Penrose site is given in Figure 42. As with the Springfield site, the capillary zone, with its high moisture content soils, completely masks out the presence of the actual water table as determined by the water observation wells. What is clearly seen is that the soils on the left side (adjacent to the river) are very different from the soils on the right side (the inland soils).

Subsequent soil testing showed that these two soil types were very different from one another and had been placed in their respective locations during past construction activity. The boundary was always present, in the same location, with contrast being the only difference between readings.

Of the many candidate techniques available to test for subsurface water nondestructively, as in seepage plume detection, the use of pulsed RF methods are likely methods. Indeed, the reflection from a well-defined water table can lead to reasonable accuracy. Results of 12 months of testing show that the greatest accuracy, approximately 14%, is during dry summer weather when there is no surface moisture. The accuracy decreases to 27% during wet winter months when moisture is contained within the soil above the water table. These results, however, are only valid for sandy (or gravelly) soils that do not contain a capillary zone. This capillary zone, which varies in thickness above the water table is saturated, or nearly so, and has a theoretical height of:

$$h_c = \cos\alpha \frac{T_o}{\gamma_\omega} \frac{1}{d_v} \qquad (34)$$

where $h_c$ = height of capillary rise

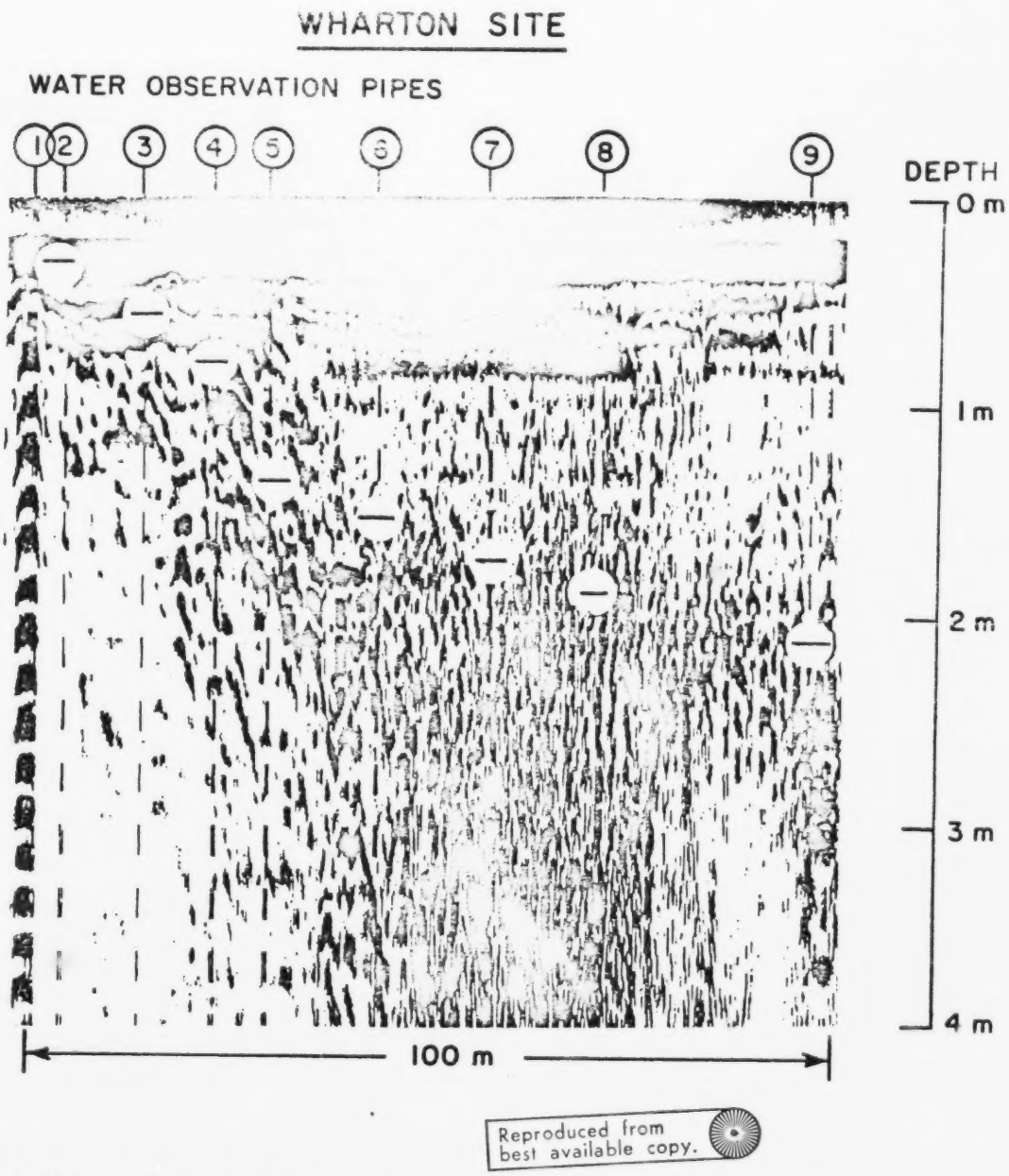


Reproduced from best available copy.

Figure 40. Pulsed-RF survey of Wharton site made on April 2, 1981, with actual water table elevations indicated by horizontal lines in circles.

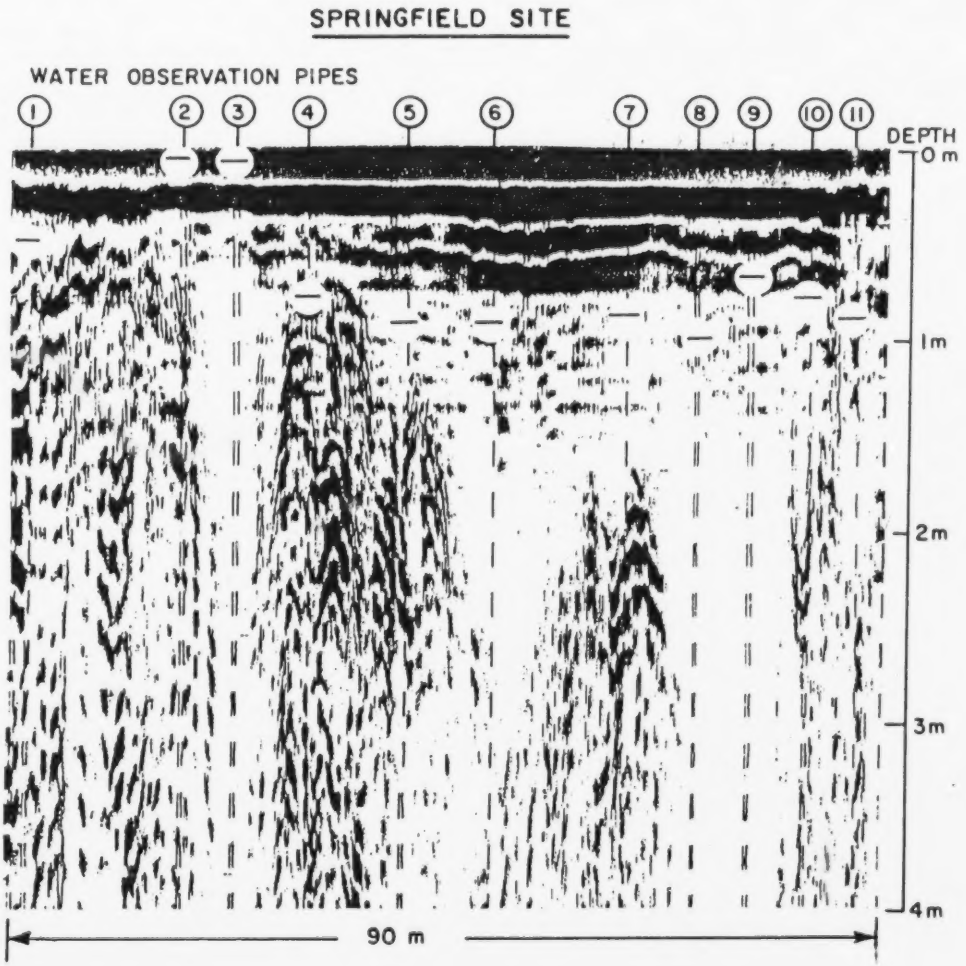


Figure 41. Pulsed-RF survey of Springfield site made on April 3, 1981 with actual water table elevations indicated by horizontal line in circle.

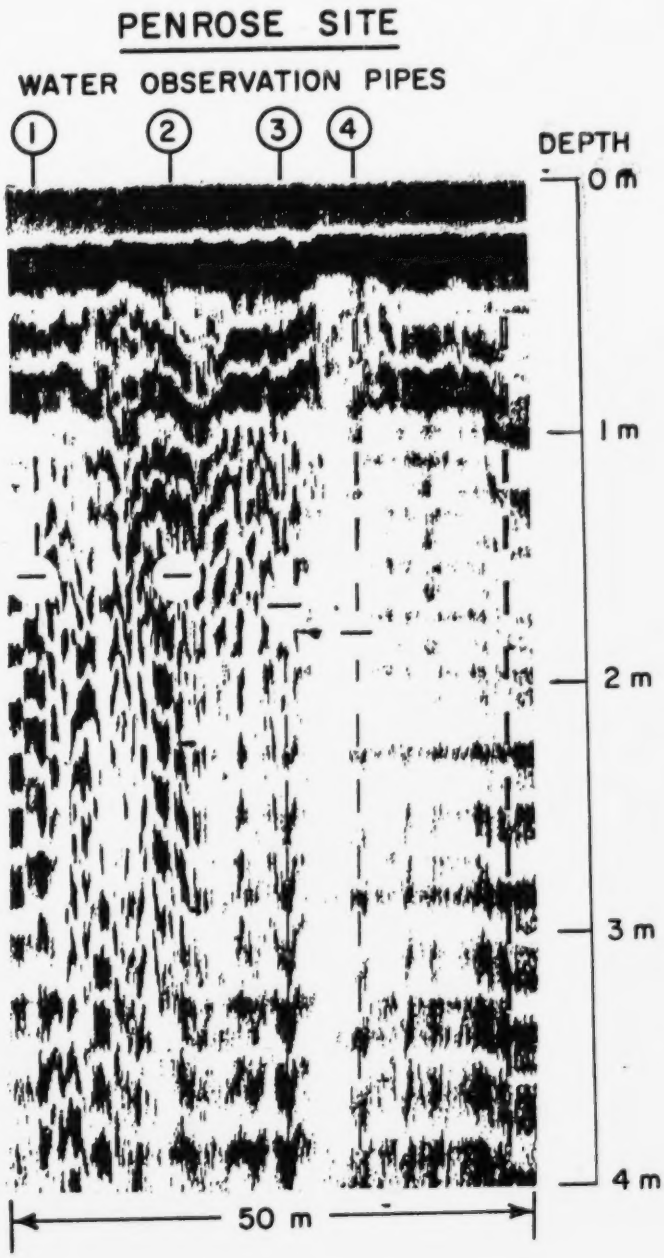


Figure 42. Pulsed-RF survey of Penrose site made on April 3, 1981, with actual water table elevations indicated by horizontal line in circle.

$\alpha$ = wetting angle of water to soil
$T_0$ = surface-tension force of water to soil
$\gamma_\omega$ = unit weight of water
$d_v$ = average soil void diameter

Thus, height of capillary rise is inversely proportional to the average soil void diameter. Easily seen is that coarse-grained soils (gravels, sand, and their mixtures), with large particle sizes (hence, proportionately large void sizes) have very narrow capillary zones, like the soils at the Wharton site.

This is not the case for the Springfield and Penrose sites, both of which had predominantly fine-grained soils (silts, clays and their mixtures). At both of these sites the actual water table could not be located and was completely dominated by stratigraphic changes in soil layers. Seen at the Springfield site was an undulating horizontal layering, while at the Penrose site the distinction was between two different soils placed beside one another.

In conclusion, pulsed-RF methods can be used in seepage detection in granular soils, but not in fine-grained soils. This is not a particularly severe limitation, because it is the granular soils that have high permeability, hence seepage problems are more acute in these soil types. For the fine-grained soils a spill or other incident involving liquids will be contained relatively close to the spill location due to the much lower soil permeability. Thus, in its proper setting, pulsed RF methods can be used for groundwater monitoring and the related problem of spill detection.

2. Buried Container Location

There are estimated to be 30,000 to 50,000 existing dump sites in the U.S.A. that contain various amounts and types of hazardous materials. Furthermore, many new sites are being discovered on a regular basis. One of the first pieces of information needed in the cleanup process is the physical extent of the dump size and resulting polluted area. This is very difficult to determine when the hazardous materials are buried. A number of geophysical or nondestructive testing (NDT) techniques can be used in the detection process, and these have been elaborated on previously. At a large number of the dump sites, the hazardous materials are placed in drums (steel or plastic) and buried. It is at such sites that the pulsed RF technique shows significant promise. Although several investigations of this type showing various degrees of success have been reported, there have been no studies to determine the accuracy ("ground truth") and limitations of such a system. The study to be described herein was undertaken to determine the detectability of the buried containers at an ideal site, with regard to the following variables:

- container material (steel or plastic)
- container size (2 gal to 55 gal)
- container burial depth (0.3 to 3 m below the surface)
- container orientation (0°, 45°, 90° with respect to the ground surface).

The site where the containers were buried was in an abandoned sand quarry that was left level and free of all vegetation and miscellaneous construction debris. This site, near Gibbsboro, New Jersey, contained no pipelines, cables or overhead wires within 1000 ft of the study area. Thus, background noise from man-made objects was minimal.

Disturbed and undisturbed soil samples indicated that the site consisted of a very uniform poorly-graded sand (specific gravity of 2.65, effective size of 0.18 mm, and coefficient of uniformity of 3.4). Its average in situ density is 1.62 g/cm$^3$ (101 PCF); the porosity is 0.40, and the relative density is 73%. For the purpose of this study, it is important to note that the in situ water content is only 2%, which corresponds to a degree of saturation of 8%. That is, the sand is almost dry.

The water table at the site was estimated to be 6 m (20 ft) below the ground surface, and the sand, with essentially no capillary zone, proved to be nearly ideal for tests.

The containers were placed in hand- and equipment-excavated holes varying from 0.3 m to 4.3 m (1 ft to 14 ft) in depth. The container burial configurations as shown in Figure 43 were as follows:

- Four steel containers (2, 5, 30, 55 gal) buried at constant depths of 1 m (3.5 ft), i.e., under 1 m of soil cover
- Four 30 gal steel containers buried at 0.3, 1, 1.8, and 3.4 m (1 ft, 3 ft, 6 ft, and 11 ft) depths
- Four 40-gal plastic containers (empty) buried at 1 ft, 3 ft, 6 ft, and 11 ft depths
- Two 40-gal plastic containers buried at 0.6 m (2 ft) depth, one filled with fresh water, the other with salt water
- Three 30-gal steel containers buried at 1 m (3 ft) depth, but at various orientations, (0°, 45°, 90° to the ground surface)
- Four 55 gal steel containers buried at 1.4 m (4.5 ft depth in two groups, one by itself, the other three side by side
- A random burial site approximately 12 ft x 12 ft x 5 ft deep, which contained 10 steel drums and 1 plastic drum in a random arrangement. (This pattern to be known as the "Trash Dump".)

All patterns were separated by sufficient distance so that interaction between them was relatively unlikely.

The real-time printouts of the scans of each container burial configuration are shown in Figures 44 to 51. Each is discussed in this section. It should be noted that no signal enhancement, other than what is built into the system, has been applied to these results.

The first pattern (Figure 44) results from a series of various size steel drums buried beneath 1 m (3.5 ft) of soil. The drums include a 55-gal, 30-gal, 5-gal, and 2-gal size from left to right on the figure. Each

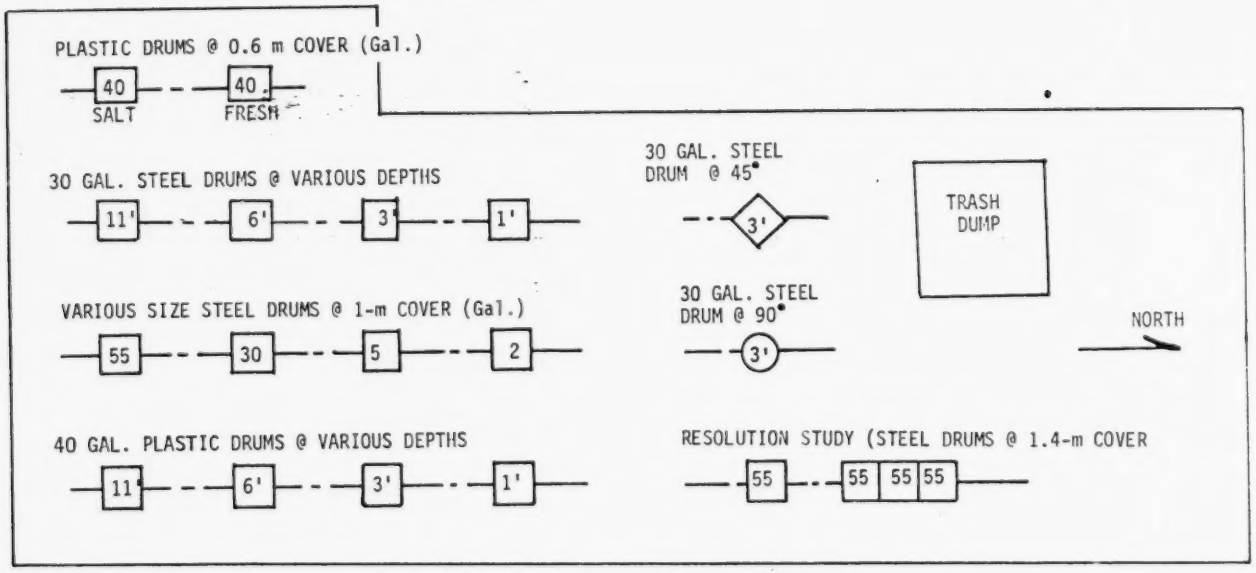


Figure 43. Plan of buried-container patterns at the Gibbsboro site. (Overall site dimensions are approximately 30 m x 60 m)

drum is characterized by a parabolic reflection which is the typical reflection from a buried cylindrical object when the antenna is moved perpendicular to the axis of the drum. The vertical scale adjacent to the printout reveals that the GPR accurately predicted the depths to the drums. This survey used a 120-MHz antenna.

The next pattern (Figure 45) to be surveyed consists of 30-gal steel drums buried at various depths including 3.4, 1.8, 1.0 and 0.3 m (11 ft, 6 ft, 3 ft and 1 ft) from left to right on the figure. All the drums are located and characterized by their parabolic reflection patterns. the drums at 3.4 and 1.8 m (11 ft and 6 ft) (a and b respectively) were surveyed with an 80-MHz antenna, and those at 1.0 and 0.3 m (3 ft and 1 ft) (c and d, respectively) were surveyed with an 120 MHz antenna. This frequency change was necessary because the higher frequency (120 MHz) was not able to penetrate to the depth of the drums at 1.8 and 3.4 m (6 ft and 11 ft) and the lower frequency (80 MHz) antenna is not capable of detecting near-surface reflectors due to direct transmission of the signal from the transmitter to the receiver. This latter limitation results in a blind area, as can be seen in Figure 45 at drums (a) and (b) for a depth of approximately 1.5 m (5 ft). Again, the vertical scale adjacent to the printout shows that the GPR accurately predicted the depths to the drums.

Four empty heavy-duty plastic drums with a 40-gal capacity were buried at different depths (3.4, 1.8, 1.0, and 0.3 m) (11 ft, 6 ft, 3 ft and 1 ft) as shown in Figure 46. Because plastic is essentially transparent to the radar waves, there is an absence of reflections from the drums. Laboratory experiments have shown that small dielectric constant changes can be observed with the GPR equipment; however, for all practical purposes, the return signal from the plastic drums is too weak to be distinguished. Careful scrutiny reveals a faint signal from the drum buried at 1.0 m (3 ft); but this was the only exception to the survey in which both 120 MHz (shown) and 30 MHz antennas were used. The drum at 0.3 m (1 ft) would probably have been detected; however, it was masked in the direct transmission of the signal from the transmitter to the receiver.

Because the plastic drums are essentially transparent to the radar signal it may be possible to detect the drums due to the reflective nature of the contents. To examine this possibility, two plastic drums (identical to those previously discussed) were buried 0.6 m (2 ft) beneath the surface. One drum was filled with fresh water to model a low conductivity waste; the other drum was filled with water and salt in a ratio of 30 g salt /liter of water. This simulated a highly ionic and conductive waste. The printout from this survey is shown in Figure 47. Both drums are clearly evident. The fresh water drum (b) is slightly more pronounced due to the better reflecting ability (lower conductivity) of the fresh water compared to the salt water.

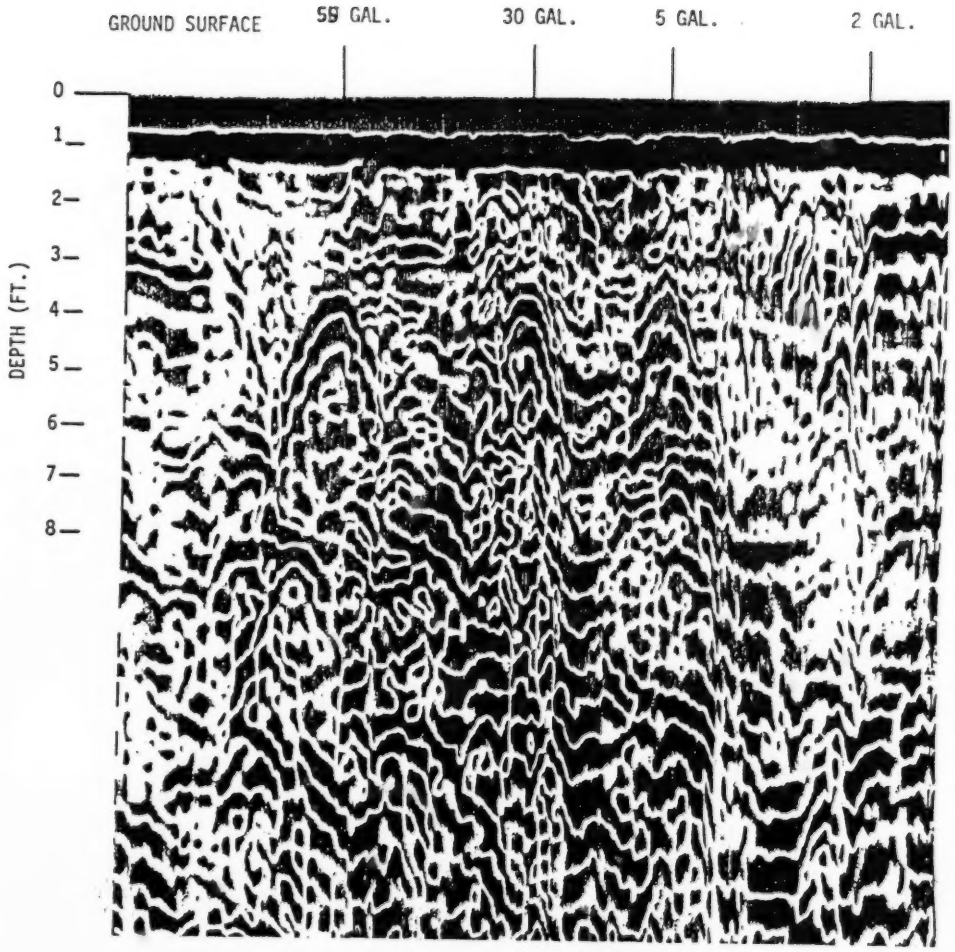


Figure 44. GPR printout showing various size steel drums with 1.1 m (3.5 ft) of soil cover.

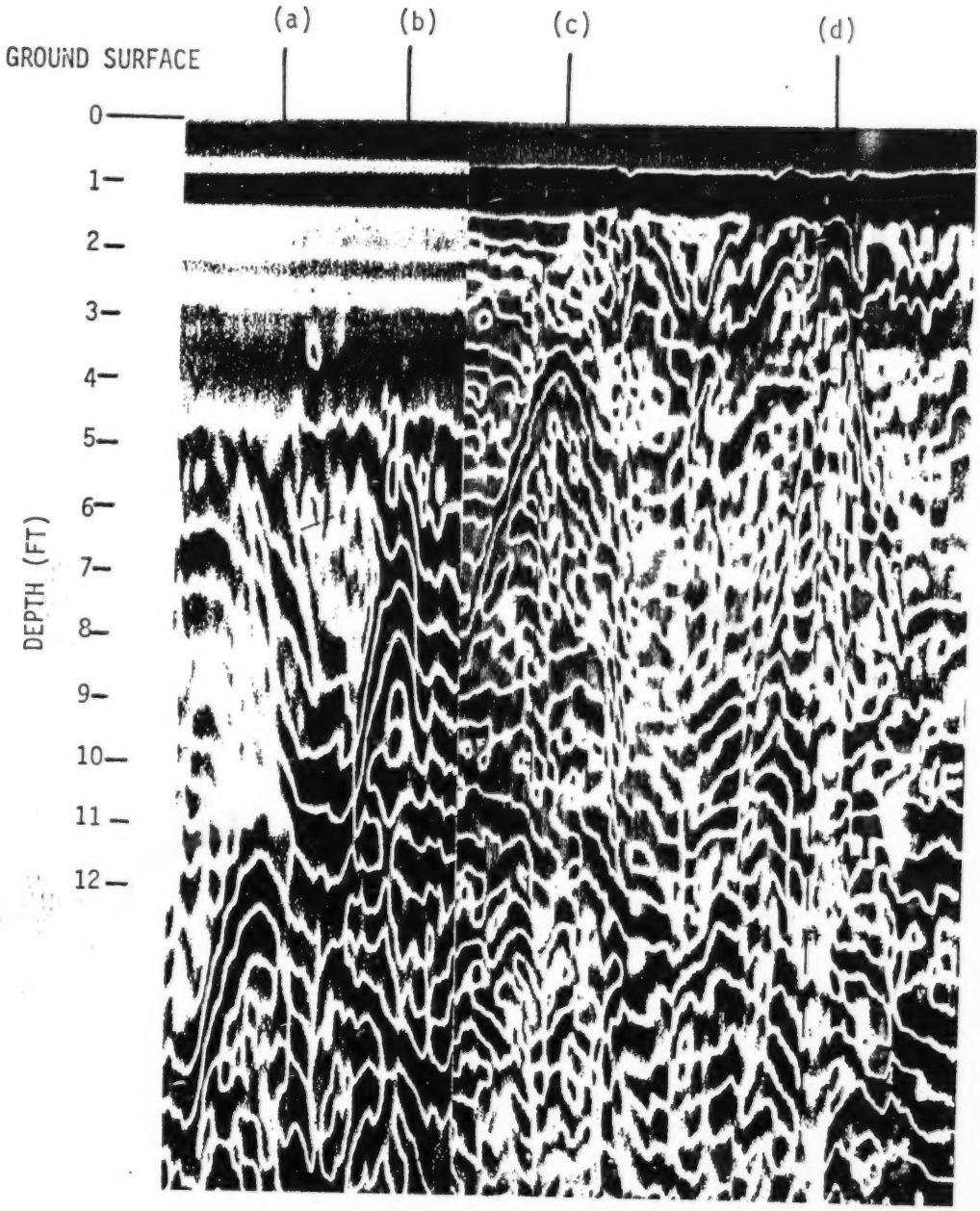


Figure 45. GPR printout showing survey of 30-gallon steel drums (empty) at various depths:

| Location | Depth (m) | Antenna (MHz) |
|---|---|---|
| (a) | 3.4 | 80 |
| (b) | 1.8 | 80 |
| (c) | 1.0 | 120 |
| (d) | 0.3 | 120 |

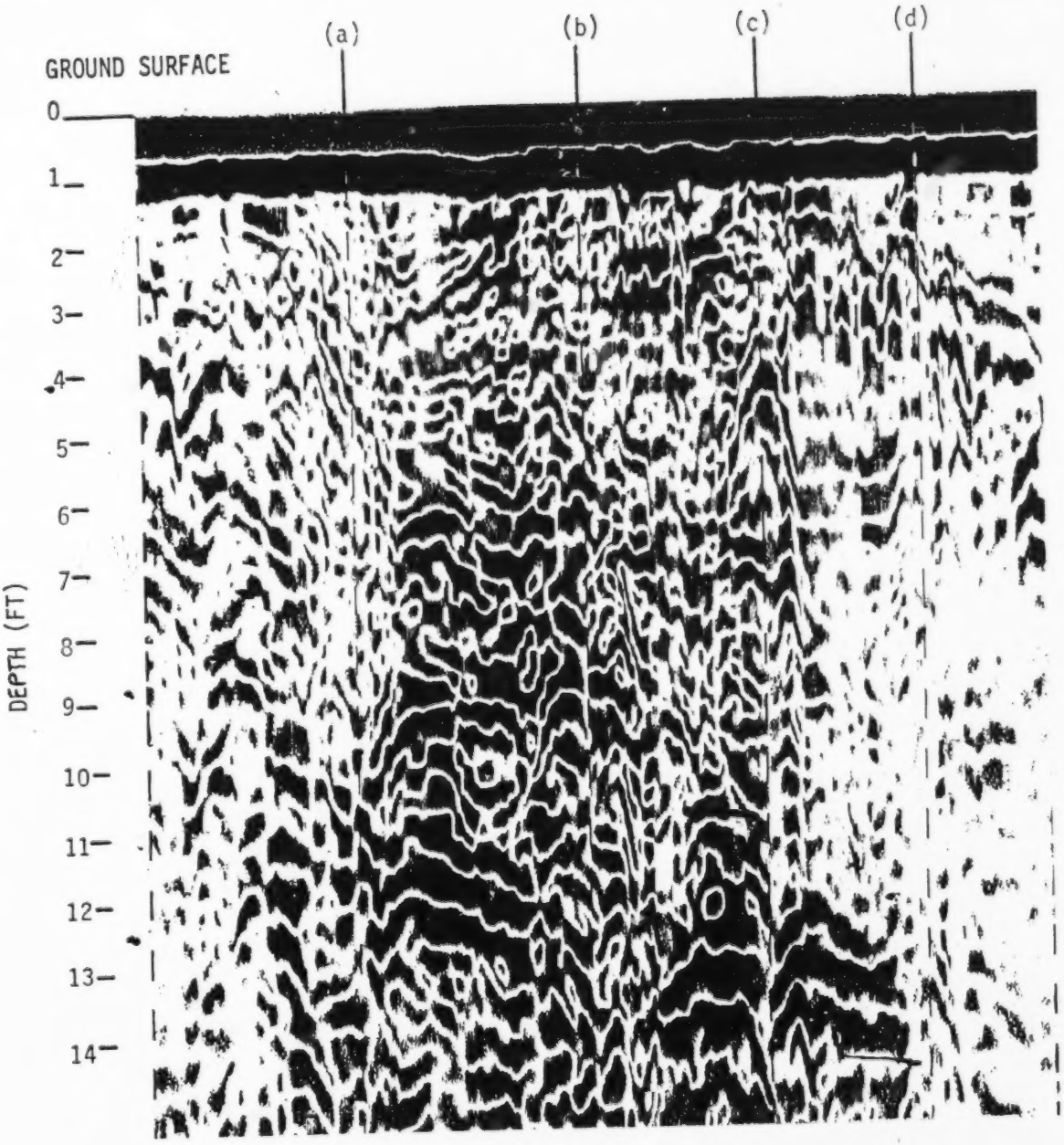


Figure 46. GPR printout showing survey of 40-gallon plastic drums (empty) at various depths, all drums surveyed with 120-MHz antenna. Burial locations and depths are the same as in Figure 45.

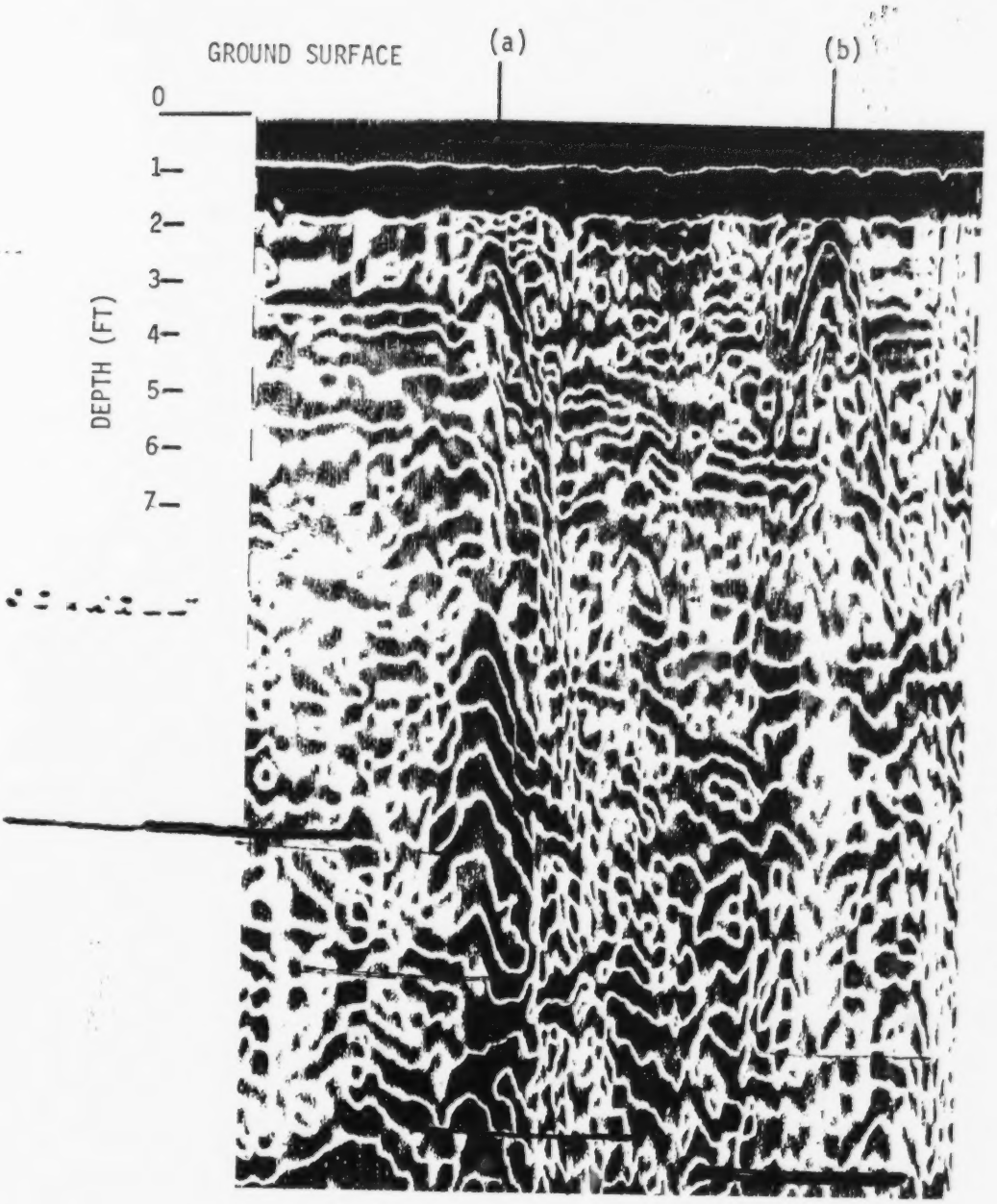


Figure 47. GPR printout showing survey of 40-gallon plastic drums buried 0.6 m (2 ft) beneath the surface, where (a) indicates the salt-water-filled drum and (b) indicates the fresh-water-filled drum.

Figure 48 shows the patterns for three 30-gal steel drums buried at various orientations with respect to the ground surface. Position (a) on the figure reveals a drum standing on its end. The reflection is no longer parabolic but rather abrupt and similar to the pattern obtained when passing over a flat steel plate. Signals are reflected only while the antenna is directly above the drum. Position (b) on the figure shows a drum buried at a 45° angle to the ground surface. Although the reflection is parabolic, due to the angle of the return signals the reflection is not as distinct or obvious as that of the drum in a horizontal orientation, as shown in postion (c) on the figure.

To examine the resolution of the GPR, a pattern of four 55-gal steel drums was arranged with three drums adjacent to one another and the fourth drum 3.6 m (12 ft) away, all buried at a depth of 1.4 m (4.5 ft). The printout for this survey is shown in Figure 49. The separation between the single and group of three drums is obvious. However, it is difficult to differentiate between the three adjacent drums. The double peaks at the three drums does indicate a larger reflecting object than the single parabolic peak at the single drum. The 120-MHz frequency was used to locate these drums and comparison with the adjacent depth scale shows that the depth was accurately predicted.

The final pattern to be examined was an excavation approximately 2.6 x 3.6 m (12 ft x 12 ft) by 2 m (7 ft) deep. Ten steel drums and one plastic drum were placed in the excavation in a random arrangement. This was covered by approximately 1.5 m (5 ft) of soil. The pattern simulates, on a small scale, a typical waste dump site. The printouts from two surveys over the site are shown in Figure 50. The center of the dump is indicated in each printout. Both surveys show a heavy black reflection at the center of the dump; however, it is not possible to resolve the individual drums within the site. Note in both surveys that the limits of the excavation, i.e., the trench boundaries, can be detected. The survey on the left of the figure shows the distinct location of the left-most boundary of the trench. It is indicated by the abrupt ending of the black horizontal band at the 0.6 m (2 ft) depth. In the survey on the right of the figure, both limits of the excavation are indicated by the abrupt end and start of the black horizontal band at the 0.6 m (2 ft) depth. The survey was conducted using a 120-MHz antenna and resulted in a good approximation of the depth to the buried drums.

Table 19 provides a concise summary of the results of the GPR surveys of each drum burial configuration.

Several major conclusions can be drawn from this study using GPR to detect buried containers:

- For steel drums, the maximum detection depth is a function of drum size (a 30 gal steel drum can be detected at a depth of 3.4 m)

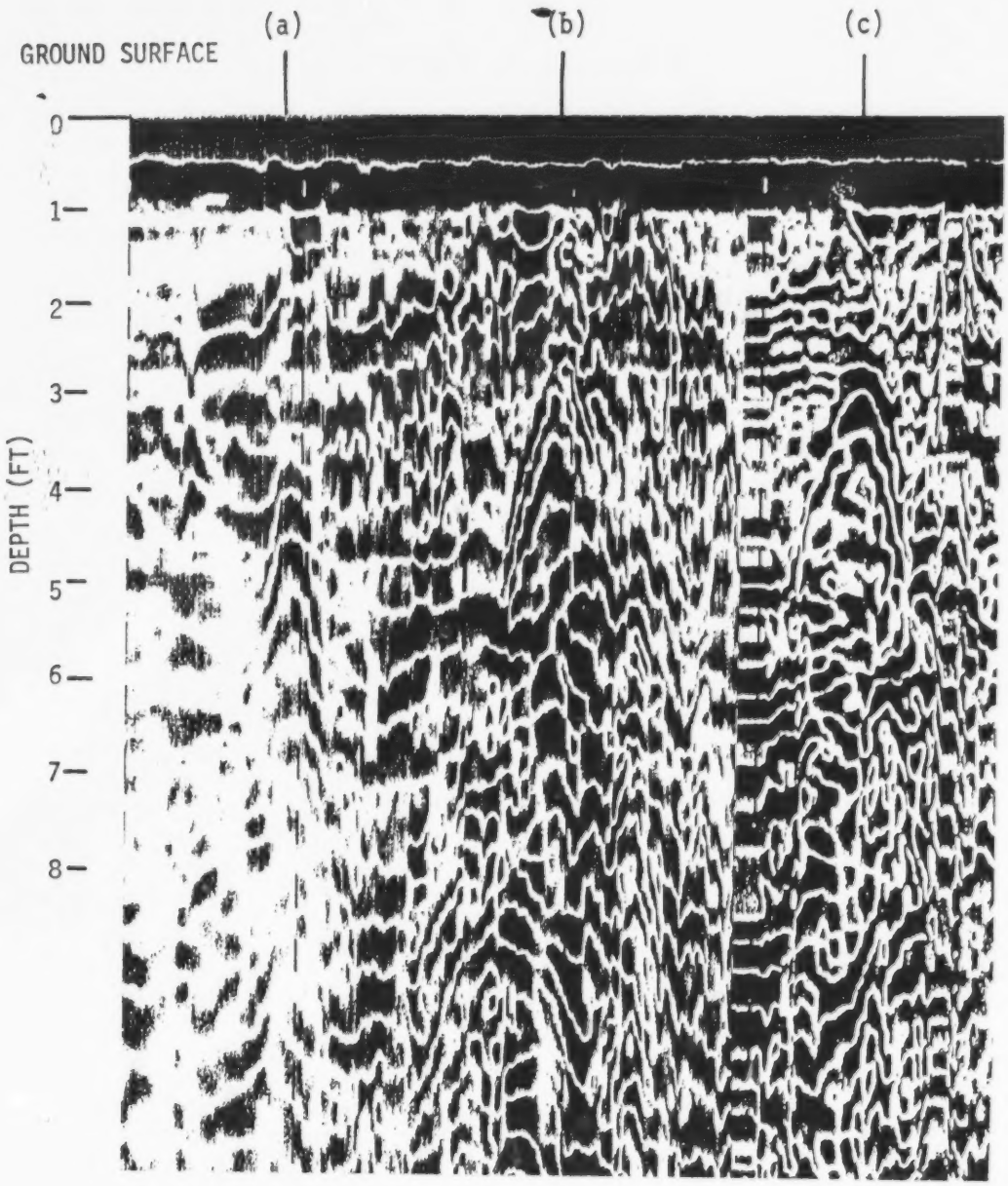


Figure 48. GPR printout showing survey of 30-gallon steel drums at various orientations buried 1.0 m (3 ft) beneath the surface.

(a) Drum standing on end
(b) Drum at 45° angle to ground surface
(c) Drum buried horizontal to ground surface

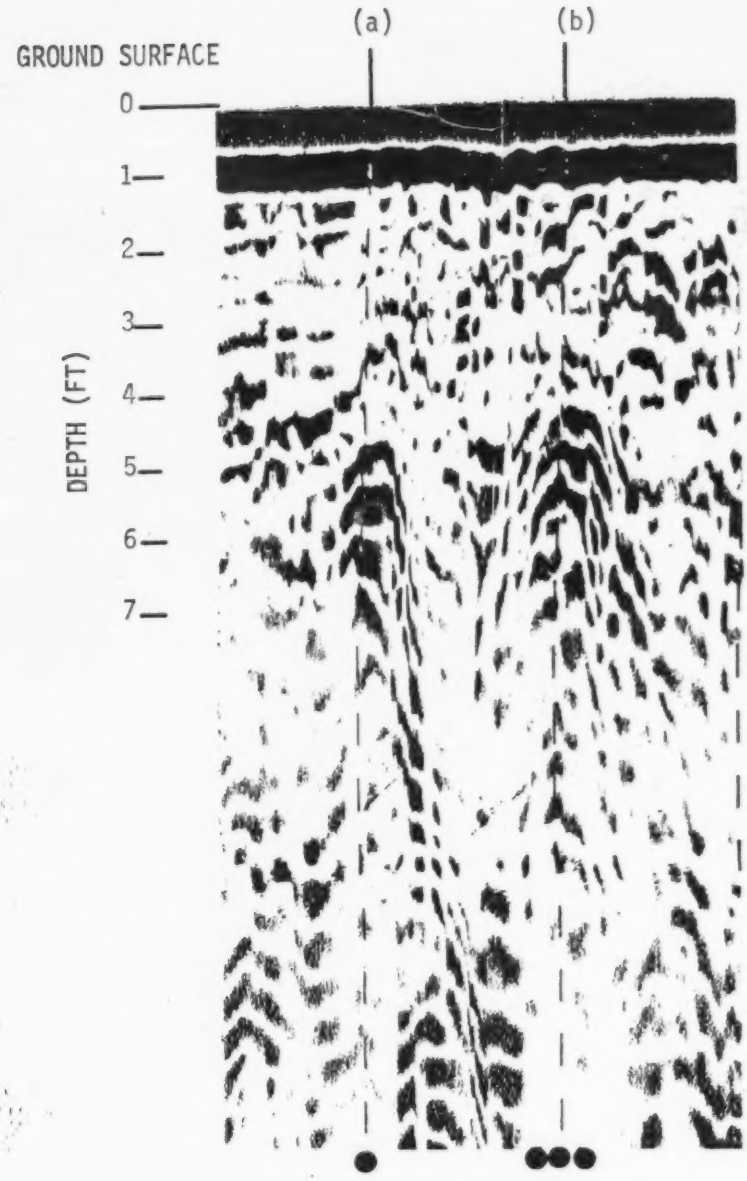


Reproduced from
best available copy.

Figure 49. GPR printout showing survey of resolution study of 55-gallon steel drums buried 1.4 m (4.5 ft) beneath the surface.

(a) Single drum
(b) Three drums adjacent to each other

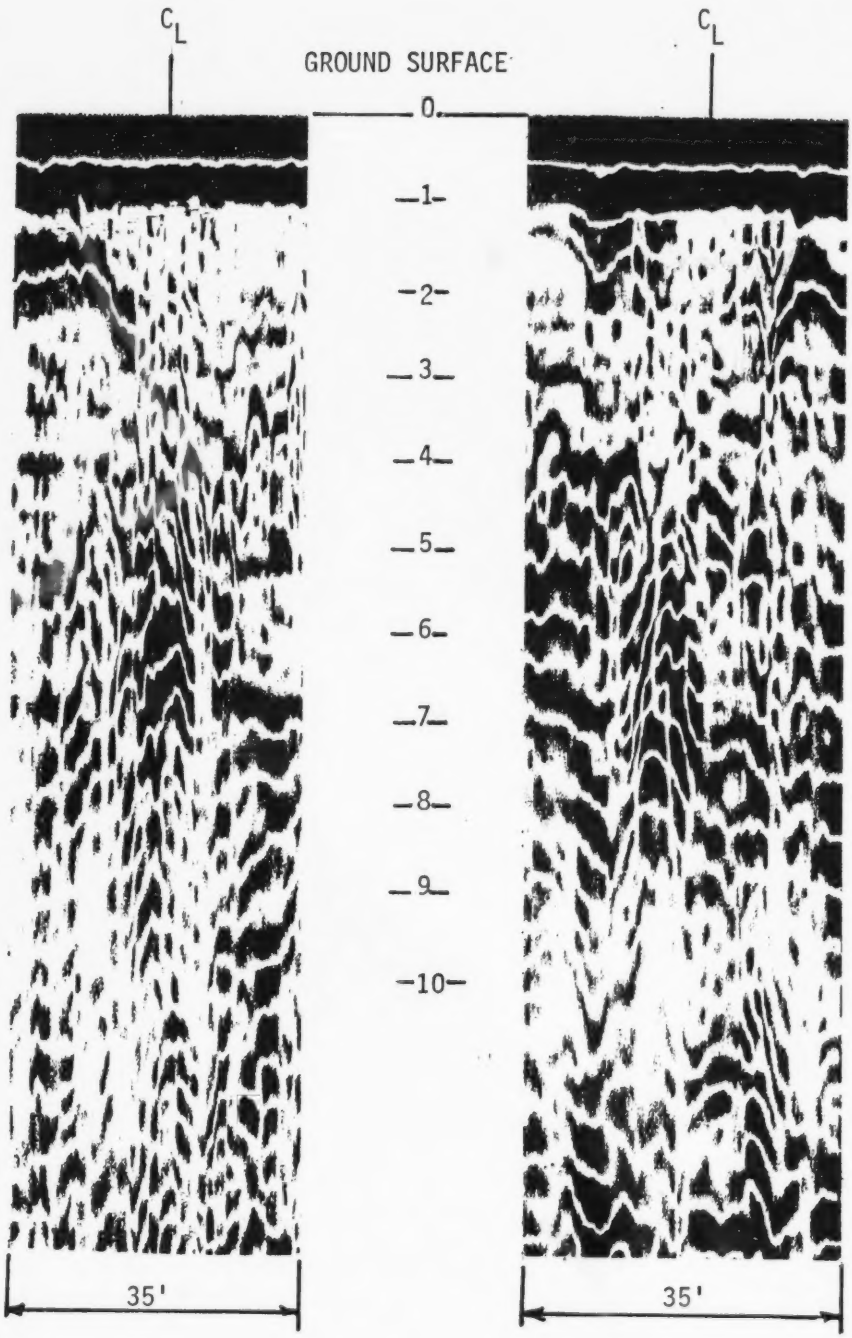


Figure 50. GPR printout showing two surveys over the trash dump.

TABLE 19. Summary Of Results From All Drum Burial Patterns

| Pattern | Resolution of Return Signal | Comments |
|---|---|---|
| STEEL DRUMS | | |
| Various depths (30 gal) | excellent | very strong parabolic reflections |
| Various sizes (55, 30, 5, 2 gal at 1-m cover) | excellent | very strong parabolic reflections |
| PLASTIC DRUMS | | |
| Various depths (40 gal - empty) | minimal | only one drum was barely discernable in one of several surveys |
| Various contents | | |
| salt water | good | average strength reflection |
| fresh water | good | strong parabolic reflection |
| Resolution | | |
| 55 gal steel drum at 1.4 m cover | good | could not resolve three adjacent drums |
| Trash Dump | minimal | could not resolve individual drums, located boundaries of the excavation |

- Steel drums at various orientations (other than horizontal) are detectable; however, the interpretation of the results is difficult.
- Adjacent or closely-spaced drums cannot be resolved making it difficult to determine the exact number of drums in a dump site; however, in some instances the boundaries of the excavation can be identifed, thereby providing an indication of the extent of the problem.

Although the GPR performance was very good overall, there are several drawbacks that should be noted. GPR has very poor lateral scan sensitivity, and it can only detect drums that are passed over by the antenna. Drums adjacent to the path of the antenna are out of the penetrating signal's path and can be easily missed, e.g., see Figure 51. Also, plastic drums are not nearly as detectable as steel drums, nor are drums located in salt water versus fresh water. Finally, GPR is very sensitive to soil conditions. This study was conducted under nearly ideal conditions in relatively dry sandy soil. Studies using GPR in clays and silts have met with less success. See reference 23.

The next phase of this project is to use the same GPR system on similar buried-container patterns in saturated fine-grained soils (silts and clays) to see if the conclusions presented herein hold or if they require modifications.

3. Detection and Location of Voids in Soil Using a GPR System

The detection of near-surface voids has been accomplished using CW microwaves as previously described. Often one is concerned with voids well below the ground surface, but the high-frequency, continuous microwaves are attenuated prior to reaching these depths. In an attempt to circumvent this problem, the ground-probing radar (GPR) system coupled with the appropriate-frequency transceiver was used to study the detection and location of voids in soil. Artificial voids were made by burying empty plastic drums placed at known depths in sand. Since the plastic is essentially transparent to the waves, any change in the received signal can be attributed to the void (air or water).

In order to carry out this test program, a series of empty plastic drums with a 40-gallon capacity were buried at various depths (3 m, 2 m, 1 m and 0.3 m). The soil consisted of a very uniform poorly-graded sand (specific gravity of 2.65, effective size of 0.18 mm, and coefficient of uniformity of 3.4). Its average in situ density is 1.62 g/cm$^3$ (101 PCF) (porosity of 0.40), which results in a relative density of 73%. For the purpose of this study, it is important to note that the in situ water content is only 2%, which corresponds to a degree of saturation of 8%, i.e., the sand is almost dry. The groundwater table was estimated to be 6 m (20 ft) below the surface, and the sand, with essentially no capillary zone, proved to be nearly ideal for tests.

The equipment used for the GPR survey was a GSSI-SIR Model No. 7 identical to that used in the previously described work.

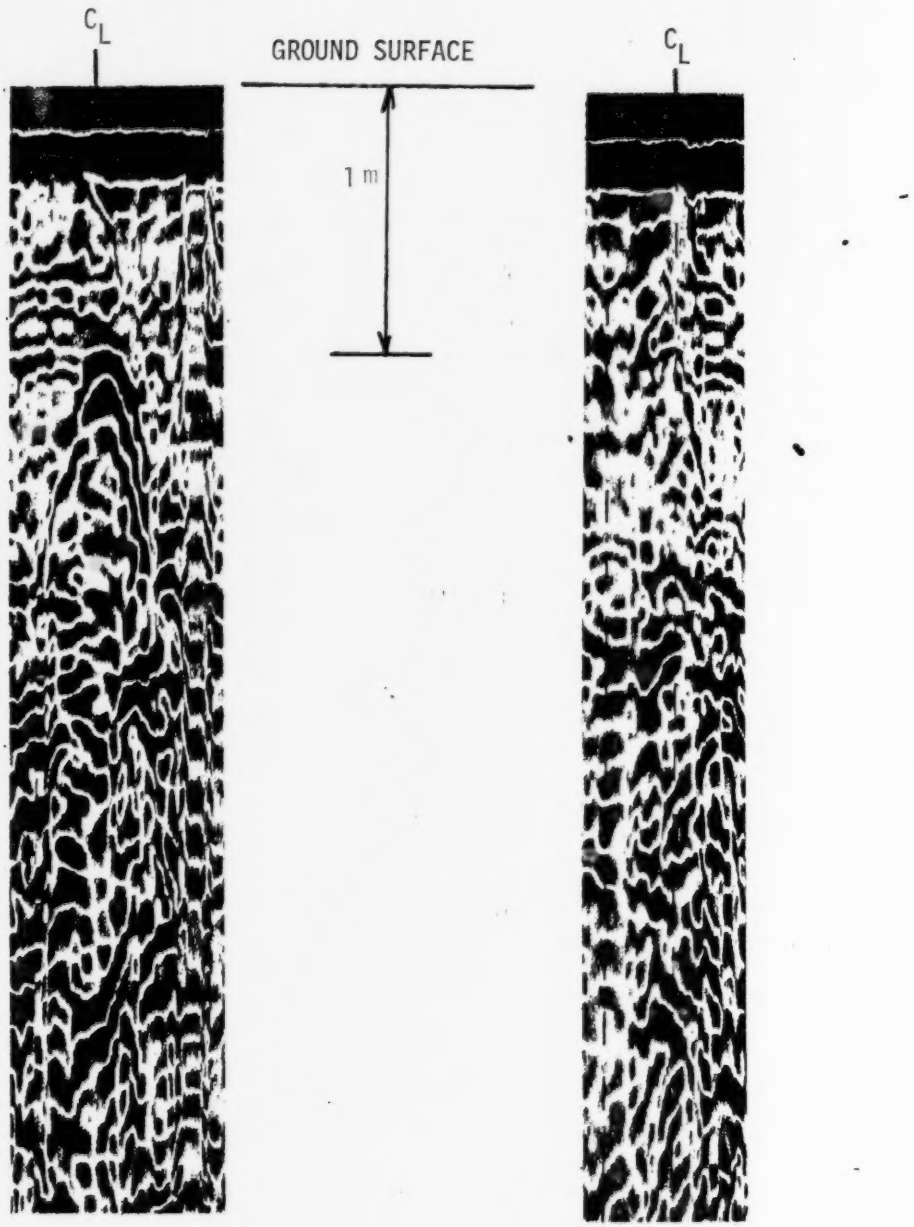


(a) ANTENNA DIRECTLY ABOVE 55 GAL. STEEL DRUM

(b) ANTENNA ADJACENT TO DRUM

Figure 51. GPR printout showing spatial sensitivity of the system (120-MHz antenna)

Figure 52 shows a typical GPR trace received when the transceiver was moved over the top of the buried plastic drums. The absence of any reflected signals indicates that the drums were transparent to the pulsed signal and the dielectric contrast between the air and the surrounding dry sand was not sufficient to provide a printable reflected signal. Careful scrutiny reveals a faint signal from the drum buried at 1.0 m (3 ft); however, this was the only exception to the survey in which both 120-MHz (shown) and 80-MHz antennas were used.

Since the preceding part of the test program proved that under these conditions air voids were not detectable, it was decided to fill another plastic drum with water and bury it. This situation represents a water-filled void. Figure 47 showed the GPR trace received from the water-filled plastic drum. The water provided a highly-contrasted dielectric constant compared to the dry sand soil, and a strong reflection is seen on the trace. Thus, water-filled voids in such a situation (dry soil surroundings) are easily detected and located using a GPR system.

In summary, it is obvious that in a soil that is relatively dry, a water-filled void is easily detected using pulsed RF methods. Along the same idea, air voids in dry soil are for all practical purposed not detectable. Both of these items are in line with the concept that to obtain a strong interpretable return signal, a large dielectric contrast is needed. Further tests for air voids in wet or high-water-content soils may provide the dielectric contrast needed to obtain an interpretable return signal; however, water pockets may no longer be detectable in this type of soil.

4. Chemical Grout Monitoring

The application described in this section involves monitoring subsurface soil conditions prior to and after chemical grouting has been completed. Chemical grouting of soil is an emerging geotechnical practice that involves pumping a liquid chemical into the soil voids to stop seepage, decrease compressibility, or increase the strength of the in situ soil. Although the practice is fairly widely used, there is presently no established method of monitoring the effectiveness of the grouting with the exception of destructive testing technqiues. This is particularly important in the formation of seepage cut-off walls in hazardous material dump sites, for example. With the addition of a pair of borehole antennas, the pulsed radar system is now capable of being used to monitor subsurface conditions between two boreholes, as shown in Figure 53. The antennas have been used on three construction projects to date.

The first investigation, in Philadelphia, Pennsylvania, involved using the pulsed radar with borehole antennas to monitor prior to and after chemical grouting (sodium silicate with DBE reactant). The objective of the grouting was to seal a 1.5 m (5 ft) thick area around a proposed 3.0 m (10 ft ft) diameter sewer tunnel. A 5-cm (2 in.) diameter PVC pipe was placed in each borehole and used for the actual grouting process. The timetable of the grouting work did not permit monitoring to be completed prior to the start of the grouting operation; however, some non-grouted boreholes were used to obtain pre-grouted data. These holes were located

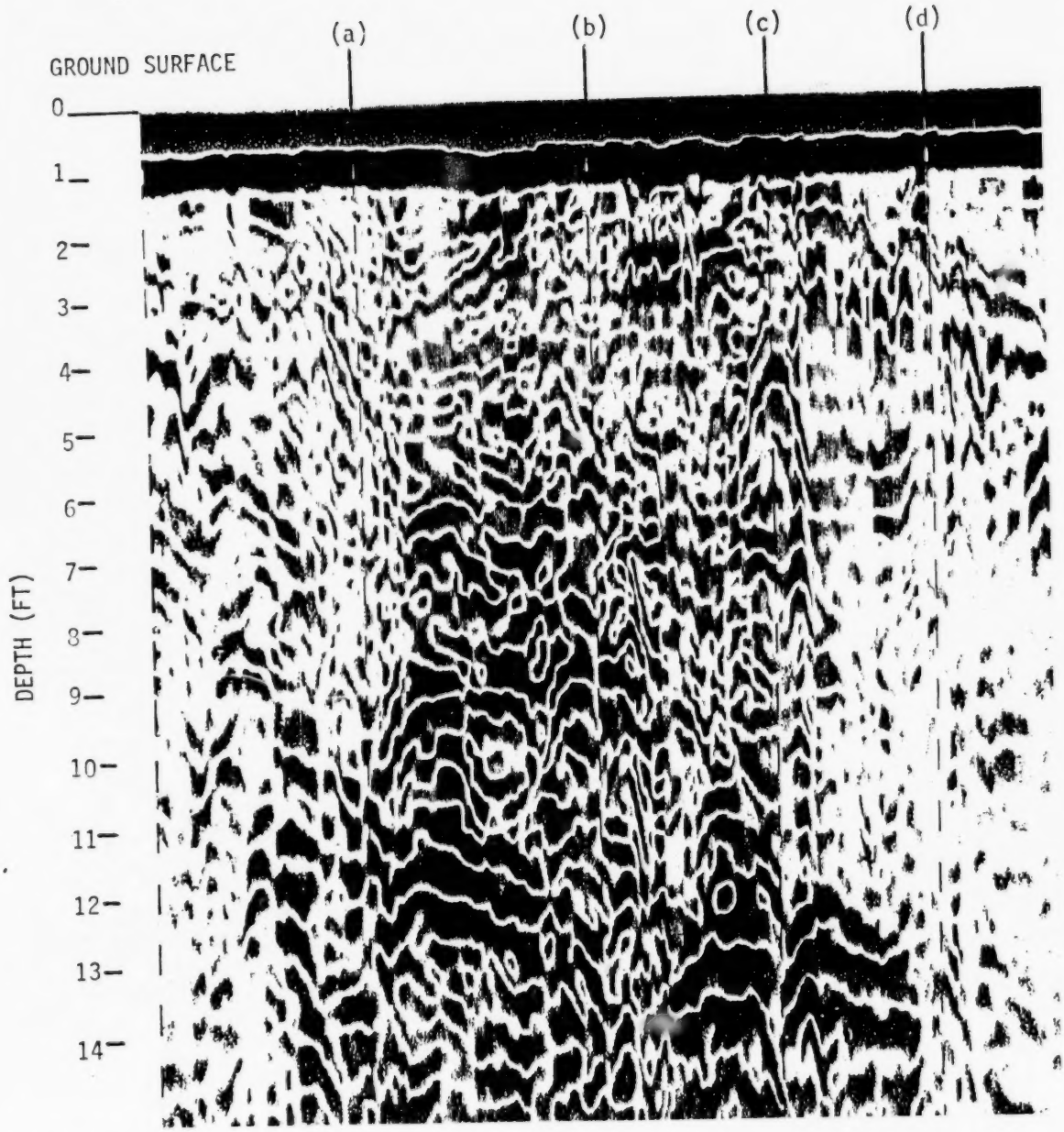


Figure 52. GPR printout showing survey of 40-gallon plastic drums (empty) at various depths, all drums surveyed with 120-MHz antenna. Burial locations and depths are the same as in Figure 45.

Figure 53. Insertion of downhole pulsed-RF antennas to monitor the effectiveness of chemical grouting.

between grouted holes. When the grouting operation was finished, post-grouting monitoring was carried out. The results were not conclusive, but a number of operational problems were resolved.

The second test site, in Pittsburgh, Pennsylvania, involved a pilot chemical grouting project where nine boreholes were drilled and cased in a 3 ft x 3 ft grid. Of the five scans taken and compared before and after grouting:

- Three were excellent and show that the travel time of the radar signals is uniform and quicker than it was in pregrouting traces, thus suggesting that grouting is complete.
- One was excellent but confusing because the hole wasn't grouted, unless the grout flowed more than 5 ft in a very uniform manner, which is somewhat unlikely.
- One was poor. The hole was grouted, but the signals were not uniform. Perhaps it wasn't grouted well?

The third test site, also in Pittsburgh, Pennsylvania, was on an actual construction job on downtown Sixth Avenue in front of the Oliver Building. A series of boreholes was drilled on approximately 1.5 m centers for a distance of approximately 120 m. The depths varied from 12 m to 18 m. Figure 54 shows GPR traces before and after grouting from the same boreholes. To interpret these results, consider the following logic. If the grout successfully enters all the soil voids, it expels all available pore water, which is usually present in the soil voids. Examination of the dielectric-constant versus moisture-content graph (Figure 5) reveals that as a soil's moisture content is decreased, as it would be when grout causes the pore water to be expelled, the dielectric constant of that soil decreases. From the following equation, it follows that, as the dielectric constant ($\varepsilon_r$) decreases, the signal travel time (t) across the same path length (d) should also decrease.

$$t = d\,(\varepsilon_r)^{1/2}/c \qquad (35)$$

where $t$ = travel time
$d$ = distance between borehole antennae
$\varepsilon_r$ = dielectric constant of soil
$c$ = speed of light in a vacuum

When comparing the post-grouting scans to the pregrouting scans, a decrease in the signal travel time may then indicate successful grout penetration into the soil.

Viewing Figure 54 in this light, the travel time from borehole to borehole in the "before grouting" trace is considerably longer (the white area), and far less uniform, than in the "after grouting" trace. The data when the antennae are near the ground surface (approximately 6 m) is not reliable.

Note should also be made of the dark zone at 7 m to 12 m depth in the "before grouting" trace of Figure 54. This anomalous dark zone represents

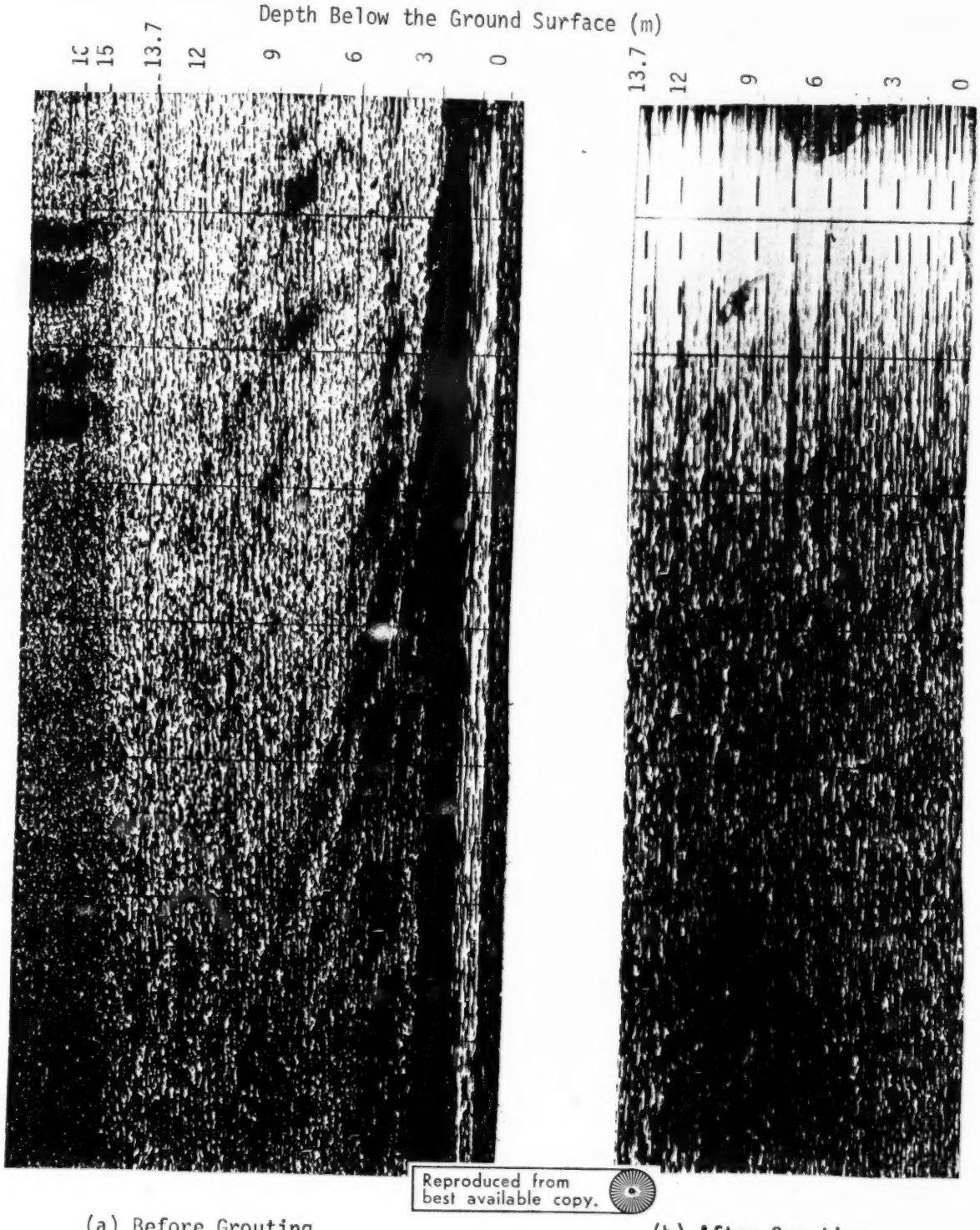


(a) Before Grouting

(b) After Grouting

Figure 54. GPR traces between boreholes 20 and 22 on Sixth Avenue in front of the Oliver Building.

some structural defect in the soil that has been completely eliminated in the "after grouting" trace. Detail such as this has tremendous impact on grout effectiveness monitoring, and it is acquired in real time where the contractor can immediately respond and correct the situation. It is possible that downhole GPR monitoring, like that shown in Figure 54, could indeed be a breakthrough in grouting technology.

## REFERENCES


1. Lord, A.E., Jr., S. Tyagi, and R.M. Koerner, Reports No. 1 through 15 submitted to U.S. Environmental Protection Agency, Edison, NJ, under Cooperative agreement No. CR80777010.

2. Okrasinski, T.A., R.M. Koerner, and A.E. Lord, Jr., "Dielectric Constant Determination of Soils at L-Band Microwave Frequencies," Geotechnical Testing Journal, American Society for Testing and Materials, Vol. 1, pp. 134-140, 1979.

3. Okrasinski, T.A., A.E. Lord, Jr. and R.M. Koerner, "Microwave Interference Detection of Subsurface Water," Technical Note, Journal of the Geotechnical Engineering Division, ASCE, Vol. 104, No. GT1, pp. 119-123. 1978.

4. Unterberger, R.R., "Electromagnetic Wave Propagation in Rock Salt," Proceedings of the Fourth Symposium on Salt, North Ohio Geological Society, 1974.

5. Holser, W.T., R.J.S. Brown, F.A. Roberis, D.C. Fredricksson, and R.R. Unterberger, "Radar Logging of Salt Dome," Geophysics, Vol. 37, pp. 899-906, 1972.

6. Lundien, J.R., "Determining Presence, Thickness, and Electrical Properties of Stratified Media Using Swept-Frequency Radar," Report M-72-4, U.S. Army Waterways Experiment Station, Nov., 1972.

7. Ellerbruch, D.A. and J.W. Adams, "Microwave Measurment of Coal Layer Thickness," Final Report NBSIR 74-387, National Bureau of Standards, Sept., 1974.

8. Cook, J.C., "Seeing Through Rock with Radar," Proceedings of the North American Rapid Excavation and Tunneling Conference, Port City Press, Baltimore, pp. 89-101, 1972.

9. Cook, J.C., "Ground Probing Radar," Proceedings: Subsurface Exploration for Underground Excavation and Heavy Construction, ASCE, New York, pp. 172-194, 1974.

10. Rosetta, J.V., Jr., "Detection of Subsurface Cavities by Ground Probing Radar," Symposium on Detection of Subsurface Cavities by Surface Remote Sensing Techniques, U.S. Army Waterways Experiment Station, pp. 120-127, 1977.

11. Morey, R.M., Continuous Subsurface Profiling by Impulse Radar," Proceedings: Subsurface Exploration for Underground Excavation and Heavy Construction, ASCE, New York, pp. 213-232, 1974.

12. Dolphin, L.T., R.L. Bollen, and G.N. Oetzel, "An Underground Electromagnetic Sounder Experiment," Geophysics, Vol. 39, pp. 49-55, 1974.

13. Unterberger, R.R., "Overview of Electromagnetic Methods in Geophysics and Application of Radar in Detection of Cavities in Salt," Symposium on Detection of Subsurface Cavities by Surface Remote Sensing Techniques, U.S. Army Waterways Experiment Station, p. 119, 1977.

14. Harrison, C.H., "Reconstruction of Subglacial Relief from Radio Echo Sounding Records," Geophysics, Vol. 35, pp. 1099-1115, 1970.

15. Rubin, L.A., J.N. Griffin, and W.L. Still, "Subsurface Site Investigation by Electromagnetic Radar, Phase I Report: Feasibility," Report NSF/RA-76-0187, ENSCO, Inc., 1976.

16. Rubin, L.A. and J.C.Fowler, "Ground-Probing Radar for Delineation of Rock Features," Engineering Geology, Vol. 12, pp. 163-170, 1978.

17. Benson, R.C. and R.A. Glaccum, "Remote Assessment of Pollutants in Soil and Groundwater," Proceedings of the 1979 Conference on Hazardous Material Risk Assessment, Disposal and Management, Information Transfer, Inc., pp. 188-194, 1979.

18. Benson, R.C. and R.A. Glaccum, "Radar Surveys for Geotechnical Site Assessment," Proceedings of the Conference on Geophysical Methods in Geotechnical Engineering, Preprint #3794, 1979.

19. Sandness, G.A., G.W. Dawson, T.J. Mathieu and J.L. Rising, "The Application of Geophysical Survey Techniques to Mapping of Wastes in Abandoned Landfills," Proceedings of the 1979 Conference on Hazardous Materials Risk Assessment, Disposal and Management, Information Transfer, Inc., 1979.

20. Hipp, J.E., "Soil Electromagnetic Parameters as Functions of Frequency, Soil Density, and Soil Moisture," Proceedings of the IEEE, Vol. 62, p. 98, 1974.

21. Hoekstra, P., A. Delaney, "Dielectric Properties of Soils at UHF and Microwave Frequencies," Jour. of Geophysical Research, Vol. 9, No. 11, p. 1699, 1974.

22. Rosenfarb, J.L., D.M. O'Shaughnessy and R.J. Krizek, "Effect of Particle Arrangement on Electrical Resistivity of Clay," Northwestern University, unpublished, 1976.

23. Koerner, R.M., A.E. Lord, Jr., S. Tyagi and J.E. Brugger, "Use of NDT Methods to Detect Buried Containers in Saturated Silty Clay Soil," Proc. 3rd Nat'l. Conf. on Management of Uncontrolled Hazardous Waste Sites, 1982.

## APPENDIX A

## LIST OF TECHNICAL PAPERS GENERATED DURING THE COURSE OF THIS PROJECT


1. Brugger, J.E., J.W. Beck, D.C. Maricovich, A.E. Lord, Jr. and R.M. Koerner, "Moisture Measurements in Sand Using a Basic Microwave Optics Setup," Amer. Jour. of Physics, Vol. 45, No. 1, pp. 88-89. 1977.

2. Okrasinski, T.A., A.E. Lord, Jr. and R.M. Koerner, "Microwave Interference Detection of Subsurface Water," Jour. of Geotechnical Engin. Div., ASCE, Vol. 104, No. GTT1, pp. 119-124, 1978.

3. Koerner, R.M., A.E. Lord, Jr., T.A. Okrasinski and J.S. Reif, "Detection of Seepage and Subsurface Flow of Liquids by Microwave Interference Methods," 1978 Conf. on Control of Hazardous Materials Spills, 1978.

4. Okrasinski, T.A., R.M. Koerner and A.E. Lord, Jr., "Dielectric Constant Determination of Soils at L-Band Microwave Frequencies," Jour. of Geotechnical Testing, ASTM, Vol. 1, No. 3, pp. 134-140, 1978

5. Lord, A.E., Jr., R.M. Koerner and J.S. Reif, "Determination of Attenuation and Penetration Depth of Microwaves in Soil," Geotechnical Testing Journal, ASTM, Vol. 2, No. 2, pp. 77-83, 1979.

6. Koerner, R.M., J.S. Reif and M.J. Burlingame, "Detection Methods for Location of Subsurface Water and Seepage," Jour. of Geotechnical Engr. Div., ASCE, Vol. 105, No. GT11, pp. 1301-1316, 1979.

7. Lord, A.E., Jr., S. Tyagi and R.M. Koerner, "Non-Destructive Testing (NDT) Methods Applied to Environmental Problems Involving Hazardous Material Spills," Proceedings of 1980 Nat'l. Conf. on Control of Hazardous Material Spills, Louisville, KY. 1980.

8. Lord, A.E., Jr., R.M. Koerner and J.E. Brugger, "Use of Electromagnetic Wave Methods to Locate Subsurface Anomalies," Proc. Management of Uncontrolled Hazardous Waste Sites Conference, pp. 119-124, 1980.

9. Koerner, R.M., A.E. Lord, Jr., J.J. Bowders, Jr. and W.M. Dougherty, "CW Microwave Location of Voids Beneath Paved Areas," Jour. Geotechnical Engr. Div., ASCE, Vol. 108, No. GT1, pp. 133-144, 1982.

10. Koerner, R.M., A.E. Lord, Jr. and J.J. Bowders, Jr., "Utilization and Assessment of a Pulsed RF System to Monitor Subsurface Liquid," Management of Uncontrolled Hazardous Sites Conference, pp. 165-170, 1981.

11. Bowders, J.J., Jr., A.E. Lord, Jr. and R.M. Koerner, "Sensitivity Study of a Ground Probing Radar System," Submitted to Geotechnical Engineering Testing Jour., ASTM, 1981, (accepted for publication).

12. Bowders, J.J., Jr., R.M. Koerner and A.E. Lord, Jr., "Buried Container Detection Using Ground Probing Radar," Submitted to Jour. Hazardous Materials, 1982, (accepted for publication).

13. Bowders, J.J., Jr., R.M. Koerner and A.E. Lord, Jr., "Potential Use of GPR in Hazardous Waste Monitoring in Unsaturated Soils," Submitted to AGU Symp., 1982, (accepted for publication).

14. Koerner, R.M., A.E. Lord, Jr., S. Tyagi and J.E. Brugger, "Use of NDT Methods to Detect Buried Containers in Saturated Silty Clay," Management of Uncontrolled Hazardous Waste Sites Conference. pp. 12-16, 1982.

APPENDIX B

LIST OF (MASTERS) THESES GENERATED
DURING THE COURSE OF THIS PROJECT

1. Okrasinski, T.A., "Determination of the Relative Dielectric Constant of Soils as a Function of Soil Type, Soil Saturation, Soil Temperature and Soil Saturated With Seawater For Electromagnetic Radiation Within the 0.3 GHz to 1.55 GHz Frequency Range," MSCE Thesis, Drexel University, 94 pgs, 1977.

2. Reif, J.S., "Determination of the Attenuation Coefficients and Relative Dielectric Constants of Three Soils as a Function of Soil Types, Water Content, Density and Frequency Within the 0.01-2.4 GHz Range," MSCE Thesis Drexel University, 121 pgs, 1979.

3. Burlingame, J.J., "A Comparison of Geophysical Methods for the Determination of Subsurface Anomalies," MSCE Thesis, Drexel University, 143 pgs, 1979.

4. Bowders, J.J., Jr., "Use of Electromagnetic Wave Methods in Geotechnical Engineering Applications," MSCE Thesis, Drexel University, 101 pgs, 1982.